The Paton WELDING JOURNAL

October 2000 # 11

English translation of the monthly «Avtomaticheskaya Svarka» journal published in Russian since 1948

«The Paton Welding Journal» monthly is published by the E.O. Paton Electric Welding Institute of the National Academy of Sciences of Ukraine with the support rendered by the International Association «Welding».

Promotion group:
V.N.Lipodaev, V.I.Lokteva
A.T.Zelnichenko (Exec. director)
Translators:
S.A.Fomina, I.N.Kutianova,
T.K.Vasilenko

Editorial and advertising offices are located at PWI, Dept. 51, 11, Bozhenko str., 03680, Kyiv, Ukraine.
Tel.: (38044) 227 67 57
Fax: (38044) 268 04 86
E-mail: paton@i.kiev.ua

Subscriptions:
$460, 12 issues

«The Paton Welding Journal» Website:
http://www.nas.gov.ua/pwj

CONTENTS

EVGENY PATON PRIZE

The International Institute of Welding regularly awards prominent scientists, engineers and public figures from different countries for making a significant contribution to development of welding science, engineering and fabrication. By submission of national delegations of Japan, France, Italy, the USA and Belgium the IIW instituted the following prizes: Y. Arata Award (Japan) — for contribution to the progress of welding science and related fields, Henry Granjion Prize (France) — for current research carried out by young scientists in the field of welding, Guerrera Medal (Italy) — for the fabrication of an outstanding welded construction, and Thomas Medal (USA) — for international standards activities. Goldschmidt-Clermont Prize (Belgium) and Andre Leroy Prize (France) are awarded every odd year and every even year, respectively, for creation of video and computer programmes.

In 1999 the Governing Board of the IIW decided to institute the international prize named after Evgeny Paton. This proves an international recognition of the outstanding services of Evgeny Paton, and this fact is especially notable that it takes place when we celebrate 130 years since his birthday. This event was preceded by a long work done by the National Welding Committee of Ukraine at working bodies of the IIW (the IIW now has 42 member countries from different regions of the world).

Institution of the Evgeny Paton Prize by the IIW was met with understanding and received an international support. The name of Evgeny Paton has been known throughout the world to many generations of welders, metallurgists, strength specialists and fabricators of different structures. His personal contribution to development of new directions of welding science and technology, creation of the Paton school, utilization of welding for fabrication of various-purpose critical structures was highly appraised by the international community. Selflessness of Evgeny Paton as a scientist and citizen has won respect of many generations.

Contribution of Evgeny Paton and his school to radical changes in many areas of machine building, metallurgy, civil engineering and materials science will retain significance on the global scale for many years to come. The Evgeny Paton Prize will be awarded every two years commencing in the year 2000 to individuals who made during their life time a considerable contribution to applied research and development in the field of advanced technologies, materials and equipment for welding and allied processes.

The Prize will be awarded in one of two categories:

Giving the honorary diploma and medal to Dr. S.J. Maddox — the first winner of the Evgeny Paton Prize of the IIW. Shown *from the right* are Dr. Maddox; Prof. Yushchenko, Chairman of the National Welding Committee of Ukraine, and Mr. Bramat, Secretary General of the IIW

Mr. B. Braithwaite, President of the IIW, is making a presentation

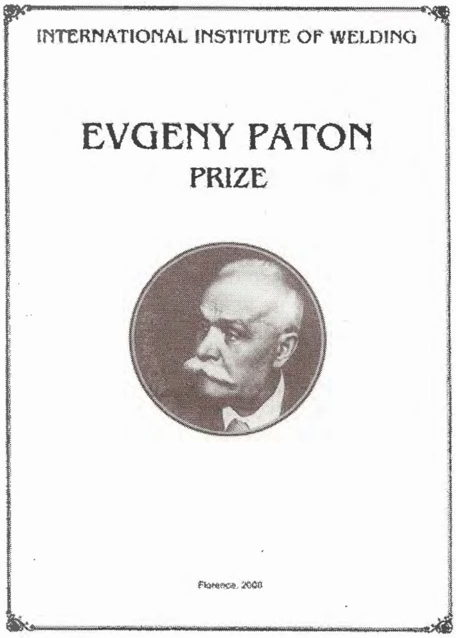

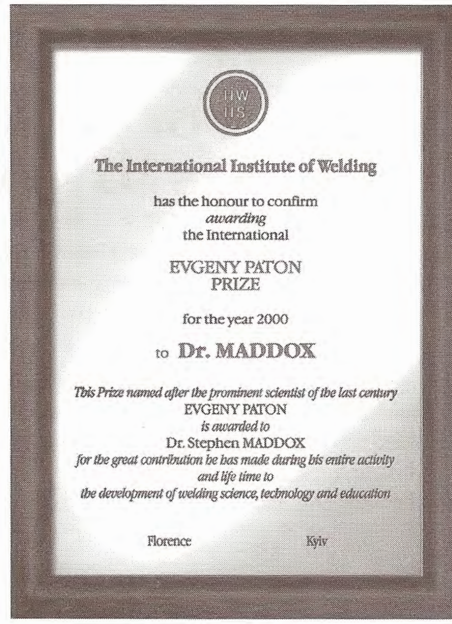

Honorary diploma given to the first winner of the Evgeny Paton Prize of the IIW

• category A: for applied research and development which has been successfully utilized in industry;

• category B: for the development of new industrial equipment, materials and structures using welding and allied processes, which has been successfully implemented by industry.

This is important also because it is for the first time in history of Ukraine that the international community institutes a prize named after our countryman. This Prize, along with the others, will continuously attract attention of specialists from different countries to Ukraine and works carried out in our country.

The first winner of the Evgeny Paton Prize for the year 2000 is Dr. S.J. Maddox, an expert in the field of fracture mechanics used for evaluation of fatigue of welded structures.

The Prize was awarded during the 53-th Annual Assembly of the IIW in Florence, Italy. The Prize was given by Mr. B. Brathwaite, President of the IIW, Mr. M. Bramat, Secretary General of the IIW, and Prof. K. Yushchenko, Chairman of the National Welding Committee of Ukraine. Those present at the Assembly warmly congratulated Dr. Maddox with this high award.

Dr. Maddox is known for high innovation activity in the field of use of fracture mechanics for evaluation of fatigue of welded structures. He was the first to prove that the fracture mechanics approaches could be equally applied along with the empirical methods for estimation of life of welded joints. Of special significance is his work on estimation of the effect of cracks propagating from toes of fillet or butt T-joint. Dr. Maddox uses to advantage the fracture mechanics approaches to determine fatigue characteristics of complicated welded joints in the cases where experiments or tests are either difficult or impossible.

Results of investigations conducted by Dr. Maddox are applied almost in all industries where equipment is subjected to cyclic loading.

Dr. Maddox is a Chairman of the Fatigue Commission at the Department of Fatigue of the British Institute of Standards. In addition to working out the methodology for estimation of the effect of defects in welds under conditions of fatigue loading, Dr. Maddox takes an active part in development of the majority of the design standards in force in Great Britain, which concern the fatigue issues.

Dr. Maddox is internationally known for being for a long time the Chairman of IIW Commission XIII. The results of his efforts are very important, as they include development of recommendations which serves as the basis for Fatigue Calculation Regulations «Eurocode 3». He is the author of a reference book on fatigue of welded structures and co-author (editor) of four other books, as well as the author of almost 60 journal publications and papers presented at conferences.

The great contribution of Dr. Maddox to investigation of fatigue properties of welded structures was highly appraised by awarding him with the Evgeny Paton Prize.

RESISTANCE OF 12KhGN2MFDRA STEEL WELDED JOINTS TO A DELAYED FRACTURE

L.I. MIKHODUJ, V.D. POZNYAKOV and A.K. YUSHCHENKO
The E.O. Paton Electric Welding Institute, NASU, Kyiv, Ukraine

ABSTRACT

Mechanical properties and resistance of T-joints of 12KhGN2MFDRA steel (hot-rolled and heat-treated) to cold crack formation were investigated relative to manual electric arc and mechanized welding in shielding gases using solid wires which provide welds of a different type of alloying (bainitic-ferritic, ferritic-bainitic, austenitic).

Key words: *high-strength steel, hot-rolled sheets, heat treatment, mechanical properties, cold resistance, T-joints, delayed fracture, diffusive hydrogen*

The low-alloyed high-strength steel of 12KhGN2MFDRA (C — 0.12; Si — 0.30; Cr, Mn — up to 1.0; Ni — up to 2.0; Mb, V, Cu — up to 1.0 wt.%) grade is used in manufacture of heavy-loaded welded structures. Unlike many other domestic high-strength steels it is supplied to manufacturers in the form of hot-rolled 4 – 20 mm thick sheets of 670 – 714 MPa yield strength [1]. This requires certain corrections in technological process of manufacture of the structure separate elements made of this steel, in particular, box-type connections, where T- and overlap joints are dominating. In this case the necessary complex of service pro-perties ($\sigma_{0.2}$ = 800 – 1000 MPa, $\delta_5 \geq 10$ % and $KCU \geq 29$ J/cm^2 at temperature –50 °C) should be provided by the 12KhGN2MFDRA steel welded joints both directly after welding and also after appropriate heat treatment (quenching with tempering).

Depending on the conditions of manufacturing and service of the 12KhGN2MFDRA steel structure the technological process of their welding envisages the use of materials of the different levels of alloying (for example, welding wires Sv-07KhG2SN2MDYu (C — 0.07; Cr, Si, Mo, Cu — up to 1.0; Mn, Ni — up to 2.0 wt.%), Sv-08GSMT (C — 0.08; Si — 0.6; Mn — 1.1; Cr ≤ 0.3; Ni ≤ ≤ 0.3; Mo — 0.2 – 0.4; Ti — 0.05 – 0.12 wt.%), electrodes of 48N-13, EA-981/15 (C — 0.1; Cr — 16.0; Ni — 25.0; Mo — 6.0; Mn — 2.0; V — 1.0 wt.%), UONI-13/45 grades, etc.), and also a number of measures directed to the increase in the welded joint resistance to a delayed fracture (reduction in concentration of the diffusive hydrogen in the deposited metal, use of preliminary and additional heating up to 200 – 250 °C). In most cases this technological process was rather labour intensive and did not always prevent the occurrence of cold cracks in the welded joints.

The present work was aimed at the searching for effective technological processes of welding 12KhGN2MFDRA steel (hot-rolled and heat-treated), which could provide the high resistance of the welded joints to a delayed fracture at lower temperatures of the preheating. It seemed rational for this purpose to test consumables for welding 12KhGN2MFDRA steel, which find application in welding other domestic high-strength steels: welding wire of Sv-08KhN2GMYu (C ≤ 0.1; Si — 0.3; Mn — 0.6; Cr — 1.0; Ni — 1.6; Mo — 0.3 wt.%) grade and electrodes of ANP-7 (C — 0.08; Si — 0.25; Mn — 1.3; Cr — 0.5; Ni — 1.8; Mb — 0.5; V — 0.04; Cu — 0.3 wt.%) grade [2, 3]. This selection was made due to the fact that the characteristic of weldability of welds, $P_{cm.\mathrm{w}}$, determined by the level of metal alloying is much lower than 0.24 – 0.28 as compared with that when, for example, the welding wire Sv-07KhG2SN2MDYu and electrodes 48N-13 are used ($P'_{cm.\mathrm{w}}$ = 0.28 – 0.31).

However, the results of similar works carried out earlier on the high-strength steel 13KhGMRB (C — 0.12; Cr, Mn, Mo — up to 1.0; Ni — up to 0.2 wt.%) [4] indicate that the decrease in level of alloying of the deposited metal should not lead to a great decrease in strength characteristics of the fillet weld metal.

As is known the selection of welding consumables is accompanied by welding of a large number of butt joints, manufacture of appropriate samples from them and their testing. From the results of these investigations the conclusion is made about the rationality of using definite technological variants in manufacture of the welded structures.

As the welded structures whose connections were made from 12KhGN2MFDRA steel consist mainly of T-joints, then the conditions of formation of structure and properties of weld metal of these joints differ greatly from the those of the butt joints. Therefore, it is rational to evaluate the mechanical properties of the weld metals from the results of testing the cylindrical samples cut out from real T-joints. The manufacture of samples for the impact bend test directly from T-joints, especially from thin metal, is seemed impossible. In this connection, special butt joints-simulators (Figure 1), recommended in [5], which could reproduce the conditions of T-joint welding, were welded for the evaluation of the impact toughness of the fillet welds.

When the present investigations were carried the T-joints and samples-simulators were manufactured from 12KhGN2MFDRA steel of 6, 10 and 15 mm thickness and the following chemical composition, %: C — 0.10 – 0.13; Si — 0.29 – 0.33; Mn — 1.08 – 1.12; Cr — 0.96 – 1.09; Ni — 1.96 – 2.05; Mo — 0.49 – 0.53; V — 0.10 – 0.12; Cu — 0.58 – 0.62; B — 0.001 – 0.002; S — 0.010 – 0.019; P — 0.012 – 0.019. Edges of butt joints of the sample-simulator were subjected to gouging under 45° angle to produce the size of a chamfer which is comparable with values of the leg (L) of welds: 7 – 8 and 10 – 11 mm. The main part of investigations was made using the 1.2 mm diameter wire Sv-08KhN2GMYu in argon-based mixture of gases ($Ar + CO_2$ and $Ar + + CO_2 + O_2$). To obtain the comparable data the other welding consumables were used, such as: wires Sv-08GSMT, Sv-08Kh20N9G7T (C — 0.08; Si — 0.5; Cr — 20.0; Ni — 9.0; Mn — 7.0; Ti — 0.8 wt.%), and also electrodes ANP-7 and EA-981/15.

To take into consideration the peculiarities of the 12KhGN2MFDRA steel the test samples were under different conditions: as-hot-rolled, and also after oil quenching at 880 °C and next tempering at 570 – 580 °C. A part of welded samples was subjected to a similar heat treatment to relieve stresses or to attain the necessary complex of properties of the welded joints.

The typical values of strength and ductile properties and also characteristics of the impact strength of metal of the fillet welds (with 7 – 8 mm leg) of the 10 mm thick 12KhGN2MFDRA steel welded joints made using the investigating consumables are given in Table 1. These data prove that required strength characteristic of the weld metals in combination with their high cold resistance at temperatures to –50 °C are guaranteed using the electrodes ANP-7 and wire Sv-08KhN2GMYu.

The susceptibility of the 12KhGN2MFDRA steel to cold cracking in the welded joints was evaluated using different methods of investigations (Implant, Tekken, «rigid T-joints» sample) that made it possible to determine the effect of concentration of hydrogen in welds ($[H]_{diff}$), rates of HAZ metal cooling, composition of deposited metal and design peculiarities of the joints.

The samples-implants for testing using the Implant method were manufactured from a hot-rolled and heat-treated steel of 10 mm thickness. Welding of the assembled samples was made by electrodes ANP-7 of 4 mm diameter using the following conditions: I_w = 170 – 175 A, U_a = 24 – 25 V, v_w = = 9.0 – 9.5 m/h. The content of the diffusive hydrogen in metal, deposited by the above-mentioned electrodes was $[H]'_{diff}$ = 2.0 – 2.5 ml/100 g and $[H]''_{diff}$ = 5.5 – 6.0 ml/100 g (when analyzing its content using a cromotographic method). This was attained by different conditions of the electrode baking. The rate of the HAZ metal cooling within the range of 600 – 500 °C temperatures ($w_{6/5}$, °C/s) which was adjusted with the help of the preliminary heating of the samples varied within the 3.0 – 18.0 °C/s ranges.

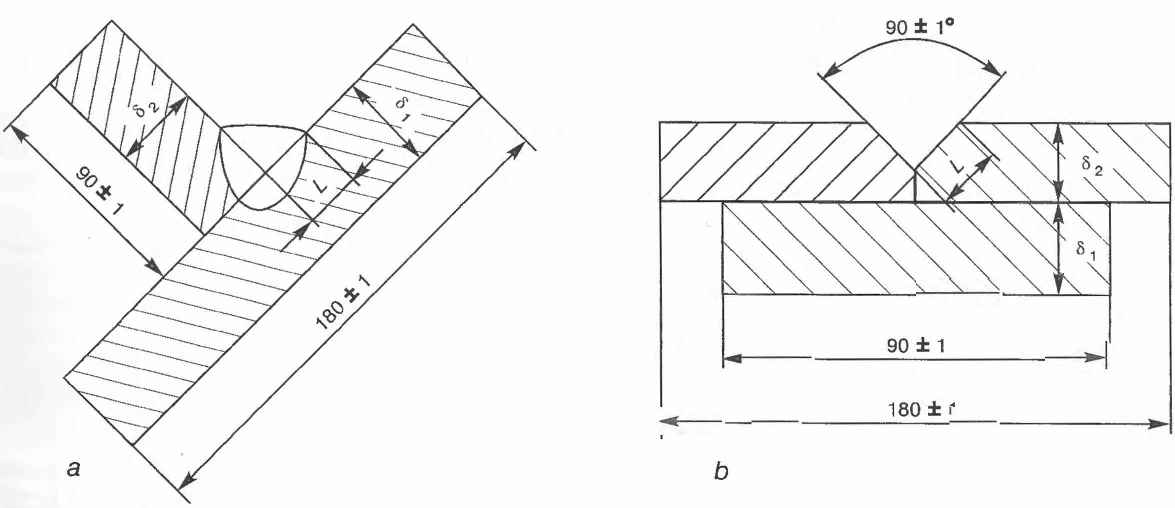

Figure 1. Scheme of making T-joint (*a*) and butt sample-simulator (*b*)

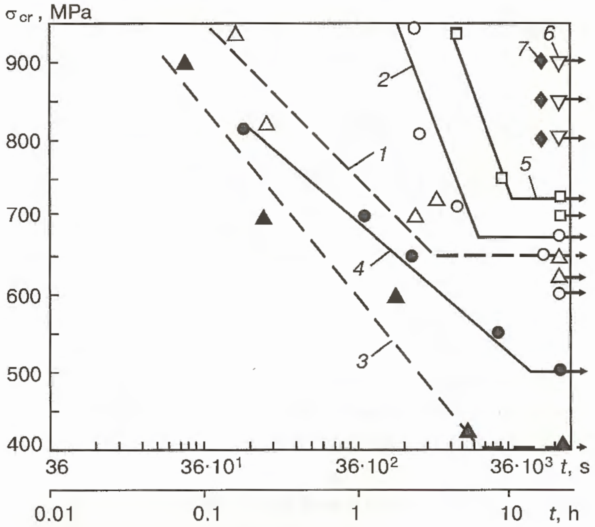

Figure 2. Resistance of Implant samples made from heat-hardened steel 12KhGN2MFDRA to a delayed fracture in changing the concentration of diffusive hydrogen in welded joints and the HAZ metal cooling rate: *1, 3* — $w_{6/5}$ = 18.0; *2, 4* — 12.5; *5* — 7.0; *6* — 3.5; *7* — 3.0 °C/s; *1, 2, 5 – 7* = $[H]_{diff}$ = 2.0 – 2.5; *3, 4* — 5.5 – 6.0 ml/100 g

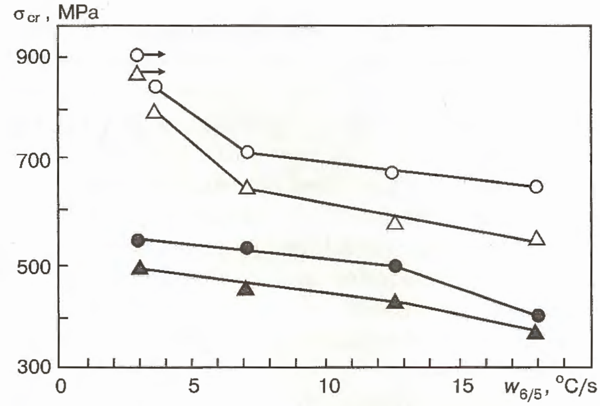

Figure 3. Effect of diffusive hydrogen concentration in welded joints and rate of HAZ metal cooling on critical stresses of Implant samples of hot-rolled (Δ, ▲) and heat-hardened (○, ●) steel 12KhGN2MFDRA: ○, Δ — $[H]_{diff}$ = 2.0 – 2.5; ●, ▲ — 5.5 – 6.0 ml/100 g

Table 1

Initial state of steel before welding	*Welding consumables, medium*	*PWHT of welded joints*	$\sigma_{0.2}$, *MPa*	σ_t, *MPa*	δ_5, *%*	φ, *%*	*KCU, J/cm², at T, °C*			*KCV, J/cm², at T, °C*	
							+20	*–50*	*–70*	*+20*	*–50*
Hot-rolled steel	Wire Sv-08KhN2GMYu Ar + CO_2	* ** *	880	948	13.8	50.0	76	69	66	38	31
	Wire Sv-08KhN2GMYu Ar + CO_2 + O_2	Same	1040	1155	12.6	58.0	88	67	61	–	–
	Electrodes ANP-7	»	858	982	15.7	55.4	78	42	27	–	–
Steel after quenching (**) and tempering (*)	Wire Sv-08KhN2GMYu Ar + CO_2	No	880	1010	13.0	50.7	80	79	73	41	32
		*	804	929	17.9	51.0	84	76	69	–	–
	Wire Sv-08KhN2GMYu Ar + CO_2 +O_2	No	953	1187	10.4	53.5	82	71	62	42	34
		*	873	960	16.6	51.0	78	72	69	41	32
	Electrodes ANP-7	No	810	930	17.3	58.6	95	60	48	–	–
			804	910	18.6	61.5	97	61	57	–	–
	Wire Sv-08GSMT CO_2	No	688	778	23.0	59.0	148	97	69	113	62
	Wire Sv-08Kh20N9G7T CO_2	No	329	875	41.3	47.6	135	92	73	124	80
	Electrodes EA-981/15	No	325	608	45.3	63.0	215	186	174	–	–

Table 2

Welding consumables, medium	$P_{cm.w}$	T_{pr}, °C	Area of cracks, %		
			at surface, C_{surf}	in section, C_{sec}	in root, C_r
Wire Sv-07KhG2SN2MDYu	0.310	20	100	100	100
CO_2		40	100	100	100
		60	100	100	100
		90	100	100	100
		120	100	100	100
		150	0	30	50
		170	0	0	0
Wire Sv-08GSMT	0.192	20	0	20	50
Ar + CO_2		40	0	10	30
		60	0	0	0
Wire Sv-08KhN2GMYu	0.273	20	100	100	100
Ar + CO_2		40	0	30	100
		60	0	10	30
		90	0	0	0
Wire Sv-08Kh20N9G7T	–	20	0	0	0
CO_2		40	0	0	0
Electrodes	0.264	20	100	100	100
ANP-7		40	20	50	70
		60	0	0	0
Electrodes	–	20	0	0	0
EA-981/15		40	0	0	0

The typical results of testing the Implant samples from heat-treated steel 12KhGN2MFDRA are given in Figure 2. The summarized results of investigations of effect of hydrogen and structural factors on the resistance of the steel examined to a delayed fracture are given in Figure 3. They indicate the negative effect of the diffusive hydrogen on the resistance of the HAZ metal of 12KhGN2MFDRA steel, having a martensitic structure [1] mainly, to cold cracking even at a rather limited its content (5.5 – 6.0 ml/100 g) in the deposited metal. At such concentrations of $[H]_{diff}$ the decrease in the rate of HAZ metal cooling from $w'_{6/5} = 18.0$ to $w''_{6/5} = 3.0$ °C/s influences negligibly the increase in values of critical tensile stresses (σ_{cr}, MPa) of 12KhGN2MFDRA steel both in as-hot-rolled condition and also after the appropriate its heat treatment from $\sigma'_{cr} \approx 370 - 400$ to $\sigma''_{cr} \approx 470 - 550$ MPa. At the same time the reduction in concentration of $[H]_{diff}$ from 5.5 – 6.0 to 2.0 – 2.5 ml/100 g 1.5 – 1.6 times increases the value σ_{cr} of the Implant samples, and consequently, the resistance to a delayed fracture of the welded joints of 12KhGN2MFDRA steel of both modifications even at a relatively intensive cooling of the HAZ metal ($w'_{6/5} = 18.0$ °C/s). At higher rates of cooling ($w_{6/5} > 7.0$ °C/s) the resistance of the welded joints to a delayed fracture was changed negligibly. In those cases when $w_{6/5} < 3.5$ °C/s, and the content of $[H]_{diff} = 2.0 - 2.5$ ml/100 g, the delayed fracture was not observed in the HAZ metal of the 12KhGN2MFDRA steel. Therefore, all next investigations on testing the technological samples using low-alloyed welding consumables were made at a very low content of the diffusive hydrogen in the deposited metal (not more than 2.5 ml/100 g).

The results of investigations of Implant samples helped to make one more conclusion, i.e. about the almost similar resistance of the HAZ metal of 12KhGN2MFDRA steel of both modifications to a delayed fracture. This is also proved by rather close relations of critical tensile stresses of Implant samples in all investigated variants of welding to the

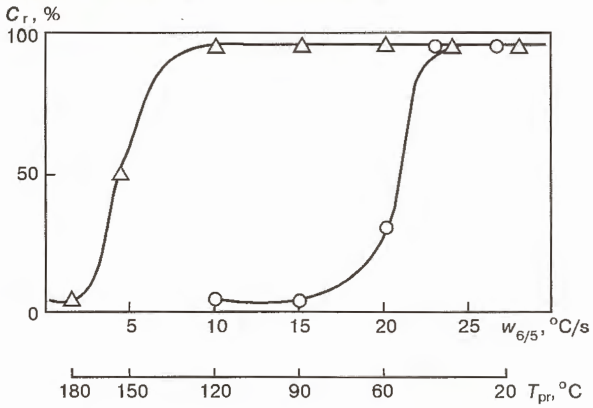

Figure 4. Effect of cooling rate (temperature of preheating) on the formation of cold cracks in weld root of the Tekken samples in welding with wire Sv-08KhN2GMYu in Ar + CO_2 mixture (O) and wire Sv-07KhG2SN2MDYu in CO_2 (Δ)

appropriate yield strengths of the hot-rolled and heat-treated steels. This is, probably, associated with the fact that the chemical composition of the steel, but not the method of its treatment, influences greatly the resistance of the HAZ metal to the cold crack formation. In this connection, all further investigations were carried out using the 12KhGN2MFDRA steel, which passed the heat treatment and possessed the highest strength characteristics.

The samples of Tekken method were manufactured from 15 mm thick steel. During their testing the resistance of welded joints made with wires Sv-07KhG2SN2MDYu, Sv-08KhN2GMYu, Sv-08Kh20N9G7T, Sv-08GSMT, and also with electrodes ANP-7 and EA-981/15, which can be used in manufacture of the 12KhGN2MFDRA steel structures, to cold cracking was evaluated. The samples were welded at the following conditions:

with coated electrodes: I_w = 170 – 175 A, U_a = = 24 – 25 V, v_w = 9.0 – 9.5 m/h;

with low-alloyed wires in Ar + CO_2 mixture: I_w = 200 – 230 A, U_a = 26 – 28 V, v_w = 20.0 – 22.0 m/h;

with low-alloyed wires in CO_2: I_w = 230 – 250 A, U_a = 28 – 30 V, v_w = 20.0 – 22.0 m/h;

with austenitic wire in CO_2: I_w = 280 – 320 A, U_a = 28 – 32 V, v_w = 20.0 – 22.0 m/h.

Results of investigations, given in Figure 4 and Table 2, show the high resistance of butt-welded technological samples made by manual and mechanized methods of welding using austenitic materials (wire Sv-08Kh20N9G7T and electrodes EA-981/15) to cold cracking. As to the crack resistance of similar technological samples, welded by low-alloyed consumables, then, their resistance to a delayed fracture was correlated to a great extend with a level of alloying of the weld metals.

The lowest level of alloying corresponds to the weld metal made by the mechanized CO_2 welding with wire Sv-08GSMT ($P_{cm.w}$ = 0.192). In this case at initial temperature of 20, 40 °C of samples the cracks were formed, but they did not escape to the surface. To prevent completely the cold crack formation in welding with this wire a preheating to 60 °C was required. On increasing the degree of alloying the deposited metal the resistance of butt technological samples to a delayed cooling was reduced. Thus, when welding was performed with wire Sv-08KhN2GMYu and in Ar + CO_2 mixture and also by manual process with electrodes ANP-7 ($P_{cm.w}$ = 0.264 – 0.273) the 12KhGN2MFDRA steel samples were preheated to 90 – 100 °C to prevent the cold cracking. As the next investigations showed this level of preheating is much lower as compared with that when the wire Sv-07KhG2SN2MDYu is used for this purpose in CO_2 welding ($P_{cm.w}$ = 0.31). In this case the preheating up to 170 °C was required to prevent the cold crack formation in Tekken samples.

However, as was earlier noted, the T-joints with fillet welds dominate in structures of the 12KhGN2MFDRA steel. Therefore, the combinations of welding consumables considered, which can find application in the mechanized welding were analyzed during « rigid T-joints» testing [6].

The T-joints of the thickest metal ($\delta_1 + \delta_2$ = = 15 mm) were welded in CO_2 using wires which are most widely used in manufacture of the 12KhGN2MFDRA steel structures: Sv-07KhG2SN2MDYu (bainitic-martensitic weld), Sv-08GSMT (ferritic-bainitic weld) and Sv-08Kh20N9G7T (austenitic weld).

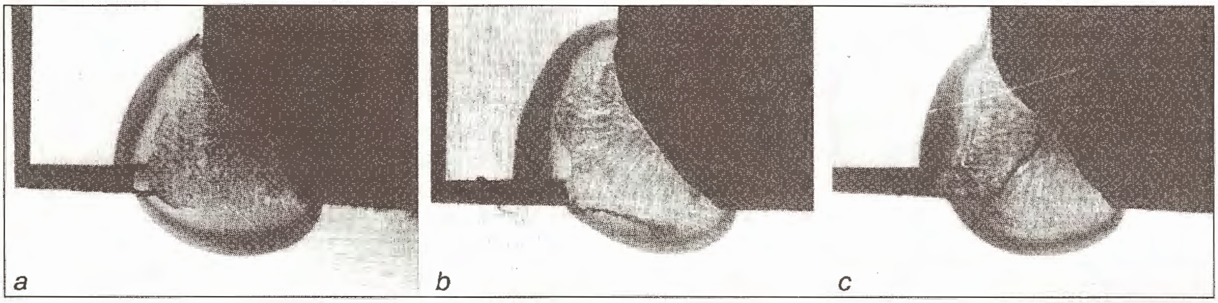

Figure 5. Macrosections of T-joints of 12KhGN2MFDRA steel

Table 3

Welding consumables, medium	*Combination of thicknesses of web and flange, mm*	*Weld leg, mm*	T_{pr}, °C	*Area of cracks, %*		
				at surface, C_{surf}	*in section,* C_{sec}	*in root,* C_r
Wire Sv-08KhN2GMYu	6 + 6	5	20	0	30	100
Ar + CO_2			40	0	25	40
			60	0	0	0
			60	100	100	100
	15 + 6	5	90	20	50	80
			120	0	10	30
			150	0	0	0
			20	20	50	100
	10 + 10	9	40	0	20	45
			60	0	0	0
			40	100	100	100
	15 + 15	9	60	0	20	45
			90	0	0	0
Wire Sv-07KhG2SN2MDYu.	15 + 15	9	60	100	100	100
CO_2			90	100	100	100
			120	30	50	80
			150	0	30	40
			180	0	0	0
Wire Sv-08GSMT	15 + 15	9	20	0	20	50
CO_2			40	0	0	0
Wire Sv-08Kh20N9G7T	15 + 15	9	20	0	0	0
CO_2						

Technological samples with the widest range of combinations of thicknesses of the flange (δ_1) and web (δ_2) of the T-joints were welded in the Ar + + CO_2 mixture using 1.2 mm diameter Sv-08KhN2GMYu wire: $\delta_1 = \delta_2 = 6$ mm; $\delta_1 = \delta_2 = 10$ mm; $\delta_1 = \delta_2 = 15$ mm; $\delta_1 + \delta_2 = 15 + 6$ mm. Depending on combination of thicknesses of the flange and web, the samples were welded with single-pass fillet welds of 4 – 5 or 8 – 10 mm legs.

Cracks in samples (Figure 5) were revealed during visual inspection of the surfaces of samples and examination of macrosections cut out from the welded joints in the direction, normal to the weld axis, after their long-time holding (not less than 72 h). It should be noted that in the samples whose weld strength was lower than that in the parent metal the cracks were propagating in the HAZ. At equal characteristics of strength of the weld metal and parent metal they were formed in the weld metal.

The investigations showed that in T-joints of an equal thickness of the web and flange (6 + 6, 10 + 10 and 15 + 15 mm) the cracks were not observed after preheating to 60 – 90 °C temperature (Table 3). It was established earlier [1] that the maximum rate of cooling the HAZ metal of the flange in these cases is $w_{6/5} \approx 6.5 - 9.0$ °C/s.

Under the unfavourable conditions the HAZ metal structure is formed in T-joints whose thickness of the flange exceeds greatly the web thickness (15 + 6 mm). In this case the leg of fillet welds ($L = 4 - 5$ mm) is set by the smaller thickness of the metal welded, i.e. the web thickness. In addition, the rate of the HAZ metal cooling of the flange during welding without the preheating possesses very high values ($w_{6/5} > 45$ °C/s), thus leading to the formation of the cold cracks in the welded joints. Only with preheating to 120 – 150 °C, when the rate of cooling HAZ metal of the flange of these T-joints was $w_{6/5} = 9.0 - 11.0$ °C/s the cracks were not observed in them.

The rest welding wires (Sv-08Kh20N9G7T, Sv-08GSMT and Sv-07KhG2SN2MDYu) were evaluated in welding «rigid T-joints», which had equal thicknesses of the web and flange $\delta_1 = \delta_2 = 15$ mm. In comparison with wire Sv-08KhN2GMYu the use of the austenitic wire can prevent completely the preheating, while in welding with wire Sv-08GSMT the preheating can be somewhat decreased (to 40 – 50 °C). The investigations show that both in welding of T-joints and also butt joints, the extrahigh level of weld alloying contributes to the great reduction in resistance of the joints to the cold crack formation. Therefore, when the wires Sv-07KhG2SN2MDYu were used, the higher-temperature preheating, i.e. up to 150 – 180 °C was required.

The investigations showed that the welded joints made from 12KhGN2MFDRA steel are characterized by the high susceptibility to cold crack formation. To prevent them, it is necessary to limit, first of all, the hydrogen enter to the welding zone. When welding with low-alloyed welding consumables its content in welds should not, probably, exceed 2.5 ml/100 g, that is difficult to attain under the real industrial conditions. The selection of the welding consumables should be made coming from the design features of definite joints and conditions in order to provide the required mechanical properties of the welded joints.

REFERENCES

1. Mikhoduj, L.I., Poznyakov, V.D., Vasiljev, V.G. *et al.* (2000) Peculiarities of welding T-joints made from 12KhGN2MDRA high-strength steel. *Avtomaticheskaya Svarka*, **3**, 6 – 11.
2. Musiyachenko, V.F., Mikhoduj, L.I. (1987) *Arc welding of high-strength steels*. Moscow: Mashinostroyeniye.
3. Mikhoduj, L.I., Melnik, I.S., Poznyakov, V.D. (1990) Resistance of low-alloyed welds to a delayed fracture in welding high-strength steels with a yield strength of above 600 MPa. *Avtomaticheskaya Svarka*, **2**, 14 – 19.
4. Musiyachenko, V.F., Mikhoduj, L.I., Poznyakov, V.D. *et al.* (1987) Selection of materials for making fillet welds of the 13KhGMRB steel joints. *Svarochnoye Proizvodstvo*, **9**, 29 – 31.
5. Asnis, A.E., Ivashchenko, G.A. (1985) *Increase in strength of welded structures*. Kyiv: Naukova Dumka.
6. Mikhoduj, L.I., Poznyakov, V.D., Zhdanov, S.L. *et al.* (1998) Delayed fracture of T-joints of high-strength steels. *Avtomaticheskaya Svarka*, **10**, 14 – 17.

SITUATION ALGORITHMS OF AUTOMATIC CORRECTION OF THE ROBOT MOTION PATH IN ARC WELDING

G.A. TSYBULKIN
The E.O. Paton Electric Welding Institute, NASU, Kyiv, Ukraine

ABSTRACT

Algorithms of a situational type with an adaptive variation of the correction step are suggested. The latter is varied on the basis of logical analysis of the formed situation characterizing current and previous positions of a tool relative to the welded joint under conditions of an incomplete information that comes from the sensing device. Results of computer modelling of the algorithms are given.

Key words: *robotic arc welding, algorithms, correction, path*

The batch-produced industrial robots used in welding production almost always have to be fitted with additional sensors. This is primarily due to the inability of the majority of the currently available robots to detect and automatically correct during arc welding the deviations of the line of the joint being welded relative to the programmed path of the end effector, arising for various reasons. This usually gives rise to the problem of adaptation of the robot motion to the above deviations based on information coming from the mounted sensor.

Based on [1], at least three different approaches to the defined problem can be indicated. In keeping with the first approach, which became developed in [2], the deviations arising in welding are corrected by introduction of correction signals into the lower (executive) level of the robot control system.

The second approach considered in [3], is based on the idea of decomposition (division) of the end effector motion on the mechanical level, into two separate motions, namely the programmed one along the assigned path and the correction motion towards the path. Implementation of such an idea envisages a greater number of axes in the control system by incorporating additional reproduction systems into it. It is obvious that both approaches result in sophistication of the control system hardware and its kinematic redundancy.

The third approach consists in automatic correction of the assigned path proper during its retrofitting [4]. Its implementation, however, runs into the following problem. Performance of correction of the path by changing the co-ordinates of its points, requires «splitting» every time the deviation measured by the sensor into components along the axes of the robot co-ordinate system. This procedure is known to involve development of additional software. Moreover, the machine time, required for performance of additional computational operations, can lead to essential limitations imposed on the welding speed.

In [4] we suggested a somewhat different from the traditional one [5] method of programming the path of the welding tool motion, allowing the above difficulties to be overcome. It consists in that between the nodal points of the path $P_s (s = 1, 2, ..., S)$ that are still assigned in the basic space of the robot with the $Oxyz$ system of co-ordinates, intermediate points $R_k (k = 0, 1, 2, ..., K)$ are placed with a certain spacing in the so-called local spaces with a special orientation of co-ordinate systems $P_s\tau nb$ and origins in the nodal points P_s. Co-ordinate axis τ is always oriented in the direction from point P_s to point P_{s+1} (Figure 1), axis b — along the longitudinal axis of the electrode, while axis n — normal to axis τ and electrode longitudinal axis.

With such a method of assigning the path, the possible deviations of the actual line of the joint being welded from the calculated line occur exactly along n co-ordinate. Therefore, adaptation of the robot motion to the possible changes in the position of the line of the joint being welded can be performed in welding by correction of n co-ordinate of intermediate points R_k.

A simple algorithm of such a correction is implemented by a recurrent relationship [6]

$$n_{k+1} = n_k - h \operatorname{sign} \psi_k, \qquad (1)$$

where n_k, n_{k+1} are the co-ordinates of points R_k and R_{k+1} along axis n, with $n_0 = 0$; h is the correction step, while sign ψ_k is the sign of signal $\psi = \psi(\varepsilon_n) +$

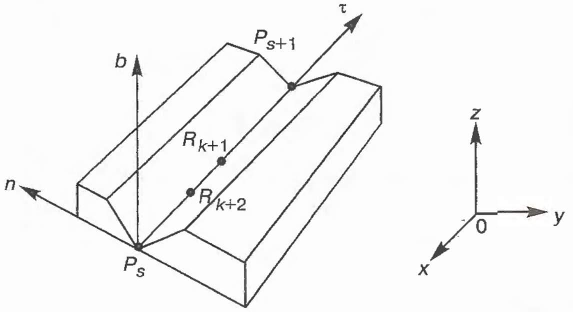

Figure 1. Orientation of the co-ordinate system $P_s\tau nb$ relative to the joint being welded

$+\ \delta$ at the sensor output, measured in point R_k and characterising the current lateral deviation ε_n of the line of the joint being welded from the calculated path in this point; δ is the measurement noise with an upper constraint by modulus imposed by a certain constant Δ: $|\delta| \le \Delta$.

The correction step $h = h(k)$ in expression (1) according to [6], can only take two values

$$h = \begin{cases} m_1\varepsilon_0, & \text{if } |\psi_k| > \psi_0, \\ 0, & \text{if } |\psi_k| \le \psi_0 \end{cases} \qquad (2)$$

depending on the situation which is in place at k-th step of ψ_k measurement.

In expression (2) $\psi_0 = \psi(\varepsilon_0)$ is the threshold based on allowance ε_0 for electrode deviation from the line of the joint being welded; $m_1 > 0$ is the parameter selected proceeding from the anticipated maximal initial deviation $\max\limits_s\ \varepsilon_n(s)$ and maximal angle of displacement $\max\limits_s\ \gamma(s)$ of the line of the joint being welded relative to the programmed line under the specific conditions of arc welding.

Use in algorithm (1), (2) of the function of sign(•) and threshold level of ψ_0 is due to the presence of an uncontrollable noise δ at the sensor output under the actual conditions of arc welding and to the fact that the actual statistical characteristics of the sensor $\psi = \psi(\varepsilon_n)$ in some cases can be non-monotonic and cannot provide sufficiently accurate information on the actual deviation of ε_n.

The above method turned out to be rather efficient, as the co-ordinates of the nodal points are assigned at the stage of programming the path of the welding tool motion, while the intermediate points are calculated by equations (1), (2). The current correction of the path during its optimisation is rather simple, namely just one co-ordinate n of subsequent point R_{k+1} is corrected directly by the results of measurement of ψ_k in the current point R_k.

This process has another valuable feature: correction of the co-ordinates of the path point R_{k+1} occurs at the moment when the welding torch is still in point R_k, and, therefore, the motion of the torch from point R_k into the already «corrected»point R_{k+1} is performed is exactly the same manner as in the absence of correction. In other words, the corrective control of the welding torch motion does not introduce any changes into the dynamics of the robot motion.

On the other hand, algorithm (1), (2) proper has an essential drawback, consisting in that the length of correction step h is assigned to be constant. Now selection of the step length under the conditions of «deficit» of the data on the actual deviation ε_n is not always an optimal one. With a too long step this may result in periodical transition of the electrode from one side of the line of the joint being welded to the other side, i.e. to an oscillatory mode, and to the loss of the effect of following the line of the joint being welded with a too short step.

Considered here is an algorithm of correction in the form of a recurrent procedure (1), but with an adaptive change of step length h in keeping with the logical function

$$h = \begin{cases} m_1\varepsilon_0, & \text{if } |\psi_k| > \psi_0, \\ m_2\varepsilon_0, & \text{if } |\psi_k| \le \psi_0, \end{cases} \qquad (3)$$

where $m_1 > 1$, $0 < m_2 < 1$ are the parameters characterising the lengthening or shortening of correction step h.

The essence of algorithm (1), (3) is as follows. The logic block functioning according to relationship (3), in each k-th step of adaptation, is presented with a certain j-th situation $\sigma_j \in \Lambda$ ($j = 1, 2, 3, 4$) which is in place by the moment of ψ_k measurement. Logic block takes a decision on the length of correction step h which should be made in this situation σ_j in point R_{k+1} in the direction indicated by sign ψ_k function.

One can see from (1) and (3) that n_{k+1} co-ordinate can take one of the four different values, depending on which of the set of four situations $\Lambda = \{\sigma_1, \sigma_2, \sigma_3, \sigma_4\}$ was in place at the moment of taking a decision in keeping with the logical function $h = f(\psi_k)$.

When algorithm (1), (3) is implemented, it is first of all necessary to correctly select the values of parameters m_1 and m_2, which largely determines the effectiveness of the use of the algorithm proper. So, if the values of parameters are close to a unity, the adaptation effect will be negligible and slow. Now, if their values are significantly different from a unity, the adaptation process will proceed quickly, but in this case «jumping» over the line of the joint being welded is possible. It is obvious that when the coefficients are selected, it is necessary to look for a reasonable compromise between

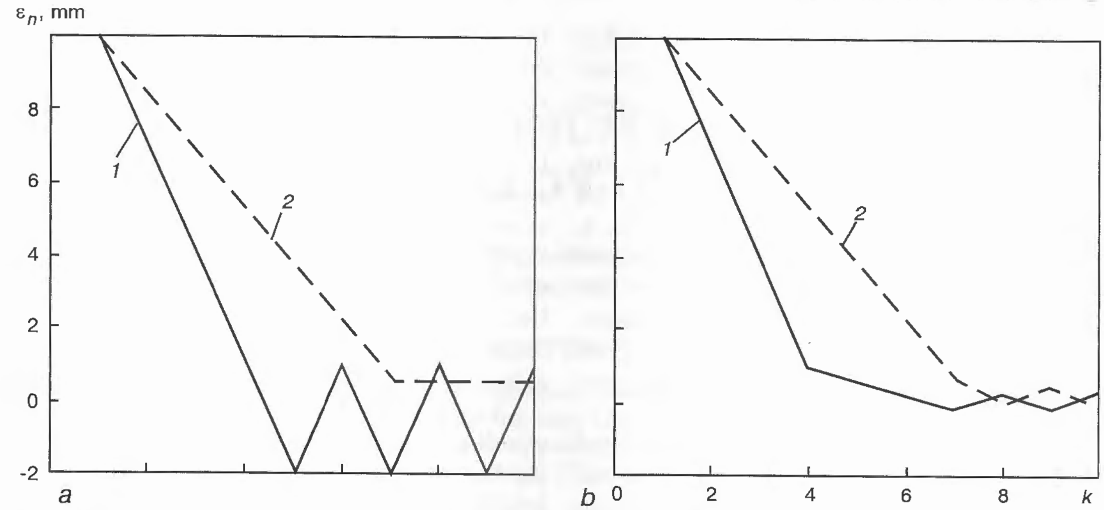

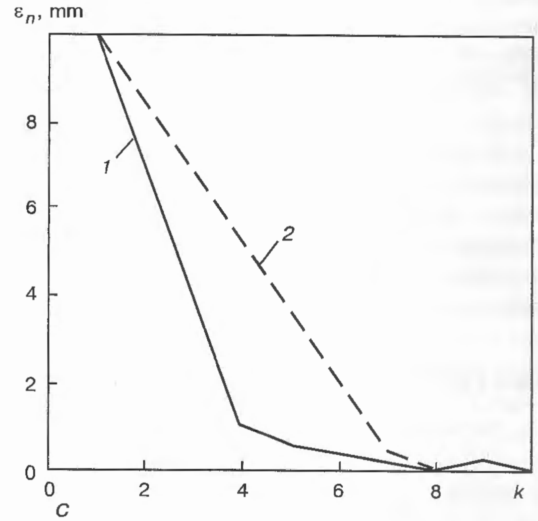

Figure 2. Results of numerical simulation of the algorithms at $m_1 = 1.6$, $m_2 = 0.4$ (curve *1*) and at $m_1 = 3$, $m_2 = 0.4$ (curve *2*)

the time of approach to the joint line and the necessary smoothness of this approach.

The adaptive properties of the situation algorithm of correction (1), (3), are illustrated by the results of computer simulation. In simulation the case was considered, when the actual line of the welded joint is shifted relative to the programmed line by a certain angle γ and, in addition, there is initial deviation $\varepsilon_n(0)$ of the electrode tip from the line of this joint. Noise δ at the sensor output was simulated by generating in the computer the pseudorandom numbers uniformly distributed in section $[-\Delta, \Delta]$

Figure 2, *b* shows the graphs of the processes of correction plotted by equations (1), (3) at $\gamma = 5^\circ$, $\varepsilon_n(0) = 10$ mm, $\varepsilon_0 = 1$ mm and different values of m_1 and m_2 parameters. For comparison, Figure 2, *a* gives the graphs of the correction processes, plotted by equations (1), (2) at the same values of γ, $\varepsilon_n(0)$, m_1, ε_0.

Comparison of equations 2, *b* and *a* shows that the characteristics of the correction process performed by algorithm (1), (3) are much better. In particular, even at a high speed of correction (at $m_1 = 3.0$), the amplitude of oscillations ε_n stays within the so-called dynamic accuracy tunnel with the radius of $\varepsilon_0 = 1$ mm.

Let us consider one more possibility for improvement of the correction algorithm. It is related to the fact that it is rational to take a decision on the length of step h not only based on measurement of ψ_k, as in (3), but also allowing for measurement of ψ_{k-1}, in the previous point, i.e. allowing for the history of the condition of the robotic system.

The logic function allowing for the previous measurements, can be represented as

$$h = \begin{cases} m_1\varepsilon_0, \text{ if } |\psi_k| > \psi_0 \text{ and } |\psi_{k-1}| > \psi_0, \\ m_2\varepsilon_0, \text{ if } |\psi_k| \le \psi_0 \text{ and } |\psi_{k-1}| > \psi_0, \\ m_3\varepsilon_0, \text{ if } |\psi_k| > \psi_0 \text{ and } |\psi_{k-1}| \le \psi_0, \\ m_4\varepsilon_0, \text{ if } |\psi_k| \le \psi_0 \text{ and } |\psi_{k-1}| \le \psi_0. \end{cases} \quad (4)$$

Here $m_1 - m_4$ are the positive parameters.

From (4) it is seen that the range of various situations $\Lambda = \{\sigma_1, \sigma_2, \ldots, \sigma_8\}$, describing the system condition, has become two times greater, compared to (3). The number of gradations of the correction step has also doubled, accordingly. This means that the adaptive capabilities of the algorithm functioning under the same conditions of limited a priori information on ε_n, have also been enhanced.

Figure 2, *c* shows for comparison purposes the graphs of the correction processes derived from (1), (4) at $m_3 = 0.6$; $m_4 = 0.2$. Parameters m_1, m_2, γ, $\varepsilon_n(0)$, ε_0 are the same as in simulation of algorithms (1), (2) and (1), (3). It is easy to see from this figure that unlike (1), (2) and (1), (3) algorithms, (1), (4) simultaneously provides the high speed and the required smoothness of the correction process.

It is important to emphasise that the considered situation algorithms can be used not only for lateral correction of the current position of the welding torch, but also for stabilisation of the specified length of the electrode extension. The structure of equations (1) and (2) (or (3) or (4)) is preserved. Just *n* co-ordinate is replaced by *b* co-ordinate in them, and instead of information signal $\psi = \psi(\varepsilon_n)$, $\varphi = \varphi(\varepsilon_b)$ signal is used, which characterises the current deviation ε_b of the electrode tip from the joint being welded along the electrode axial line.

Correction can certainly be performed also by *n* and *b* co-ordinates simultaneously. In particular, such a possibility is readily provided, when the industrial robot is fitted with just one electric arc sensor. In this case ψ and φ signals can be generated in the following form [7]:

$$\psi_k = \frac{\delta_R(k) - \delta_L(k)}{\delta_R(k) + \delta_L(k)} (A - vT_{\text{w}}),$$

$$\varphi_k = a\left(\delta_0 - \frac{\delta_R(k) + \delta_L(k)}{2}\right) \qquad (5)$$

In expressions (5), $\delta_R(k)$, $\delta_L(k)$ are the welding current deviations measured in the vicinity of point R_k, to the right and left of the average current position of the electrode tip, respectively, at transverse oscillations of the torch with amplitude A; δ_0 is the assigned nominal deviation of welding current; a is the coefficient of proportionality; v is the speed of transverse motion of the torch; T_{w} is the time constant, found from equation $T_{\text{w}} = R/EM$; where R is the total ohmic resistance of the electric circuit of the welding loop; E is the electric field intensity in the arc column; M is the slope of the electrode melting characteristic.

Thus, the results of numerical simulation have provided convincing evidence to the effect that situation algorithms (1), (3) and (1), (4) guarantee a more stable property of the welding robot adaptability to the environment, i.e. to various kinds of unforeseen changes in the spatial position of the line of the joint being welded and to the initial deviations of the welding tool from this line, than algorithm (1), (2).

Application of the above algorithms for the longitudinal and lateral channels of the welding robot correction, will provide stabilisation of the nominal length of the electrode extension and the minimal deviation of the welded joint from the sought position in robotic arc welding under the conditions of «deficit» of the information coming from the sensor.

Note that the proposed algorithms are quite simple and can be readily implemented in the computer which is part of the control system of a modern industrial robot, using just the programming means available to the user without any change in the basic software.

REFERENCES

1. Tsybulkin, G.A. (1990) Multi-constraint control of the motion of a material point with an assigned diversity in a three-dimensional space. In: *Thesis of 6th All-Union Meet. On Multi-Constraint System Control*, Suzdal, March 1990. Moscow: IPU.
2. Tsybulkin, G.A. (1991) Co-ordinating control of robot motion with error correction. In: *Thesis of 1st All-Union Conf. on Co-ordinating Control in Eng. and Nat. Systems*, Maly Mayak, Oct. 1991. Kharkov.
3. Tsybulkin, G.A. (1995) Two-level co-ordinating control of a manipulation robot with a kinematic redundancy. *Problemy Upravl. i Informatiki*, **3**, 143 – 150.
4. Lebedev, V.K., Timchenko, V.A., Tsybulkin, G.A. (1989) Control of spatial motion of the adaptive welding robot. In: *Thesis of XI All-Union Meet. On Control Problems*, Tashkent, 1989. Moscow.
5. Fu, K., Gonsales, R., Li, K. (1989) *Robotics*. Moscow: Mir.
6. Tsybulkin, G.A., Vlasov, O.V. (1990) On one method of correction of a programmed path of the robot end effector motion. In: *Thesis of All-Union Meet. On Robotic Systems*, Gelendzhik, Oct., 1990. Moscow.
7. Tsybulkin, G.A. (1999) On evaluation of current deviation of the electrode from the line of the joint being welded. *Avtomaticheskaya Svarka*, **12**, 53 – 54.

EFFECT OF SCANDIUM ADDITIONS ON WELDABILITY OF ALLOY OF Al–Zn–Mg SYSTEM

A.Ya. ISHCHENKO, V.O. CHAPOR and **M.R. YAVORSKAYA**
The E.O. Paton Electric Welding Institute, NASU, Kyiv, Ukraine

ABSTRACT

Data are presented about the effect of scandium additions in parent metal and filler wires on mechanical properties of welded joints. The susceptibility of joints to hot crack formation in welding experimental aluminium alloy Al–6Zn–2Mg is evaluated. Results of investigations confirmed the high effectiveness of using scandium in the parent metal of alloys of Al–Zn–Mg system and in all filler wires of Al–Mg system which are used in welding alloys of this type.

Key words: *aluminium alloys, zinc, magnesium, scandium, welding, hot cracks, filler wire, heat treatment, strength, ductility, angle of bending*

Additions of scandium to aluminium-based high-strength alloys improve greatly their technological and service characteristics. Now, there are scandium-containing promising alloys of the main systems of alloying, including Al–Mg (1570), Al–Mg–Li (1421), Al–Zn–Mg (1970, 1975) [1, 2]. The high-strength alloys of Al–Zn–Mg system are characterized by an effect of «self-hardening», i.e. formation of oversaturated solid solution at a comparatively low rate of cooling in air from high temperatures. This hardens significantly the weld metal due to a natural or artificial ageing without a repeated hardening. It should be noted that the alloys of this system of alloying are characterized by a much better adaptability in manufacture of prefabrications than the alloys of system Al–Mg and Al–Mg–Li. Researchers observed the capability of alloys to a large deformation within the wide ranges of temperatures and rates that improves greatly the adaptability in manufacture of prefabrication from them in the conditions of a superplasticity [1, 3].

One of the main drawbacks of these alloys is an increased susceptibility to hot crack formation in welding, and also the sensitivity of the parent metal and welded joint of the high-alloyed aluminium-zinc-magnesium alloys to a corrosion stress cracking that prevents their application in critical large-sized welded structures [4, 5].

Investigations of alloys developed in 1970 and 1975 in Russia showed that the introduction of scandium additions does not only affect favourably the mechanical properties of prefabrications made from alloys of Al–Zn–Mg system, but also improves noticeably their resistance to a stress corrosion and a delayed fracture [1]. As there are a little data about the scandium effect on the weldability of alloys of the above-mentioned system it is rational to investigate the effect of scandium on mechanical, corrosion properties and also the susceptibility to hot cracking in welding of alloys of the Al–Zn–Mg system. Actuality of these works in Ukraine is also stipulated by large resources of scandium-containing ore.

The present article gives the results of investigations of effect of scandium additions in parent metal and filler wire on the mechanical properties of welded joints and susceptibility to hot cracking during welding the experimental alloy Al–6Zn–2Mg. For this purpose, the batches of experimental alloys of the parent metal (Table 1) and filler wires (Al–5Mg, Al–5Mg–0.5Sc, Al–6Mg–0.45Sc) were produced.

Heat treatment of 3 mm thick sheets was performed using condition T8: water quenching from 45 °C, cold rolling with a deformation level of up to 5 %, artificial ageing at 120 °C for 24 h. The mechanical properties of sheets are given in Table 2. It was established that the presence of scandium improves negligibly the characteristics of strength and ductility of the parent metal.

Table 1. Chemical composition of sheets made from experimental alloys of Al–Zn–Mg system, mass %

Alloy	*Zn*	*Mg*	*Cu*	*Zr*	*Cr*	*Mn*	*Sc*	*Fe*	*Si*
Al–6Zn–2Mg	6.0	2.1 – 2.3	0.20 – 0.22	0.17 – 0.20	0.18	0.30	–	0.08	0.011
Al–6Zn–2Mg–0.2Sc	5.7 – 6.1	1.8 – 1.9	0.02	0.14 – 0.16	0.18	0.27	0.18 – 0.21	0.10	0.014

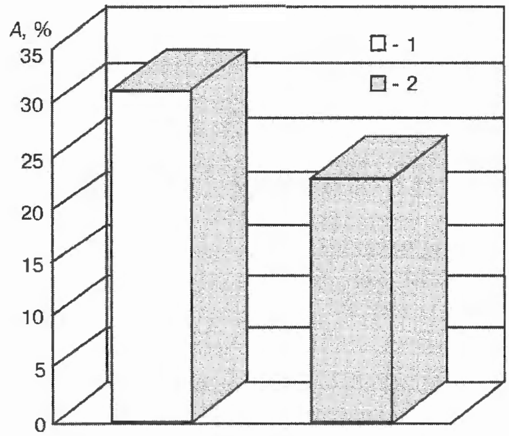

Susceptibility of experimental alloys of Al–Zn–Mg–(Sc) system to hot crack formation during welding using Trans-Varestraint sample: *1* — Al–6Zn–2Mg; *2* — 6Al–6Zn–2Mg–0.2Sc

The automatic butt welding of joints was performed with a non-consumable electrode in argon using three 1.6 mm diameter filler wires: Al–5Mg, Al–5Mg–0.5Sc and Al–6Mg–0.45Sc. Welding condition was as follows: I_w = 280 – 305 A, v_w = = 10 m/h, $v_{f.w}$ = 96 – 98 m/h. Strength of the welded joint with a weld convexity σ_t^w and strength of the weld metal $\sigma_t^{w.m}$ were evaluated at testing flat specimens with a narrowed working part in the weld zone. Mechanical properties of the welded joints were determined after welding in a state without an additional heat treatment.

Susceptibility of alloys to the hot cracking during welding was evaluated on two welding samples: «fish-bone» and Trans-Varestraint. The specimens of the first sample were not subjected to an additional load. They were subjected to the action of natural welding and shrinkage stresses only. The specimens of the second sample were subjected to an additional external load [5, 6]. Both samples are rather informative, that provides a feasibility to evaluate more precisely the alloy hot brittleness.

Welding of specimens of the «fish-bone» sample was performed with a non-consumable electrode using approximately the same conditions that in

Table 2. Mechanical properties of parent metal after heat treatment using condition T8

Alloy	σ_t, *MPa*	σ_y, *MPa*	δ, *%*	α, *deg*
Al–6Zn–2Mg	489.5	443.1	9.3	42
Al–6Zn–2Mg–0.2Sc	496.6	469.7	10.4	56

butt welding of the joints. Tests were conducted on specimens without a filler wire and using three fillers: Al–5Mg, Al–5Mg–0.5Sc, Al–6Mg–0.45Sc.

Tests on Trans-Varestraint sample were conducted on 6 mm thick 150 × 150 mm specimens. The welding condition was as follows: I_w =320 A, v_w = 2.8 mm/s. Deformation level of weld metal was 1.2 % [5 – 7].

The results of testing the susceptibility of alloys to the hot cracking on «fish-bone» sample are given in Table 3.

In welding of parent metal specimens without a filler wire the long cracks are formed which are located in the weld centre. The introduction of 0.2 % scandium into the parent metal of alloy Al–6Zn–2Mg made it possible to reduce the susceptibility to the hot crack formation (*A*, %) from 53.9 to 16.0 %.

During welding of reference alloy with fillers of Al–Mg system with scandium and without it the cracks are formed in the fusion zone, their length is 2.8 and 7.4 %, respectively. Introduction of 0.2 % Sc into the parent metal when welding using Al–5Mg–0.5Sc wire prevented the formation of cracks in weld and in fusion zone. The use of the Al–6Mg–0.45Sc filler wire when welding alloys with and without scandium prevents the hot crack formation.

Minimum level of susceptibility to hot cracking in welding of alloy Al–6Zn–2Mg–0.2Sc using the filler wires Al–5Mg–0.5Sc or Al–6Mg–0.45Sc makes it possible to assume that application of scandium additions is effective in welding alloys which contain the higher amount of zinc and magnesium

Table 3. Results of testing the susceptibility of alloys of Al–Zn–Mg–(Sc) system to the hot crack formation using a «fish bone» sample*

Alloy	*Filler*	*Sc, %*	*A, %*	
			weld	*fusion zone*
Al–6Zn–2Mg	Without filler	0	53.9	0
	Al–5Mg	0	0	7.4
	Al–5Mg–0.5Sc	0.25	0	2.8
	Al–6Mg–0.45Sc	0.23	0	0
Al–6Zn–2Mg–0.2Sc	Without filler	0.20	16.0	0
	Al–5Mg–0.5Sc	0.35	0	0
	Al–6Mg–0.45Sc	0.33	0	0

*Averaged results of testing three specimens are given.

Table 4. Mechanical properties of welded joints of experimental alloys of Al–Zn–Mg–(Sc) system

Alloy	*Filler wire*	*Scandium content in weld metal, %*	σ_t^w, *MPa*	$\sigma_t^{w.m}$, *MPa*	α, *deg*
Al–6Zn–2Mg	Al–5Mg	0	336.9	$\frac{253.9 - 267.7}{260.8}$	$\frac{67 - 131}{90}$
	Al–5Mg–0.5Sc	0.25	349.3	$\frac{286.1 - 305.3}{293.4}$	$\frac{68 - 76}{72}$
	Al–6Mg–0.45Sc	0.23	364.8	$\frac{302.1 - 303.9}{303.0}$	$\frac{78 - 96}{87}$
Al–6Zn–2Mg–0.2Sc	Al–5Mg–0.5Sc	0.35	380.1	$\frac{313.8 - 318.3}{315.8}$	$\frac{63 - 86}{75}$
	Al–6Mg–0.45Sc	0.33	381.1	$\frac{308.4 - 330.2}{314.6}$	$\frac{57 - 63}{60}$

Note. In numerator the minimum and maximum values are given, in denominator the averaged results of testing three specimens are given.

and, consequently, possess higher characteristics of strength.

Tests on Trans-Varestraint sample were conducted only in welding parent metal without using a filler wire. Results were evaluated visually by measuring a total length of the cracks. With introduction of 0.2 % Sc into the alloy their length was decreased from 31 to 23 mm (Figure).

Results of testing the mechanical properties of welded joints are given in Table 4. The strength of weld metal in welding alloy Al–6Zn–2Mg using the filler wire Al–5Mg was about 261 MPa, angle of bending was 90°. The application of the Al–5Mg–0.5Sc filler with a scandium led to the increase in strength to 293 MPa, the angle of bending was decreased to 72°. The application of Al–6Mg–0.45Sc wire in welding provided the weld metal strength above 300 MPa, the angle of bending was not almost changed.

Introduction of 0.2 % Sc into the parent metal and using Al–5Mg–0.5Sc and Al–6Mg–0.45Sc filler wires during welding provided the weld metal strength at the level of 315 MPa, angle of bending was varied from 60 to 75°.

As the specimens fractured in HAZ, then the strength of the parent metal with 0.2 % Sc addition could increase the strength of the welded joint by 7 – 8 % on average.

The test results showed that the scandium addition into the parent metal and filler wire promotes the increase in strength characteristics of the welded joint. Moreover, at increase of scandium content in weld metal from 0.20 to 0.35 % leads to the growth in strength of the weld metal. In this connection, to provide the necessary scandium content in weld during welding alloys, not containing scandium, it is rational to use the wire which contains 0.5 % scandium.

Thus, the high effectiveness of using scandium in the parent metal of Al–Zn–Mg system alloys and in Al–Mg filler wires which are used in welding alloys of this series is confirmed.

CONCLUSIONS

1. Introduction of scandium into the parent metal makes it possible to decrease the susceptibility to the hot cracking during welding by 3 times.

2. Combined alloying of the parent metal and filler wires with scandium almost prevents the hot crack formation and provides the increase in weld metal strength during welding by 20 %

REFERENCES

1. Davydov, V.G., Elagin, V.I., Zakharov, V.V. *et al.* (1996) About alloying of aluminium alloys with additions of scandium and zirconium. *Metallovedeniye i Term. Obr. Metallov*, **8**, 25 – 30.
2. Ishchenko, A.Ya., Labur, T.M. (1998) Weldable aluminium alloys with scandium. *Avtomaticheskaya Svarka*, **8**, 3 – 6.
3. Khan, G.M., Nikiforov, A.O., Zakharov, V.V. *et al.* (1993) Effect of scandium content on structure and characteristics of superplasticity of aluminium alloys of Al–Zn–Mg–Sc–Zr system. *Tsvetnye Metally*, **11**, 55 – 58.
4. Elagin, V.I., Zakharov, V.V., Drits, A.M. (1982) *Structure and properties of alloys of Al–Zn–Mg system*. Moscow: Metallurgia.
5. Rabkin, D.M. (1986) *Metallurgy of fusion welding of aluminium and its alloys*. Kyiv: Naukova Dumka.
6. Gavrilin, S.V. (1997) Methods of determination of resistance of aluminium alloys to hot cracking. *Avtomaticheskay Svarka*, **8**, 9 – 14.
7. Seda, T., Matsuda, F., Takano, G. (1972) Studies on solidification crack susceptibility for weld metals with Trans-Varestraint test. *Transact. of JWS*, **6**, 113 – 127.

PECULIARITIES OF DIFFUSION BONDING OF MAGNETIC SYSTEM PARTS

T.G. TARANOVA and **G.M. GRIGORENKO**
The E.O. Paton Electric Welding Institute, NASU, Kyiv, Ukraine

ABSTRACT

Diffusion bonding used for the manufacture of hyroscopic devices provides the guaranteed quality of the bonds in magnetically soft materials with high mechanical and magnetic properties, causing no changes in their initial electrophysical characteristics. Optimal parameters of the process, involving thermal cycling that allows structure and properties of the formed bonds to be controlled, are given.

Key words: *diffusion bonding, hyroscopic devices, magnetic materials, permalloys, bonds, common grains*

To ensure control of modern flying vehicles it is necessary to manufacture high-precision and reliable navigation equipment, including gyroscopic devices.

At the final stage of the manufacture of magnetic systems, instruments, automation and computation facilities, where there is no possibility to conduct restoration annealing [1 – 3], no stresses, whatever insignificant they are, are permitted in magnetic elements of magnetically soft materials. Magnetic characteristics of these materials are deteriorated in heating to a temperature above the Curie point. For example, a dramatic decrease in magnetic saturation occurs in the case of permalloy 50N. Because there is no way of heating such alloys, is it extremely difficult to achieve a tight contact between the mating surfaces.

Besides, in a magnetic system even minor discontinuities or remains of oxide films in the joining region add to resistance to the magnetic flux, which causes losses of the effective magnetomotive force.

Therefore, the technology for joining magnetic materials should meet the following requirements:

1. Temperature of the process of formation of a joint should not be in excess of that of the beginning of changes in magnetic properties of the materials joined.
2. Macroscopic plastic deformation of parts of magnetically soft materials should be kept at minimum.
3. Defects in the joining zone (discontinuities, pores, cavities, contaminants, etc.), which increase resistance to the magnetic flux, are not permitted.

The brazing technology commercially used for such purposes has substantial drawbacks, as in a number of cases it involves heating of materials to a temperature above the Curie point. Besides, a brazing filler metal used in the process tends to flow over the mating surfaces, and this makes it necessary to subject the brazed joint afterwards to machining, which leads, among other things, to unstable readings of devices and insufficient strength of the joints [4].

In this connection, the use of diffusion bonding is indicated, as it provides quality bonds in magnetic materials without deterioration in their initial characteristics. Diffusion bonding enables a decrease in temperature of the process, elimination of formation of chemical heterogeneity within the bond zone, restriction of plastic deformation of the

Compositions of reagents and parameters of etching of the sections

No. of reagent	*Sample materials*	*Composition of reagent*	*Electropolishing and etching parameters*
1	NP-2, 79NM, 50N	60 % H_3PO_4, 20 % H_2SO_4, 5 – 7 % CrO_3, 13 – 15 % H_2O	U_{el} = 75 V, t_{el} = 5 – 10 s
2	79NM, 50N	50 cm^3 of each of HNO_3 and CH_3COOH	t_{el} = 2 – 3 min
3	NP-2	20 % solution of $(NH_4)_2SO_4$ with addition of a few drops of N_2SO_4	U_{et} = 10 – 12 V, t_{et} = 5 – 10 s

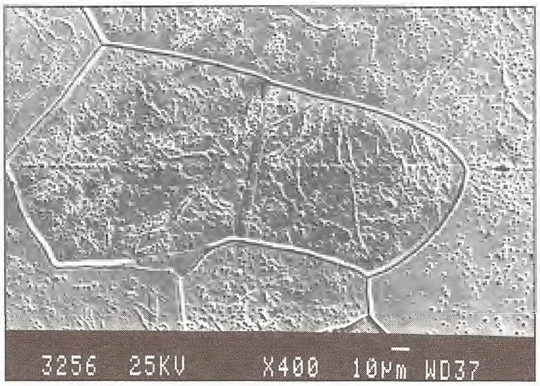

Figure 1. Microstructure of the diffusion bond in nickel NP-2 made at $T = 900$ °C, $t = 30$ min and $P = 20$ MPa (reduced by 2/3)

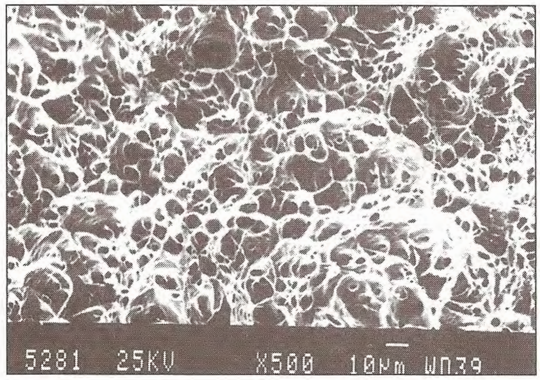

Figure 2. Fractogram of fracture of the diffusion bond in nickel NP-2 made at $T = 1000$ °C, $t = 30$ min and $P = 15$ MPa (reduced by 2/3)

parts joined and thus maintenance of their initial magnetic properties and geometry [5, 6].

The purpose of the work described in this article was to develop the technology for diffusion bonding of parts of magnetic materials that would provide a minimum plastic deformation within the contact zone.

Magnetically soft alloys 50N and 79NM (belonging to a group of permalloys), and nickel of the commercial grade NP-2 (in the form of rolled and annealed rods with a diameter of 20 mm) were used as materials for the investigations. Nickel NP-2 was chosen for the investigations as the model material because it forms only one oxide (NiO), undergoes no phase transformations and is part of the composition of magnetically soft materials. In addition, its physical-technological properties are well studied, as it is widely applied in industry as a structural material. Diffusion bonding was performed on combinations of samples of similar materials, which made it possible to analyse the most favourable conditions of formation of a physical contact, activation and adhesion of the mating surfaces, as well as migration of the interface. The bonding experiments were conducted on samples 12 mm in diameter within a temperature range of $T = 673 - 1323$ K and a bonding pressure of $P = 5 - 25$ MPa in vacuum. The time of bonding ranged from 5 to 60 min.

The metallography sections were cut out from the bonds normal to the bonding direction. They were made successively in several stages (Table): to reveal microstructure the sections were first subjected to electropolishing in reagent No. 1 and then to chemical etching in reagent No. 2 for NP-2 and in reagent No. 2 — for magnetically soft materials.

Metallography was done using the «Union» (Japan) device «Versamet-2». Fractography of fractures in the bonds was done using the «JEOL» (Japan) scanning electron microscope JSM-840 equipped with the «Link Analitic» and «Optek» microanalysers. The investigations were conducted in the secondary electrons mode at an accelerating voltage of $U = 20$ kV and electron beam current of $10^{-10} - 10^{-7}$ A.

Diffusion bonding of the model samples of NP-2 performed using the above parameters allowed the most favourable conditions of the process of formation of a physical contact, localization of plastic deformation in the contact zone, formation of common grains and migration of their boundaries to be analysed and predicted. Results of metallography of the samples show that within the bond zone a high-angle interface oriented in the plane of contact migrates during the bonding process, primarily by growth of grains. The contact zone is characterized by an intensive formation of common grains, which occurs by the mechanism of collective recrystallization. In this case impact toughness of the bond metal is at a level of that of the base metal [7].

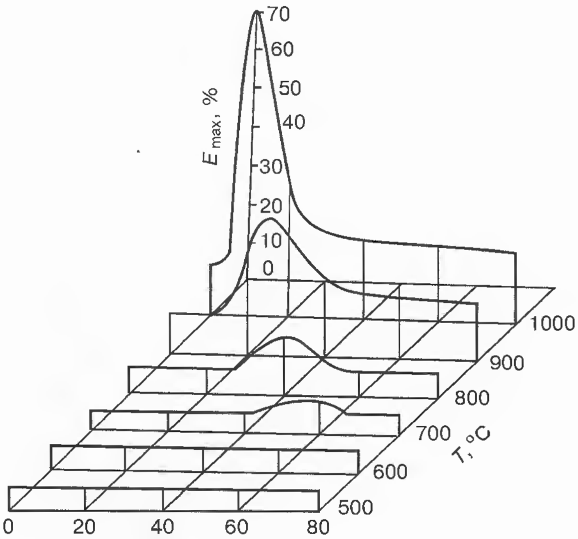

Figure 3. Maximum plastic deformation in the bond zone vs. pressure and temperature (nickel NP-2, $t = 30$ min)

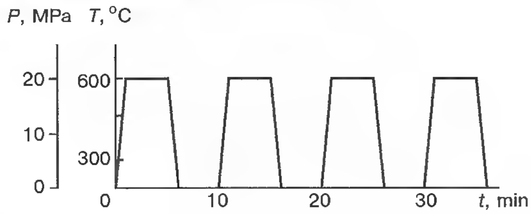

Figure 4. Variations in pressure and temperature during the thermal cycling process

This structure has no defects in the form of narrow and long discontinuities (type 1), while in the contact plane the defects detected are less than 0.1 μm in size and have the form of individual fine pores (type 2). Chains of etching pits are also detected. They are points of escape of individual dislocations, which persisted at their initial locations after migration of the interface (Figure 1).

It should be noted that whereas as a result of contact plastic deformation the defects of type 1 decrease to critical sizes, the defects of type 2 are removed owing to the diffusion processes.

Fractography of fractures of the model samples shows that their structure becomes of a purely tough character over the entire contact surface, which is indicative of high mechanical properties of the bonds (Figure 2).

It follows from extrapolation of curves of the pressure dependence of maximum plastic deformation E_{max} [7] (Figure 3) that bonding of parts of magnetically soft materials can be performed at a temperature of 500 – 600 °C. Therefore, the minimum permissible temperatures of bonding for permalloys should be within the above range. In this case it should be taken into account that formation of a physical contact at extreme values of the diffusion bonding parameters (pressure, temperature and time) is difficult and requires extra technological arrangements. Thus, the use of electropolishing of surfaces provide a maximum possible physical contact and led to retention of magnetic properties of the materials. The bonding time was additionally increased, as the diffusion processes were insufficiently activated at low temperatures and pressures [8].

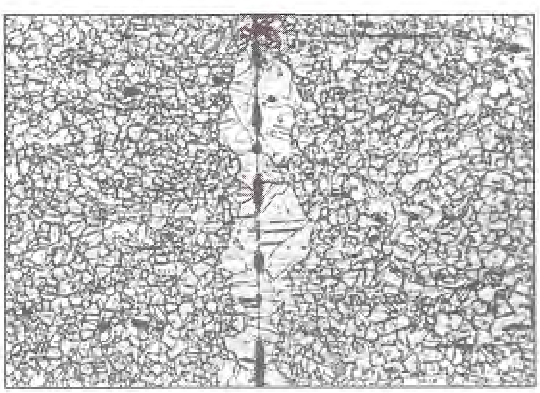

Figure 5. Microstructure of the bond in permalloy 50N (×100) (reduced by 2/3)

One of the methods leading to intensification of plastic deformation in the contact zone, which favours formation of a strong bond free from defects of both type 1 and type 2, and formation of a controllable amount of common grains in the bond zone, is thermal cycling. This method makes it possible to preset the value of deformation, constant or varying within a wide range.

Thermal cycling leads to a more intensive development of processes of formation of a physical contact, «healing» of discontinuities and migration of the plane-oriented interface of the bond [9, 10]. The method of thermal cycling of permalloys is schematically shown in Figure 4.

Figure 5 shows microstructure of the bond in permalloy 50N made by diffusion bonding at T = = 600 °C, P = 20 MPa and t = 1 h, involving thermal cycling. Under the above conditions the process of formation of the bond is identical to that in the model material. Common grains appear in the bond zone as early as in 5 min. Further increase in the process time leads to an insignificant growth of the physical contact surface area.

Therefore, the collective recrystallization was found to occur in the bond zone. At the same time, the interface migrates over the entire interaction area. Strength of the bond in materials used for the manufacture of gyroscopic devices meets the requirements.

CONCLUSIONS

1. The investigations conducted made it possible to work out technological recommendations and substantiate selection of parameters for diffusion bonding of gyroscopic devices of permalloy 50N and 79NM. The optimal parameters of diffusion bonding for permalloys are as follows: T = 500 – 600 °C, P = 20 MPa and t = 1 h. Combined with electropolishing used as the surface preparation method, these parameters provide the guaranteed quality of the bond with high mechanical and magnetic properties and with no change in the initial electrophysical characteristics.

2. The use of thermal cycling allows bonding to be performed by cyclically changing the deformation rate at stresses not in excess of yield strength of the materials joined. This makes it possible to control the process of formation of the bond, its structure and properties.

3. The use of diffusion bonding for the manufacture of parts of magnetic materials (sensors of accelerometers) enables avoidance of labour-con-

suming milling operations and provides saving of about 45 % of expensive permalloy.

REFERENCES

1. Pelpor, D.S., Yagodkin, V.V. (1977) *Gyroscopic systems*. Moscow: Vysshaya Shkola.
2. Fevraleva, N.E. (1969) *Magnetic materials and permanent magnets*. Kyiv: Naukova Dumka.
3. Gavrilov, A.N., Chizhikov, V.F. (1974) *Technology of magnetic elements for devices and means of automation and computer facilities*. Moscow: Energia.
4. Khulkov, V.A. (1966) *Machining of parts of magnetic materials in instrument making*. Moscow: Mashinostroyeniye.
5. Kazakov, N.F., Mashkova, N.A., Gerberg, A.H. (1967) Diffusion bonding of magnetic alloys in vacuum. *Svarochnoye Proizvodstvo*, **12**, 21 – 29.
6. Kazakov, N.F., Shishkova, A.P., Mashkova, N.A. (1971) On the problem of creation of precision joints by the method of diffusion bonding in vacuum. In: *Diffusion bonding in vacuum*. Moscow: Mashinostroyeniye.
7. Taranova, T.G., Grigorenko, G.M., Tayanovskaya, A.V. *et al.* (1993) Deformation processes in the contact zone during diffusion bonding of nickel. *Avtomaticheskaya Svarka*, **1**, 17 – 20.
8. Karakozov, E.S., Kotelkin, A.S., Matveev, G.M. *et al.* (1968) On the kinetics of formation of a bond in solid-state joining of similar materials. *Fizika i Khimiya Obr. Materialov*, **3**, 113 – 122.
9. Karakozov, E.S. (1986) *Pressure joining of metals*. Moscow: Mashinostroyeniye.
10. Abramov, V.V., Karakozov, E.S., Petrov, B.A. (1970) Kinetics of formation of a bond in solid-state joining by static and cyclic loading with preheating. *Fizika i Khimiya Obr. Materialov*, **4**, 104 – 117.

EFFECT OF WELDING PARAMETERS ON THE RATE OF HEATING OF THE WELD ZONE METAL

A.M. SAVITSKY, M.M. SAVITSKY and **D.A. DUDKO**
The E.O.Paton Electric Welding Institute, NASU, Kyiv, Ukraine

ABSTRACT

Peculiarities of implementation of high-rate heating in arc welding are considered. The use of the N.N. Rykalin's numerical methods made it possible to prove the possibility of achieving high heating rates (1000 °C/s and higher) in arc welding, and analyse peculiarities of the effect of welding parameters on the rate of heating of a welded joint. The heating rate was found to be in inverse relationship with the welding heat input.

Key words: *arc welding, heating rate, thermal power of the arc, welding heat input, thermochemical activation of the arc, activator*

Results of investigations described in [1 – 3] are indicative of the positive effect of high heating rates on the kinetics of structurization of welded joints. High-rate heating initiates shifting of points A_{c1} and A_{c3} to the region of higher (as compared with isothermal conditions) temperatures. Depending upon the heating rate and chemical composition of steel, temperature A_{c3} can increase by 150 – 300 °C [1, 3]. This results in a dramatic decrease in the time during which the welded joint metal dwells in a high-temperature region of the intensive growth of secondary austenite grain and homogenization of austenite [1]. This leads to a decrease in stability of austenite in overcooling and shift of its decomposition to the region of higher temperatures, close to the diffusion one [1 – 4], which shows up even in the case of high-carbon steels [2, 3].

To achieve such changes in the kinetics of structurization of welded joints, it is necessary to provide high heating rates (above 1000 °C/s), which seems to be a problem in arc welding.

The purpose of this work was to estimate the capability of the welding arc of initiating high (above 1000 °C/s) heating rates in the overheated region of the HAZ metal, and identify the welding parameters having a decisive effect on the rate of heating of a welded joint.

The capability of the welding arc of initiating high-rate heating can be estimated by calculations using the N.N. Rykalin's numerical methods [5]. The rate of cooling of a welded joint is known to be in an inverse relationship with the welding heat input (q/v_w). Therefore, it is apparent that the heating rate also depends upon this parameter. To prove this assumption, calculations were made to estimate the temperature field in the limiting state, using methods of a high-power fast-moving spot heat source on the surface of a semi-infinite body, and a high-power fast-moving linear heat source [5] for a plate of steel 40KhN (C — 0.4; Cr — 1.0 wt.%).

The welding heat input is determined by the ratio of thermal power of the arc, q, to welding speed v_w. Therefore, to identify principles of the effect of each of the parameters on the heating rate, the calculations were made in two stages. At the first stage the welding speed was varied and the q value was kept constant, whereas at the second stage, vice versa, the thermal power of the arc was varied and the welding speed was kept constant. In both cases the calculations were made for a case of automatic gas-shielded welding, which was allowed for by a corresponding value of the arc efficiency. The temperature of 1390 °C (temperature in the overheated region of the HAZ) was assumed to be a limiting temperature. Initial data for the calculations are given in Tables 1 and 2.

Welded joint heating and cooling conditions are determined by the character of the welding thermal cycle. Therefore, results of the calculations are given in the form of curves of the welding thermal cycle at points with a limiting temperature of 1390 °C.

As shown by these curves calculated by the method of a high-power fast-moving spot heat source (Figure 1, *a*), the character of the effect of the welding speed on the heating rate is determined by a direct proportional relationship. The higher the welding speed (at a constant thermal power of the arc), the higher the rate of heating of a welded joint. Data of Table 1, which gives the mean values of the rate of heating up to a maximum temperature, show that at a constant thermal power of the arc equal to

$$q = UI\eta = 340 \cdot 32 \cdot 0.75 = 8160 \text{ W}$$

and a welding speed of 10 m/h the time of heating to the maximum temperature is 3.34 s. In this case the heating rate is 421 °C/s. An increase in the welding speed to 30 m/h is accompanied by reduction of the time of heating to the maximum temperature to 1.09 s. In this case the heating rate increases to 1263 °C/s. Further increase in the welding speed to 45 m/h reduces the time to achieving the maximum temperature to 0.72 s and increases the heating rate to 1925 °C/s. At a welding speed of 60 m/h the time needed to reach the maximum temperature is reduced to 0.54 s and the heating rate is increased to 2574 °C/s.

The thermal cycle curves shown in Figure 2, *a*, describing the effect of the thermal power of the arc on the heating rate at a constant welding speed (the calculations are made by the method of the high-power fast-moving spot heat source), prove that in this case the dependence is inversely proportional. A decrease in the thermal power of the arc leads to an increase in the heating rate.

Values of the time of heating to a maximum temperature for each welding thermal cycle are given in Table 2. These data indicate that at a welding speed of 15 m/h and arc thermal power of 13500 W, the time needed to reach the maximum temperature is 3.56 s. In this case the heating rate is 390 °C/s. A decrease in the thermal power of the arc to 6750 W is accompanied by a decrease in the time needed to reach the maximum temperature to 1.78 s and increase in the heating rate to 781 °C/s. Further decrease in the thermal power of the arc to 2250 W reduces the time of heating to 0.6 s. In this case the heating rate is increased to 2316 °C/s.

Similar results were obtained also in the calculations by the method of a high-power fast-moving linear heat source in a infinite plate 10 mm thick, which is proved by the thermal cycle curves shown in Figures 1, *b*, and 2, *b*, and data given in Tables 1 and 2. In this case the investigations also showed an increase in the heating rates in the HAZ metal with an increase in the welding speed or decrease in the thermal power of the arc.

The thermal power of the arc and the welding speed are the parameters which determine the welding heat input. Any change in their values leading to a decrease in the welding heat input is accompanied by an increase in the heating rate. The calculations show that in arc welding it is possible to achieve heating rates of 1000 °C/s and higher, at which the substantial changes in structurization were detected to take place in a welded joint [1, 3, 4]. Results of quantitative estimation of the capacity of the welding arc to initiate a high-rate heating were proved experimentally. Figure 3 (curves *1* and *2*) shows the welding thermal cycles obtained by calculations and experimentally, using

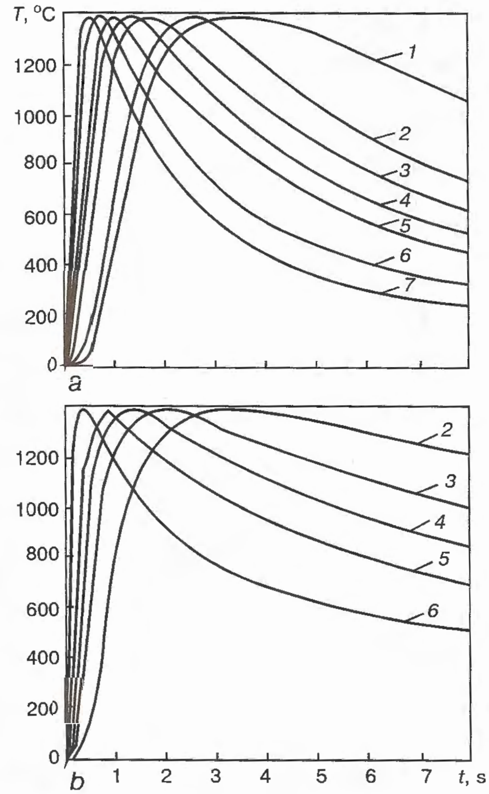

Figure 1. Influence of welding speed on conditions of heating of a welded joint at constant thermal power of the arc, q = 8160 W; calculation methods — high-power fast-moving spot (*a*) and linear (*b*) heat sources: *1* — v_w = 10; *2* — 15; *3* — 20; *4* — 25; *5* — 30; *6* — 45; *7* — 60 m/h

the above method of a fast-moving spot heat source for the given steel at a heat input of q/v_w = 2670 J/cm, which corresponds to the following welding parameters: I = 300 A, U = 30 V, v_w = 91 m/h and η = 0.75.

Table 1. Influence of welding speed on heating rate of a welded joint

v_w, m/h (cm/s)	q/v_w, J/cm	t, s	v_h, °C/s
	Spot heat source		
10 (0.27)	30222	3.34	421
15 (0.42)	19428	2.50	556
20 (0.56)	14571	1.61	863
25 (0.69)	11757	1.30	1069
30 (0.83)	9831	1.09	1263
45 (1.25)	6528	0.72	1925
60 (1.67)	4886	0.54	2574
	Linear heat source		
15 (0.42)	19428	3.41	407
20 (0.56)	14571	1.92	724
25 (0.69)	11757	1.26	1103
30 (0.83)	9831	0.87	1598
45 (1.25)	6528	0.39	3564

Note: Here T_{max} = 1390 °C, q = 8160 W.

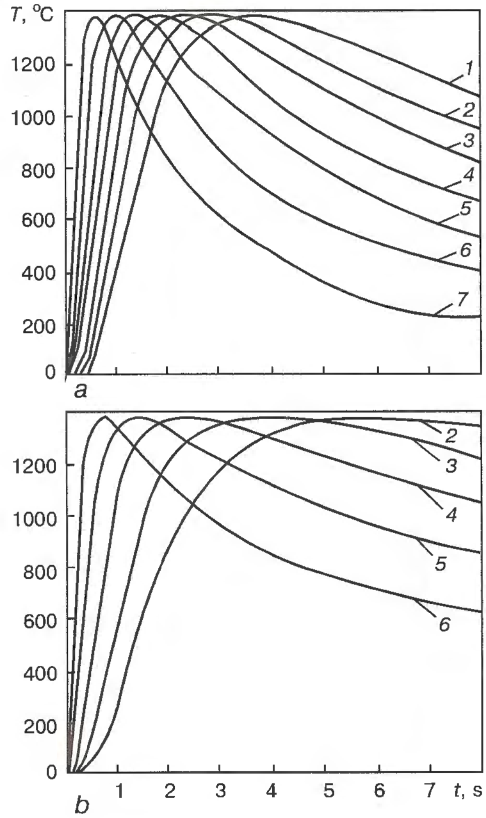

Figure 2. Influence of thermal power of the arc on conditions of heating of a welded joint at constant welding speed v_w = = 15 m/h; calculations methods — high-power fast-moving spot (*a*) and linear (*b*) heat sources: *1* — q = 13500; *2* — 10800; *3* — 8662; *4* — 6750; *5* — 5602; *6* — 3601; *7* — 2250 W

As it follows from the above data, the heating rate at the given value of the welding heat input is more than 3000 °C/s. Differences between the experimental and calculated welding thermal cy-

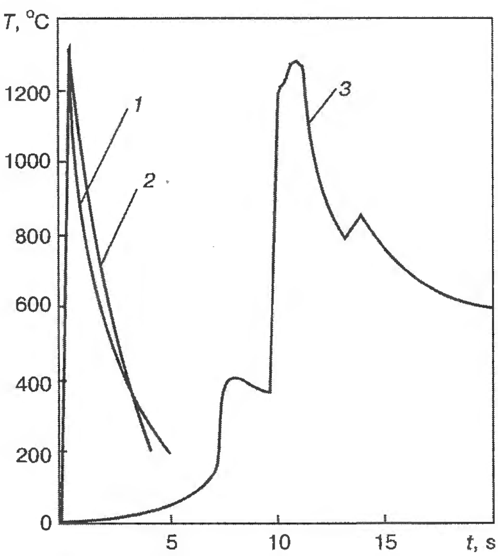

Figure 3. Welding thermal cycles: *1* — calculated; *2* — experimental; *3* — experimental (complex, with delayed cooling)

Table 2. Influence of effective thermal power of the arc on heating rate of a welded joint

I_w, A	U, V	q, W	q/v_w, J/cm	t_h, s	v_h, °C/s
Spot heat source					
450	40	13500	32143	3.56	390
400	36	10800	25714	3.00	463
350	33	8662	20625	2.20	632
300	30	6750	16071	1.78	781
250	27	5062	12053	1.33	1045
200	24	3601	8571	0.95	1467
150	20	2250	5357	0.60	2316
Linear heat source					
400	36	10800	25714	5.98	232
350	33	8662	20625	3.84	362
300	30	6750	16071	2.33	597
250	27	5062	12053	1.31	1058
200	24	3601	8571	0.66	2106

Note: Here T_{max} = 1390 °C, v_w = 15 m/h and η = 0.75.

cles are insignificant and can be seen only at the cooling branch of the curve.

Figure 3 (curve *3*) also shows a complex welding thermal cycle with a delayed cooling, demonstrating a heating rate of above 3000 °C/s. This thermal cycle, obtained experimentally for q/v_w = = 3204 J/cm, corresponds to the following welding parameters: I = 300 A, U = 36 V, v_w = 91 m/h and η = 0.75. Welding and deposition were performed using wire of the Sv-08G2S (C — 0.08; Si — 0.8; Mn — 2.0 wt.%) grade in a shielding gas mixture of 85 % Ar + 15 % CO_2 in an automatic mode. The base material was steel 40KhN with a thickness of not less than 50 mm.

However, the increase in the heating rates to 1000 °C/s and higher is possible only at comparatively low values of the welding heat input (not more than 11000 – 12000 J/cm). This corresponds to the following welding parameters: I = 250 A, U = 27 V, v_w = 15 m/h and η = 0.7.

Therefore, in the case of using traditional approaches the necessity of improving the quality of the welded joints in quenching steels involves difficulties associated with maintaining high productivity of welding. This requires a change from the principle of raising productivity of welding by increasing the deposition efficiency to the principle based on increasing the penetration depth.

One of the methods for raising productivity of welding is thermochemical activation of the arc. Implementation of this process in tungsten-electrode argon-arc welding allowed a not less than 2 – 4 times increase in the penetration depth without an increase in the welding current. At present the similar process is available also for metal-electrode welding.

Addition of special electronegative activating elements to the arc burning zone enables achievement of different degrees of de-ionization of peripheral regions of the arc column. This makes it possible to limit sizes of a current-conducting plasma channel (contraction of the arc). In turn, the arc contraction is accompanied by an increase in the current density in the arc, concentration of heating and rise in the gas-dynamic pressure of the arc on the weld pool. As a result, the penetration depth is increased more than twice without any increase in the welding current. The ratio of an increase in the penetration depth depends upon such factors as chemical composition of an activator, method of its introduction to the arc burning zone and diameter of the electrode wire.

Comparing the capabilities of metal electrode welding using the thermochemically activated arc with CO_2 welding proved the former to be obviously advantageous.

To perform single-pass welding of the steel VSt.3sp (C — 0.2; Si — 0.25; Mn — 0.6 wt.%) samples 10 mm thick with complete penetration by the CO_2 method using the 1.6 mm dia. electrode, it is necessary to use the following pro-cess parameters: $I = 550$ A, $U = 40 - 42$ V and $v_w = 25$ m/h. In this case the welding heat input is not less than 24948 J/cm.

The use of the activator applied to the surface to be welded and ensuring the not less than two-fold increase in the penetration depth makes it possible to achieve penetration to 10 mm in a single pass at $I = 400$ A, $U = 34$ V and $v_w = 40$ m/h. The welding heat input in this case decreases (as compared with CO_2 welding) by a factor of not less than 2.5 and is 9180 J/cm.

If we compare these results with the data of Tables 1 and 2, we can see that in CO_2 welding the heating rate is within a range of 200 to 300 °C/s, while in welding using the activator it exceeds 1500 °C/s, i.e. an increase in the heating rate in gas-shielded arc welding to 1000 °C and higher is not accompanied by any substantial decrease in productivity of welding.

CONCLUSIONS

1. In gas-shielded arc welding the possibility exists of achieving the rates of heating of welded joints in excess of 1000 °C/s.

2. As any change in the welding heat input is accompanied by an inversely proportional change in the heating rate, with the conventional welding methods it is difficult to combine the high heating rate and welding productivity.

3. Thermochemical activation of the arc enables an increase in its penetrating power at decreased currents, and makes it possible to achieve high heating rates by maintaining high productivity of welding.

REFERENCES

1. Shorshorov, M.Kh., Belov, V.V. (1972) *Phase transformations and variations in properties of steel during welding*. Moscow: Nauka.
2. Gridnev, V.N., Meshkov, Yu.Ya., Oshkaderov, S.P. *et al.* (1973) *Physical principles of electrothermal strengthening of steel*. Kyiv: Naukova Dumka.
3. Dudko, D.A., Savitsky, A.M., Vasiliev, V.G. *et al.* (1996) Peculiarities of structure and properties of welded joints in steels with an increased carbon content of welded joints formed by thermal cycling. *Avtomaticheskaya Svarka*, **2**, 6 – 10.
4. Shorshorov, M.Kh., Smirnov, B.A. (1960) Kinetics of growth of austenite grain in increased-strength steels during arc welding. *Ibid.*, **5**, 17 – 20.
5. Rykalin, N.N., Pugin, A.I. (1959) *Thermal processes in fusion welding*. Moscow: Profizdat.

WELDED JOINT FORMATION IN EXPLOSION WELDING OF METALS

S.V. KUZMIN, V.I. LYSAK, E.A. CHUGUNOV and **A.P. PEEV**
Volgograd State Technical University, Volgograd, Russia

ABSTRACT

Investigations into characteristic ranges of collision of metal plates in the kinematic coordinates resulted in proving of existence, phenomenological description and quantitative determination of boundaries of the ranges of explosion welding for a case of formation of the wave-free interface and development of abnormal waves in the weld zone. It is shown that a change in the mechanism of formation of a welded joint with variation of parameters of a high-velocity collision has a substantial effect on the character of distribution of maximum shears in the weld zone metal.

Key words: *waveless welding mode, explosion welding, wave formation, angle of collision, plastic deformation, welded joints*

In metals welding by explosion, the welded joint forms due to high-velocity joint plastic deformation of shear in the near-contact layers of the materials being welded, which is most often manifested in the form of regular waves in the joint zone or of a waveless flow. The latter is found in welding of dissimilar metals for the following modes:

• near the lower limit of weldability the modes are characterised by the low energy input and are insufficient for formation and development of the wave profile on the layer interface [1];

• with small values of the velocity of the point of contact v_c when the waves do not form [2, 3].

In the latter case, various researchers explain the process of wave disappearance in the joint zone

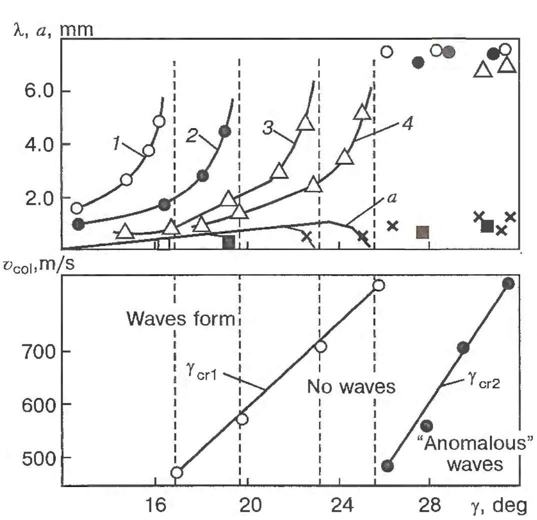

Figure 1. Influence of the parameters of collision of aluminium plates on the nature of wave formation process at v_{col}: 460 (*1*); 540 (*2*); 715 (*3*); 830 m/s (*4*)

[4, 5] either by the existence at small v_c of anomalous back mass flows with the velocity essentially lower than that of the cumulative jet (calculated by the hydrodynamic theory), or existence of a certain critical angle of collision γ_{cr} [2, 3, 6] for various pairs of the metals being welded, which, when exceeded, prevents wave formation.

This study was aimed at investigation of the conditions of joint formation in explosion welding and study of the main laws of plastic deformation of the metal in the HAZ.

The most convenient form of description and analysis of the external features of the process of explosion welding of metals, is its representation in kinematic co-ordinates of collision angle γ – velocity of the point of contact v_c [7]. They are usually used to determine the welding region, limited, on the one hand, by the critical and limit boundaries and, on the other, by the areas of the supersonic and waveless collision modes, that have by far not yet been completely studied or fundamentally described. A detailed and systematic study of the left part of γ – v_c plane revealed a number of still unknown anomalous phenomena here.

Bimetal samples (aluminium AD1 + aluminium AD1, aluminium AD1 + aluminium alloy AMg6, steel St.3 + steel St.3) of various thickness, were used for investigations. They were welded with variation of the angle of collision γ within 10 – 40°, as well as the velocities of the point of contact v_c and collision v_{col} in the ranges of 500 – 3200 and 300 – 1100 m/s, respectively, controlled by the rheostat and electric contact procedures [8, 9]. Metallographic investigations and mechanical tests of samples showed that the dynamic angle of collision γ (Figure 1) largely determines the parameters of the waves, forming in the joint zone, this being in agreement with the data of [2, 10]. Also, γ has greater influence on wave length λ, which grows continuously with its increase up to $\lambda = \lambda_{cr1}$. In the latter case λ, tending to infinity, is responsible for absence of wave formation in the welded joint. Wave range a increases less intensively with γ increase up to a certain value, somewhat smaller γ_{cr1}, and goes to zero at $\gamma = \gamma_{cr1}$ (Figure 1). Similar changes in λ and a are found for St.3 + St.3 pair. However, absence of wave formation at the same values of v_{col} is found at greater values of γ, this being, apparently, related to increase of welded materials strength.

At the values of the collision angle above the critical value ($\gamma > \gamma_{cr1}$), its further increase leads to a somewhat unexpected result, not found earlier by other researchers. With a certain value of γ_{cr2}, waves of an unusual elongated shape (λ = 7 – 8 mm) are again observed in the joint zone, with preservation of the wave range, found prior to the absence of wave formation (a = 0.8 – 1.2 mm).

The critical angle of collision γ_{cr1}, responsible for the transition to the waveless welding mode, mainly depends on the collision velocity v_{col}. So, in explosion welding of aluminium plates with v_{col} = 460 m/s, γ_{cr1} = 17°, while with v_{col} increase up to 830 m/s, its value rises up to 26°. The graph of $\gamma_{cr1} = f(v_{col})$ function plotted by experimental data for the case of explosion welding of aluminium plates, is shown in Figure 1. Angle γ_{cr2} at which the joint zone again shows the secondary or «anomalous» waves, also depends on v_{col} (Figure 1). However, the slope of straight line $\gamma_{cr2} = f(v_{col})$ to the abscissa axis is smaller, than that of $\gamma_{cr1} = f(v_{col})$ curve, which results in the waveless mode range becoming narrower with the increase of v_{col}.

The area of formation of waveless joints is more readily demonstrated in the traditional plane of co-ordinates γ — v_c, in which at least 5 characteristic areas can be singled out, depending on the weld profile (Figure 2). They differ from each other not only by the produced profile of welded joints, but also by the nature of plastic flow of the metal in the HAZ, evaluated by the maximal shear deformation g_{max} [11] at different distances from the joint line.

The area of the «traditional» wave modes of explosion welding (*1* in Figure 2; 3, *a*) is defined, on the one hand, by the position of the lower limit (LL) of welding, below which the welded joint tear strength is lower, than that of the base metal, while their ratio — relative strength of the joint $\sigma \leq 1$. There are no waves in this joint zone, because of insufficient energy input (*5* in Figure 2). From the side of greater values of v_c, area *1* borders with

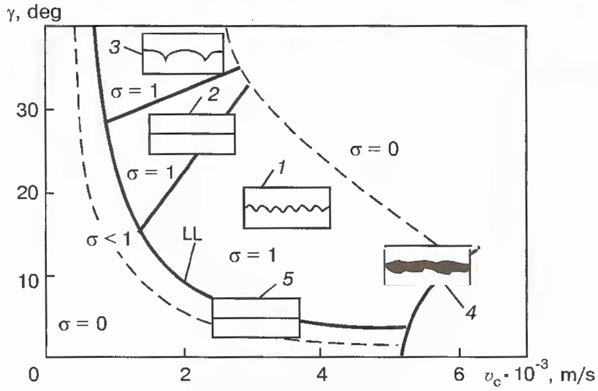

Figure 2. Location of characteristic areas (*1* – *5*) in explosion welding of aluminium plates

area *4*, within which a continuous interlayer of the melt forms along the joint line, and on the third side — with area *2* of low-intensity waveless modes. The latter is characterised by the absence in the welded joint zone of waves, molten metal inclusions or other defects (Figure 3, *b*), despite a considerable variation of the specific energy of plastic deformation under the experimental conditions.

The joint strength within this area, is on the level of that of the base metal, which is of great practical importance in welding of pipes and rods by a cylindrical schematic, when the internal element has a conical surface, in explosion spot welding, etc.

Within area *3* (Figure 2) strong joints are produced with formation of «anomalous» waves of elongated non-sinusoidal shape on the interface of the materials being welded (Figure 3, *c*). The appearance of such waves, apparently, is the result of the changing geometry of collision of the plates being welded. Qualitatively, the mechanism of such waves formation can be explained by analysing the kinetics of alternative interaction of the colliding surfaces for the cases of explosion welding in the «traditional» and the low-intensity modes (Figure 4). So, if the conditional angle between the vector of the velocity of the «deformation hump» top and the surface of the stationary plate φ exceeds

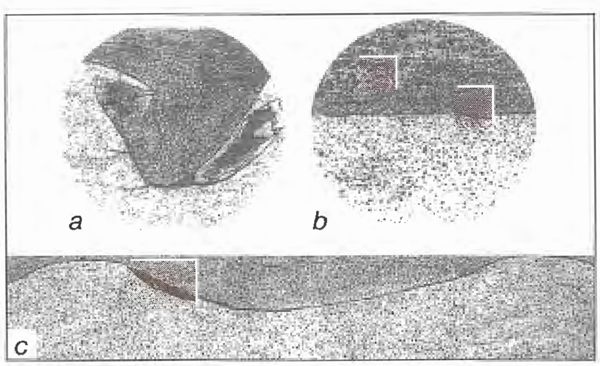

Figure 3. Structures of characteristic areas (*a* – *c* — areas *1* – *3* in Figure 2) of AMg6 + aluminium welded joints (AMg6 on top)

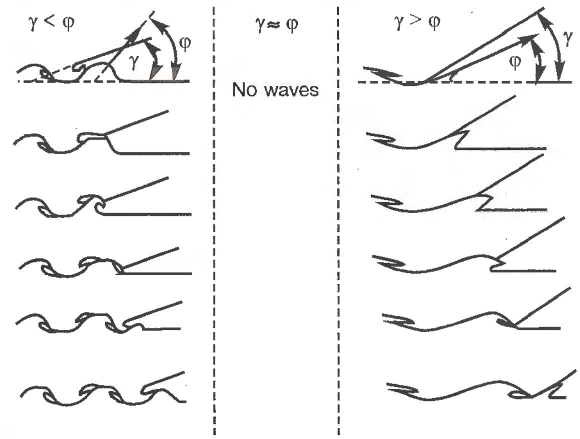

Figure 4. Kinematics and phenomenological nature of macroplastic flow of metal in the HAZ in various collision modes

angle γ, collision of metals proceeds by alternative «butting in» of the deformation humps into the surface of the opposite blank with formation of regular sinusoidal waves in the joint zone [12]. At γ > φ collision of the plates occurs with «pressing out» of the deformation hump from the surface of just the stationary plate and its «ricocheting» from the surface of the flyer plate with subsequent «closing» of the elongated «deformation hump» by the rolling-on surface of the flyer element, which results in the melt being present only on one side of the plate. No waves are formed in the transition area (γ ≈ φ).

Change of the collision conditions when moving over from one area of the weldability region to another one (Figure 2) qualitatively changes the pattern of distribution of the shear deformations in the HAZ metal, which were studied by the procedure of [13]. So, in explosion welding of model aluminium plates 8 mm thick in the modes providing the formation of a straight waveless joint near the LL of weldability region (area *5* in Figure 2), the maximal shear deformation g_{max} at distance $y \approx \approx 0.03$ mm is up to 250 %. Then it is markedly decreased with the increase of the distance from the welded joint line (Figure 5, *a*). In this case, the depth of the deformed metal layer does not exceed 2 mm.

In subsonic modes of explosion welding (area *4* in Figure 2), the deformation is localised in an even narrower HAZ 0.1 to 0.2 mm wide, this leading to formation of a continuous interlayer of molten metal, while the recorded values of residual maximal shear outside this layer do not exceed 50 % (Figure 5 , *b*).

Lowering of the contact velocity with a simultaneous increase of the collision velocity, leading to absence of wave formation in the joint (area *2* in Figure 2), and then to formation of «anomalous» waves of an elongated shape with the melt location from one side (area *3* in Figure 2), promotes the involvement into plastic deformation of the deeper lying layers of the metal of the plates being welded. In this case g_{max} = 250 – 300 % in the immediate vicinity of the line of the welded joint (Figure 5, *c, d*). Thus, aluminium samples of the initial thickness of 8 mm deform through practically their entire depth in explosion welding in the modes with formation of «anomalous» waves, the level of maximal shear recorded at the back surface of the plates, being about 100 %. In welded elements of the same thickness, produced by welding in the modes with absence of wave formation, the maximal shear deformation measured at the free surface, does not exceed 10 %.

The most interesting in terms of science, however, are the results of investigation of the plastic flow of the HAZ metal of the samples, obtained in the region of the traditional wave formation (area *1* in Figure 2). A characteristic feature found for

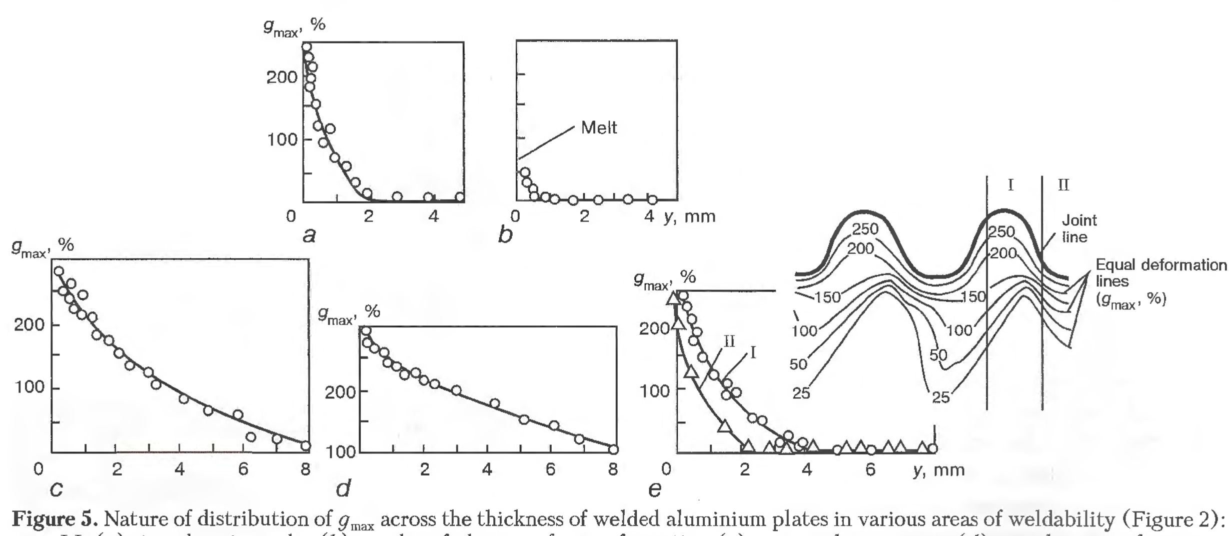

Figure 5. Nature of distribution of g_{max} across the thickness of welded aluminium plates in various areas of weldability (Figure 2): near LL (*a*), in subsonic modes (*b*), modes of absence of wave formation (*c*), «anomalous» waves (*d*), regular wave formation (*e*)

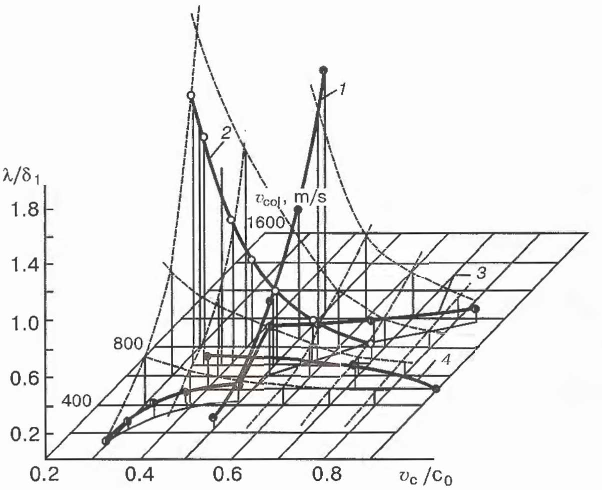

Figure 6. Influence of velocities of collision v_{col} and point of contact v_c on the relative wave length in welding of steel plates (δ_1/δ_2 << 1): *1* — [10]; *2* — [14]; *3, 4* — authors' data

this type of joints, is an essential non-uniformity of the field of the residual shear deformations in the direction of the vector of the contact point velocity (Figure 5, *e*). With the presence of the layers of maximal shear deformations g_{max} = 250 – 300 % in the immediate vicinity of the wavy interface, the intensity of their decrease across the plate thickness is essentially different within one wave. Not only the surface, but also the in-depth sections of the materials being welded participate in the formation of the «deformation hump», pressed out ahead of the contact line. In this connection, the metal under the wave crest, is involved into the plastic deformation to a much greater depth compared to the metal, which is under the depression, where the deformation is smaller, because of the limited capability of its implementation. In this case, the non-uniformity of the field of the residual maximal shear across the microsection, on the whole, is of a periodical nature, which is repeated within the adjacent waves.

A detailed study of the change in the relative length of the waves at variation of the main kinematic parameters within area *1* (Figure 2) allowed revealing the dependence of $\lambda/\delta_1 = f(v_{col}, v_c)$, where λ is the wave length, δ_1 is the thickness of the flyer plate. It is represented by a surface (Figure 6) which can be readily described by a system of mathematical equations

$$\begin{cases} \gamma = 2\arcsin\dfrac{v_{col}}{2v_c} \quad [8], \\ \dfrac{\lambda}{\delta_1} = k\cdot\sin^2\dfrac{\gamma}{2} \quad [2, 12]. \end{cases}$$

Solving this problem, at k = 26, we obtain the following equation which satisfactorily describes the experimental results:

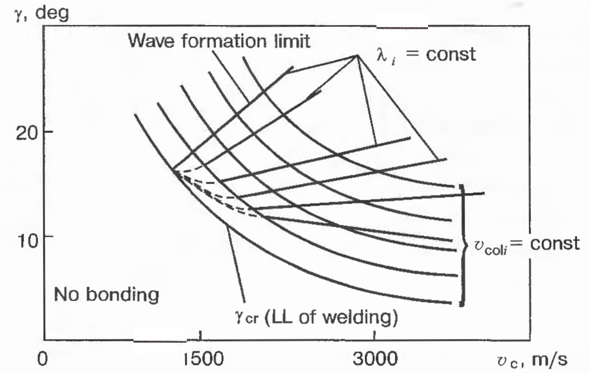

Figure 7. Lines of equal velocities of collision v_{coli} and isodimensional waves in the zone of the aluminium alloy joints

$$\frac{\lambda}{\delta_1} = 6.5\left(\frac{v_{col}}{v_c}\right)^2.$$

Simultaneous analysis of these data and of the position of the critical limits in the region of the «traditional» welding modes showed that the lines of equal wave lengths formed in the HAZ, are represented by a family of straight lines, turning around a certain point. Analysis of the dependencies in Figure 7, proves the correctness of the assumptions made by individual researchers to the effect that the wave parameters proper cannot be a criteria of assessment of the position of critical limits or the quality of the produced joints, as different collision conditions correspond to one and the same wave length.

CONCLUSIONS

1. The existence of the areas of welding with formation of a waveless line of contact and development of «anomalous» waves in the HAZ, was established, proceeding from investigation of the characteristic regions of collision of the metal plates in the kinematic co-ordinates $\gamma(v_{col}) - v_c$. The mechanism and kinetics of formation of these waves are determined by the values of angle φ between the vector of velocity of the «deformation hump» top and the surface of a stationary plate. The regular wave formation mode implemented at $\gamma < \varphi$, in the situation when $\gamma > \varphi$ gives way to an anomalous mode, due to «ricocheting of the deformation hump» from the surface of the flyer plate. This leads to development in the HAZ of markedly elongated waves with the melts located from one side. The waves do not propagate in the transition zone ($\gamma \approx \varphi$), despite the fact that deformation of the near-contact layers of the metal reaches hundreds of percent.

2. Change of the mechanism of welded joint formation with the change of parameters of high-speed collision significantly affects the distribution of maximal deformations of the metal in the HAZ.

With the increase of the velocity of the point of contact v_c, as with the increase of the strength of the materials being welded, the plastic shear deformations are localised near the interface of the plates being welded. Lowering of v_c and increase of the collision velocity v_{col}, provides a more uniform distribution of the maximal shear across the thickness of the samples being welded. Deeper lying metal layers are involved into the plastic deformation.

REFERENCES

1. Lysak, V.I., Sedykh, V.S., Trykov, Yu.P. (1981) Determination of the critical limits of the process of explosion welding. *Svarochnoye Proizvodstvo*, **6**, 15 – 17.
2. Gordopolov, Yu.A., Dremin, A.N., Mikhailov, A.N. (1976) Experimental determination of the dependence of the wave length on the angle of collision in explosion welding of metals. *Fizika Goreniya i Vzryva*, **4**, 601 – 605.
3. Bahrani, A.S., Black, T.I., Crossland, B. (1967) The mechanics of wave formation in explosive welding. *Proc. of Roy. Soc.*, **1445**, 123 – 136.
4. Deribas, A.A., Zakharenko, I.D. (1974) On surface effects at oblique collisions of metal plates. *Fizika Goreniya i Vzryva,* **3**, 409 – 421.
5. Petusknov, V.G., Zotov, M.I., Dobrushin, L.D. (1988) Features of plastic flow in explosion welding. *Avtomaticheskaya Svarka*, **6**, 12 – 13, 22.
6. Godunov, S.K., Deribas, A.A., Mali, V.I. (1975) On the influence of the material toughness on the process of jets formation in collision of metal plates. *Fizika Goreniya i Vzryva*, **1**, 3 – 18.
7. Wittman, R.H. (1973) The influence of collision parameters on the strength and microstructure of an explosion welded aluminium alloy. In: *Mater. of 2nd Int. Symp. on Use of Explosive Energy in Manufacturing Metallic Materials of New Properties*. Marianske Lasne.
8. Deribas, A.A. (1980) *Physics of strengthening and welding by explosion*. Novosibirsk: Nauka.
9. Kuzmin, G.N., Mali, V.I., Paj, V.V. (1972) On throwing flat plates by layers of condensed explosives. *Fizika Goreniya i Vzryva*, **4**, 558 – 562.
10. Deribas, A.A., Kudinov, V.M., Matveenkov, F.I. *et al.* (1968) On simulation of the process of wave formation in explosion welding. *Ibid.*, **1**, 100 – 107.
11. Kriventsov, A.N., Sedykh, V.S. (1969) On the role of plastic deformation of metal in explosion welding. *Fizika i Khimiya Obr. Materialov*, **1**, 133 – 141.
12. Kudinov, V.M., Koroteev, A.Ya. (1978) *Explosion welding in metallurgy*. Moscow: Metallurgia.
13. Kuzmin, S.V., Chugunov, E.A., Lysak, V.I. *et al.* (1998) Development of a procedure of investigation of plastic deformation of metal in the HAZ of joints welded by explosion. In: *Inercollege Transact. on Explosion Welding and Properties of Welded Joints.* Volgograd: GTU.
14. Sedykh, V.S., Sonnov, A.P. (1975) Quantitative estimate of metals surface melting in explosion welding. In: *Transact. on Explosion Welding and Properties of Welded Joints.* Volgograd: VPI.

HIGH-TEMPERATURE TRIBOLOGICAL PROPERTIES OF THERMAL SPRAY COATINGS CONTAINING SOLID LUBRICANTS

A.L. BORISOVA, A.Yu. TUNIK, G.M. GRIGORENKO, V.A. KOSTIN and **E.A. ASTAKHOV**
The E.O. Paton Electric Welding Institute, NASU, Kyiv, Ukraine

ABSTRACT

Results of investigations of tribological properties of thermal spray coatings containing solid lubricants under conditions of dry friction and increased temperatures are given. Addition of solid lubricants (Fe_mO_n or CaF_2) to the cast iron based coatings allows a substantial improvement in their anti-friction properties at increased temperatures. Friction coefficient of detonation coatings with Fe_mO_n at 400 °C is decreased 1.5 times and that of plasma coatings with CaF_2 is decreased 3 times, as compared with friction coefficient of cast iron. Wear resistance, respectively, is increased by 30 % on the average.

Key words: *thermal spray coatings, solid lubricants, dry friction, wear resistance*

Because of increasingly stringent requirements to quality of anti-friction materials, special consideration is given now to solid lubricants applied as coatings to working surfaces of friction units. Such solid lubricant-containing coatings are used to protect surfaces of parts from friction and wear under conditions of a limited lubrication or without any lubrication.

Earlier the authors [1 – 3] developed a series of powders for thermal spraying of anti-friction coatings containing graphite, calcium fluoride and iron oxides used as solid lubricants. The coatings were deposited by the thermal spraying methods and their structure, phase composition and properties were investigated. As such coatings are intended for operation under extreme conditions, further comprehensive investigations should be conducted to study them. In particular, it applies to investigation of the effect of temperature on anti-friction properties.

The purpose of this work was to study tribological properties of thermal spray coatings containing solid lubricants under conditions of dry friction in air at increased temperatures (up to 400 °C).

The specially developed tribological system was used to evaluate anti-friction properties of coatings on friction parts [4]. The system comprises devices for positioning of samples and registration of friction forces (Figure 1), a drive for relative displacement of friction surfaces, electric heating furnace with a temperature sensor and devices for generating a certain pressure in a place of contact of the friction pair and registering geometrical characteristics of the friction strip surfaces.

During the friction process the flat test samples with coatings were brought into contact by a diagram «sphere-plane». Steel ShKh-15 (C — 0.95 – 1.05; Mn — 0.2 – 0.4; Si — 0.17 – 0.37; Cr — 1.3 – 1.65 wt.%) balls with a diameter of 6 mm and hardness of *HRC* 63 – 64 were used as the indenter (*8* in Figure 1). Pressure in contact of the investigated friction pair of the samples was generated by a load of $N = 10 - 120$ N applied using a set of weights.

The coated samples were tested to evaluate friction force F, linear wear of a sample, I (to depth h of the wear pit), surface area of the worn out region of the coating, S_w, and diameter of the contact spot, P_c. The mean value of the friction force was used in the investigations, and it was determined from the following formula:

$$F = \sum_{i=1}^{n} F_i/n,$$

where F_i is the friction force of the i-th measurement and $n = 3$ is the number of the measurements.

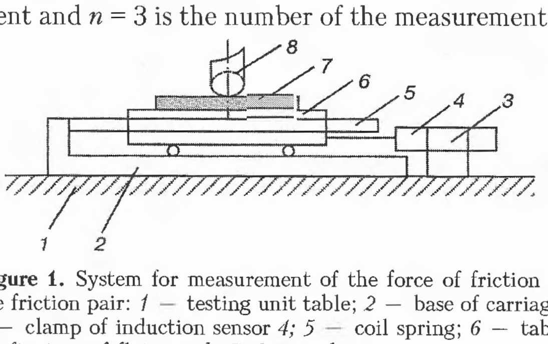

Figure 1. System for measurement of the force of friction in the friction pair: *1* — testing unit table; *2* — base of carriage; *3* — clamp of induction sensor *4*; *5* — coil spring; *6* — table for fixation of flat sample *7*; *8* — indenter

Table 1. Compositions and conditions of spraying of the coatings

Composition of spraying material, vol.%	*Spraying method*	*Working gas*	*Gas flow rate, m^3/h*	*Current, A*	*Voltage, V*	*Spraying distance, mm*
100 FeCSi	DS	C_3H_8 O_2	0.5 1.0	–	–	100
80 FeCSi + 20 CaF_2	DS	C_3H_8 O_2	0.5 2.0	–	–	100
Same	SAGPS	Air P = 0.4 MPa	12.0	180	380	230
80 FeCSi + 20 Fe_mO_n	DS	C_3H_8 O_2	0.5 2.0	–	–	100
Same	SAGPS	Air P = 0.4 MPa	12.0	160	420	230

Table 2. Characteristics of the thermal spray coatings

Composition of spraying material, vol.%	*Spraying method*	*Coating thickness, μm*	*Phase composition*	*Microhardness, MPa*
100 FeCSi	DS	290	γ-Fe, α-Fe, Fe_3C, Fe_8Si_2C, α-Fe_2O_3 (traces)	4410 – 5410
80 FeCSi + 20 CaF_2	DS	300	γ-Fe, α-Fe, Fe_3C, Fe_8Si_2C, CaF_2, γ-Fe_2O_3 (traces)	4510 – 5840
Same	SAGPS	350	α-Fe, Fe_3C, γ-Fe, Fe_8Si_2C, CaF_2, α-Fe_2O_3 (traces)	4800 – 6000
80 FeCSi + 20 Fe_mO_n	DS	150	γ-Fe, Fe_3C, α-Fe, Fe_3O_4, Fe_8Si_2C, α-Fe_2O_3	4410 – 5490
Same	SAGPS	330	α-Fe, γ-Fe, Fe_3C, Fe_3O_4, Fe_8Si_2C, FeO (traces)	5400 – 7010

Note: Phases are given in decreasing order of the intensity of reflection of X-rays.

Table 3. Results of tribological tests

Composition of spraying material and spraying method, vol.%	*T, °C*	*F, N*	*I, μm*	*$S_w \cdot 10^3$, μm²*	*P_c, mm²*	*f*
80 FeCSi + 20 Fe_mO_n (DS)	20 100 250 400	8.99 9.91 9.28 6.71	7.55 6.53 6.24 6.38	2.1 1.7 1.9 1.6	1.82 2.04 1.93 2.11	0.30 0.33 0.31 0.22
80 FeCSi + 20 Fe_mO_n (SAGPS)	20 100 250 400	9.57 10.81 9.93 8.40	9.11 7.75 7.34 7.48	1.8 2.2 2.6 2.0	1.88 1.92 1.97 2.20	0.32 0.36 0.33 0.28
80 FeCSi + 20 CaF_2 (DS)	20 100 250 400	7.48 8.98 7.81 5.41	8.89 8.50 8.12 8.40	2.2 2.1 2.3 2.7	1.91 1.97 2.04 2.15	0.25 0.30 0.26 0.18
80 FeCSi + 20 CaF_2 (SAGPS)	20 100 250 400	7.96 8.42 7.53 3.32	8.51 7.96 7.58 7.62	2.1 2.3 1.9 2.0	1.89 2.01 1.94 2.06	0.26 0.27 0.25 0.11
100 FeCSi (DS)	20 100 250 400	12.09 12.30 11.43 9.32	10.53 8.71 8.91 9.30	2.9 2.2 2.3 2.7	1.97 1.98 2.10 2.23	0.40 0.43 0.40 0.30

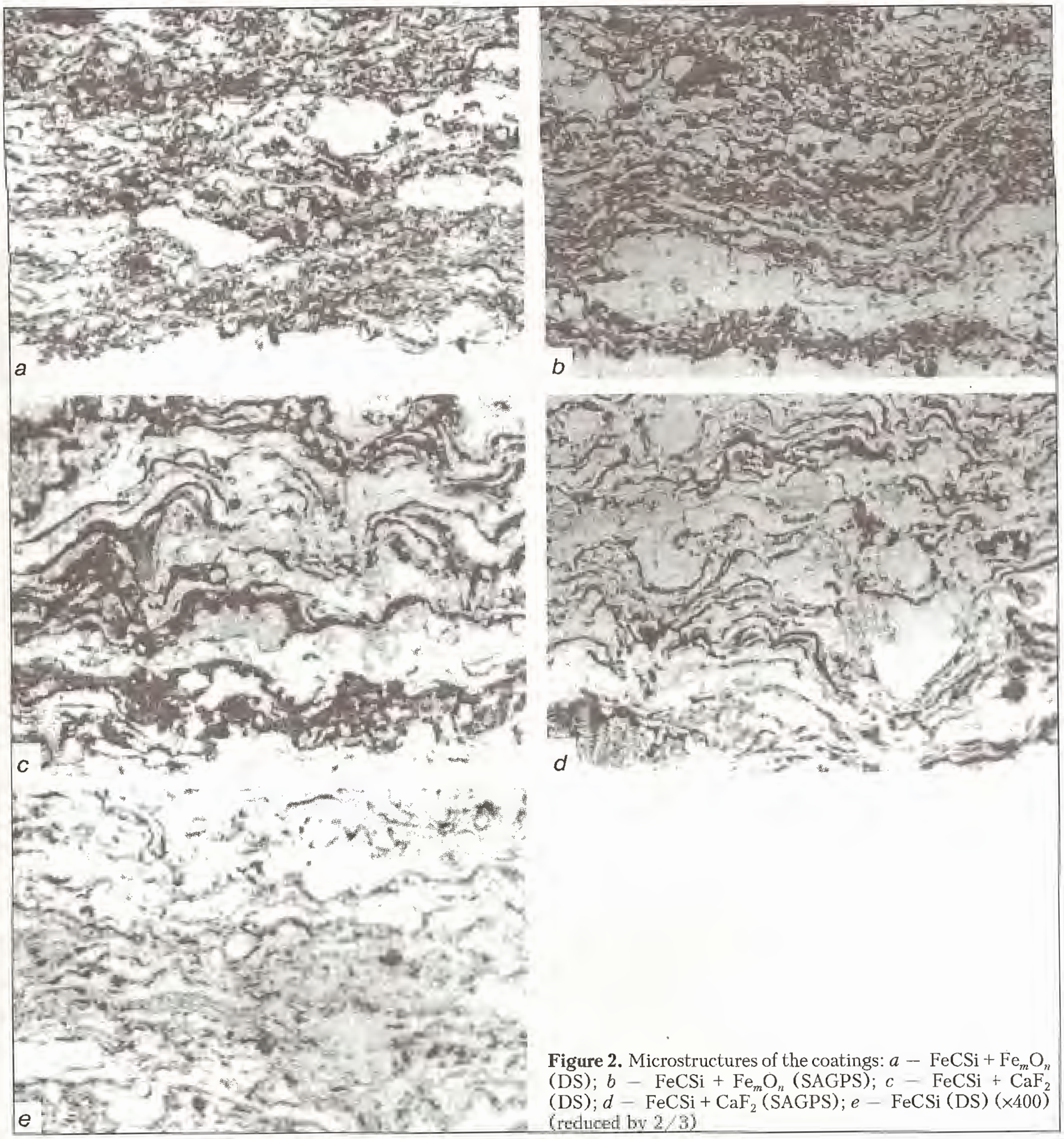

Figure 2. Microstructures of the coatings: *a* — FeCSi + Fe_mO_n (DS); *b* — FeCSi + Fe_mO_n (SAGPS); *c* — FeCSi + CaF_2 (DS); *d* — FeCSi + CaF_2 (SAGPS); *e* — FeCSi (DS) (×400) (reduced by 2/3)

The error of measurement of the friction force F_i and, respectively, F, was no more than 5 %.

The friction coefficient was calculated as the friction force to load ratio: $f = F/N$. Linear wear $I \sim h$ of the samples was registered after the tests using profile patterns of the friction strip surfaces (at three locations), recorded using the «Kalibr» profilograph-profilometer P-201. In this case the error in determination of the pit depth and, accordingly, linear wear was not in excess of 1 %. Diameter of the spot contact between the spherical indenter and flat surface of the sample was measured using the MIM-7 microscope with a magnification of ×7, the measurement error being no more than 1 % either.

The basic component of the anti-friction coatings investigated is the FeCSi cast iron powder containing 2.16 wt.% C and 5.18 wt.% Si. Solid lubricants CaF_2 or Fe_mO_n in an amount of 20 % each were added to this initial powder by mechanical mixing. Particles of the produced mixtures were 40 – 80 μm in size. The coatings were deposited on samples of steel 45 preliminarily subjected to jet-abrasive blasting using synthetic corundum of the M100 grade. The deposition methods were detonation spraying (DS) and supersonic air-gas plasma spraying (SAGPS). Compositions of the coatings, process conditions and deposition methods are given in Table 1.

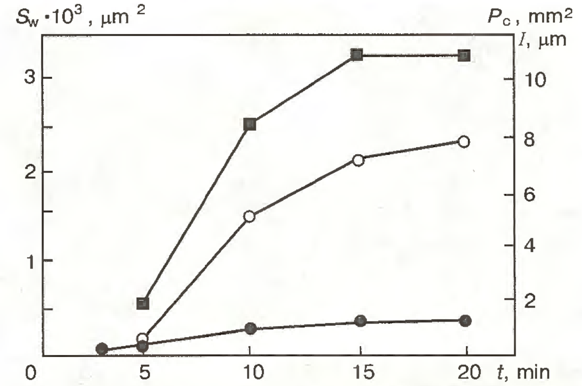

Figure 3. Dependence of linear wear, I (■) of the coating of FeCSi (DS), cross section area of the material, S_w (O) and contact spot of the mating body, P_c (●) upon the test time (speed 0.5 m/s, load 30 N)

The coatings sprayed were investigated by metallography using the Neophot-32 microscope and X-ray phase analysis (XPA) using the DRON-3 diffractometer in a characteristic CoK_α radiation. Microhardness of structural components was measured using the LECO hardness meter M-400 under a load of 0.49 N for 10 – 12 s. After the tribological tests the samples were investigated also by scanning electron microscopy (SEM) and X-ray spectrometry using the JEOL (Japan) device JSM-840 with an attachment of the «Link System» microanalyser.

The high-temperature measurements of microhardness HV of the preliminarily polished samples (not less than 7 indentations at each temperature) were made in vacuum using the VIM-1 device by standard procedures under a load of 0.24 N, the loading time being 10 – 12 s.

Table 2 gives phase composition and microhardness of the coatings investigated. As proved by metallography, the resulting coatings are sound, almost pore-free, containing no cracks, separations or other defects at the interface with the substrate (Figure 2, $a - e$).

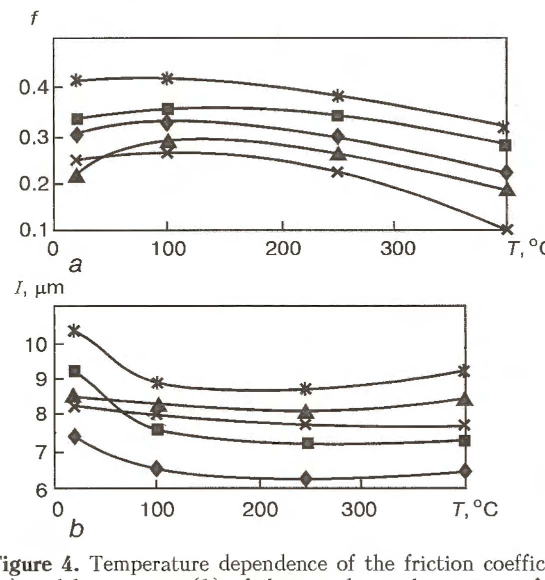

Figure 4. Temperature dependence of the friction coefficient (a) and linear wear (b) of the samples with coatings: ◆ – FeCSi + Fe_mO_n (DS); ■ – FeCSi + Fe_mO_n (SAGPS); × – FeCSi + CaF_2 (DS); ▲ – FeCSi + CaF_2 (SAGPS); ✱ – FeCSi (DS)

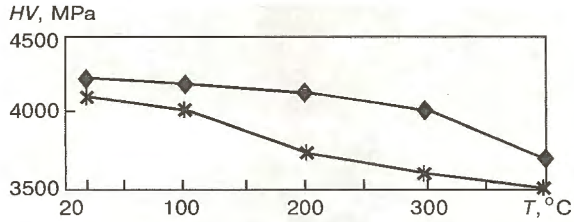

Figure 5. Temperature dependence of microhardness of the coatings: ◆ – FeCSi + Fe_mO_n (DS); ✱ – FeCSi (DS)

The tribological test procedure was tried out first at normal temperature on cast iron samples with detonation coatings. Analysis of the derived time dependencies of S_w, I and P_c (Figure 3) showed that stabilization of the friction force and the best reproducibility of the measurement results (minimum variance coefficient) were observed under a load of 30 N, sliding speed of 0.5 m/s and test time of 20 min. It is under these conditions that the time dependence of the friction coefficient and linear wear of the thermal spray coatings with solid lubricants was estimated (Figure 4).

Results of the tribological tests of different compositions of the thermal spray coatings are given in a summary Table 3.

According to the data obtained, addition of the Fe_mO_n or CaF_2 solid lubricants to the cast iron based coatings leads to a decrease in wear and friction coefficient over the entire temperature range investigated.

The extreme temperature dependence of the friction coefficient (Figure 4, a) can be explained as follows. According to the molecular-mechanical (termed abroad as «adhesion-deformation») theory of friction, in relative displacement of solid bodies the friction resistance F_{fr} is made up of the molecular (adhesive) F_a and cohesive F_c components [5]: $F_{fr} = F_a + F_c$. An increase in temperature leads to a decrease in the molecular component of the friction coefficient caused by intensification of the oxidation processes and decrease in shear resistance of the molecular bond. However, this is accompanied by a decrease in hardness of the material, which leads to formation of deeper irregularities on its surface and increase in a mechanical component of the friction coefficient. The resulting character of the temperature dependence of the friction coefficient depends upon the interaction of these factors.

Judging from the measurement results, starting from 100 °C an increase in temperature is accompanied by a monotonous decrease in hardness (Figure 5), leading to an increase in the mechanical component of the friction coefficient. At the same time, formation of secondary structures responsible for its molecular component takes place at high temperatures. As proved by SEM and XPA analysis

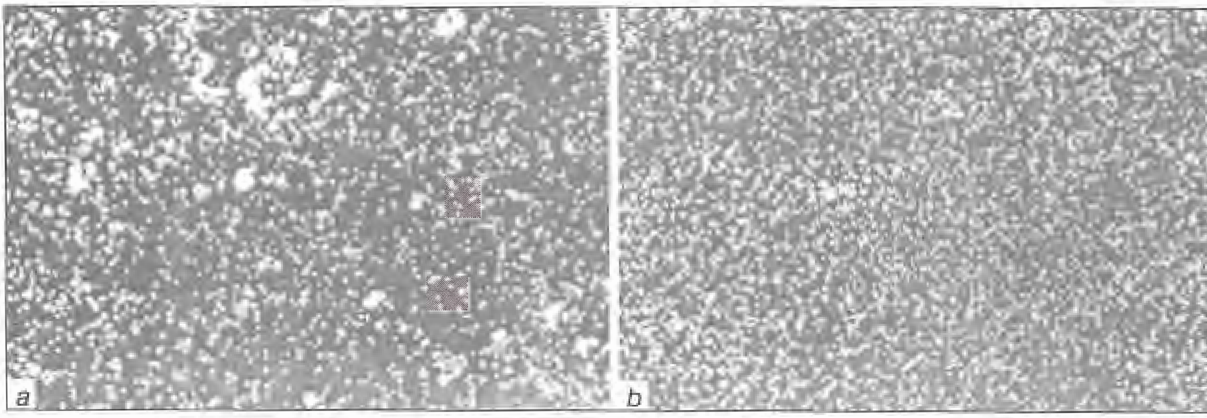

Figure 6. Surface of the FeCSi + CaF_2 coating (SAGPS) in characteristic calcium radiation before (*a*) and after (*b*) tribological tests (×230) (reduced by 2/3)

of the friction strips, the content of oxides Fe_3O_4 and FeO providing the highest wear resistance and lowest friction coefficient increases on the surface of the coating which contains (in the initial state) iron oxide Fe_mO_n. The surface of the coating containing calcium fluoride is characterized by the presence of an almost continuous film of the latter, which is formed at increased temperatures that facilitate its destruction (Figure 6, *a, b*).

The surface state of the friction strips after the tribological tests conducted at a temperature of 400 °C (Figure 7) is indicative of occurrence of such processes as smoothing of a microrelief (*a*), formation of wear products primarily in the form of dispersed spheroidal particles (*b*), and presence of a network of cracks (*c*). Traces of brittle cleavage near the latter are noted extremely rarely, which is indicative of a high ductility of the coating and its ability to withstand further multiple deformation. The fact that the coating wears out uniformly, without separation and fatigue defects, is proved by the character of the temperature dependence of the linear wear (Figure 4, *b*).

The investigations conducted evidence that an addition of solid lubricants (Fe_mO_n or CaF_2) to the cast iron based coatings allows a substantial improvement in their anti-friction properties at increased temperatures. Thus, the friction coefficient at 400 °C decreases from 0.3 for cast iron to 0.2 for a detonation coating containing Fe_mO_n, and to 0.1 for a plasma coating containing CaF_2. At the same time, wear resistance of the coatings increases by 30 % on the average. The data on the effect of temperature on tribological properties of the

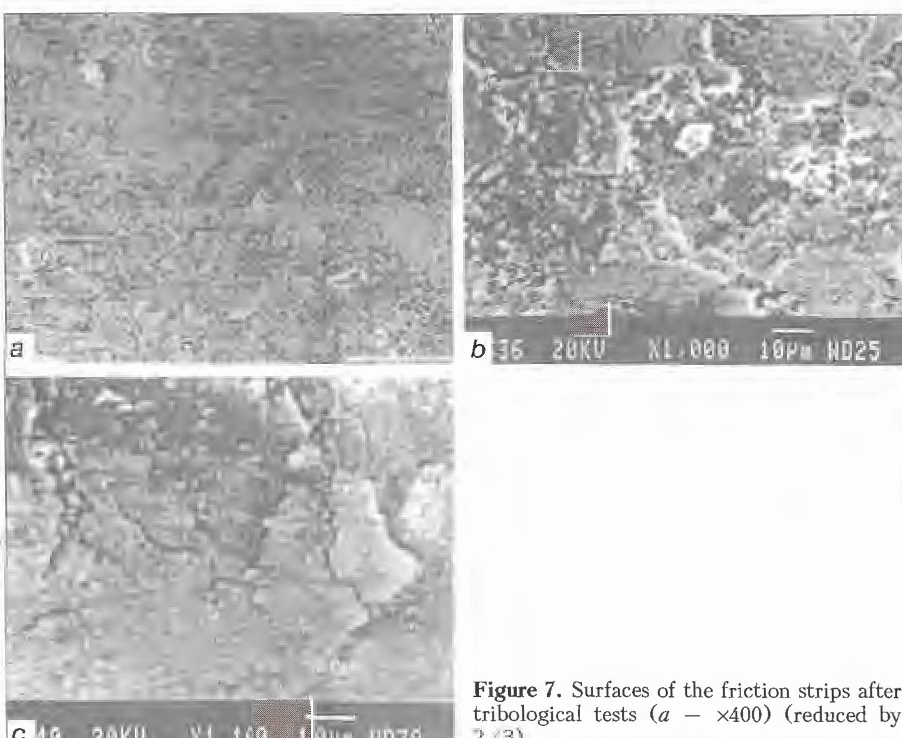

Figure 7. Surfaces of the friction strips after tribological tests (*a* — ×400) (reduced by 2/3)

plasma coatings of the Kh20N80–CaF_2 composite powders are given in [6] (Kh20N80 – Cr – 20.0; Ni – 80.0 wt.%). According to these data, the values of wear and friction coefficient (I = = 1 μm/h, f = 0.21) are close to the results obtained in this work. However, the test conditions used in [6] were less rigid: speed was 0.5 m/s, pressure was 0.05 MPa, and the mating body was cellular glass ceramic. Owing its high anti-friction properties, as compared with nichrome, cast iron shows much promise for use as the base material for thermal spray coatings containing solid lubricants.

REFERENCES

1. Borisova, A.L., Adeeva, L.I., Tunik, A.Yu. *et al.* (1999) Structure and properties of thermal spray coatings based on titanium carbide and titanium-chromium oxides, containing solid lubricants. *Avtomaticheskaya Svarka*, **1**, 22 – 31.
2. Borisova, A.L., Adeeva, L.I., Tunik, A.Yu. *et al.* (1999) Anti-friction thermal spray coatings of mechanical mixtures of cast iron and calcium fluoride powders. *Ibid.*, **7**, 20 – 29.
3. Borisova, A., Borisov, Y., Tunik, A. *et al.* (1999) Thermal spraying of coatings containing solid lubricants. In: *Proc. of the 1st Un. Thermal Spray Conf.*, Aachen, Germany, March 1999.
4. Grinkevich, K.E., Latsko, D.V., Yefimov, N.A. (1996) Investigation of the influence of laser treatment and dynamic force effect on tribological and physical properties of steel Kh18N10T. *Problemy Tribologii*, **2**, 23 – 31.
5. Kragelsky, I.V., Dobychin, M.N., Kombalov, V.S. (1977) *Principles of friction and wear calculations*. Moscow: Mashinostroyeniye.
6. Lekarev, Yu.G., Maksimov, V.V., Barvinok, V.A. *et al.* (1988) Anti-friction plasma coatings based on composite materials «metal–solid lubricant». In: *Transact. on Diffusion Saturation and Coatings on Metals. Kyiv: IPM.*

CHALLENGING TECHNOLOGIES FOR HIGH-STRENGTH STEEL WELDING WITHOUT PREHEATING AND HEAT TREATMENT

V.V. SNISAR, E.L. DEMCHENKO and **E.V. IVANCHENKO**
The E.O. Paton Electric Welding Institute, NASU, Kyiv, Ukraine

ABSTRACT

Technologies and welding consumables for manual arc and mechanized welding of high-strength hardenable steels without preheating and postweld heat treatment (PWHT) to provide a welded joint equal in strength to the base metal are presented. Structure, physical-chemical properties, susceptibility to a delayed fracture and corrosion cracking of welded joints made from 15Kh2N4MDA (C — 0.15; Cr — 2.0; Ni — 4.0; Mo, Cu — 1.0 wt.%) high-strength steel are described.

Key words: *welding consumables, hardenable steel, weld metal, welded joint, mechanical properties, microstructure, crack resistance, cold resistance, fatigue strength*

One of the main tasks facing the domestic machine-building is the reduction in a structure metal content. Therefore, the application of resources-saving technologies during their manufacture is especially actual. In this connection, many branches of industry use more and more widely the high-strength steels of yield strength at the level of 600 – 1000 MPa. Welding of such steels as 40Kh, 30KhGSA, 15Kh2N4MDA, 30Kh2N2M, etc. presents a complex technological problem. Susceptibility to formation of coarse-grained quenched structures in weld-adjacent zones under the action of the welding thermal cycle, the presence of high welding stresses and also the hydrogen embrittlement of metal in HAZ cause the risk of occurrence of the weld-adjacent cold cracks.

The existing technologies of welding of the mentioned steels envisage the measures which contribute to deterioration of a negative effect of the above-mentioned factors. First of all, the preheating and PWHT of the welded joints are used. However, when these measures are used in welding of large-sized and thick-walled structures the technological process becomes more complicated and, in several cases, impossible for realization.

It is known, that the application of welding consumables, which provide weld metal of an austenitic class, makes it possible to eliminate the preheating and PWHT from the technological process in welding of products from medium-alloyed hardenable steels. Welded joints with austenitic welds are not susceptible to cold cracking. However, such technological variant has a following drawback: due to a low strength of the austenitic weld metal it is necessary to perform the weld with a large reinforcement to provide the equal strength of the welded joint. This leads to the great increase in volume of welding jobs and consumption of expensive welding consumables. Moreover, the increased reinforcement of the weld creates a stress raiser which in several cases decreases the serviceability of the welded joint.

A new method of welding high-strength hardenable steels was suggested at the E.O. Paton Electric Welding Institute [1]. It consists in application of welding consumables which provide a structure in the weld with a decomposition of austenite at temperature below 200 °C and formation of the decomposition products which impart high strength characteristics at a good ductility and toughness to the weld metal. This method of welding is based on a positive effect of the austenitic weld metal on the kinetics of phase transformations in the HAZ of the high-strength steel and on changing in a mode of distribution of stresses in the welded joint. This method makes it possible to weld high-strength hardenable steels without preheating and PWHT of the product, the same as in case of using the austenitic weld, and to produce here the welded joints which are equal in strength. One of the variants of a practical realization of the suggested method is the application of the welding consumables which provide weld metal of chemical composition and structure of the low-carbon martensitic or austenitic-martensitic steel. Technologies and consumables for the manual and mechanized welding have been developed at the PWI [2 – 4]. The technology of the manual electric arc welding envisages the use of the new electrodes of ANVP-60, ANVP-80 and ANVP-100 (C — 0.05;

Mechanical properties of weld metal in welding steel 15Kh2N4MDA

Welding consumables	$\sigma_{0.2}$, *MPa*	σ_t, *MPa*	δ, *%*	ψ, *%*	KCV^{+20}, *J/cm²*	KCU^{-60}, *J/cm²*
			Manual welding			
ANVP-60	600	1000	15	40	105	60
	700	1100	18	50	110	80
ANVP-80	780	1050	15	40	100	60
	850	1150	18	50	110	80
ANVP-100	950	1150	12	25	70	50
	1050	1200	16	35	90	70
			Mechanized welding in CO_2			
PP-ANVP80	750	1000	14	30	60	45
	900	1200	16	40	70	50
			Mechanized submerged arc welding			
EK-17VI	840	1150	18	45	65	50
	910	1190	22	50	75	55
PP-ANVP80	750	900	18	35	65	50
	800	1000	25	40	75	55

Cr — 11.0 – 13.0; Ni — 7.0 – 9.0; Mo — 1.5 – 2.0; Mn — 1.5 – 2.0; Si — up to 0.5; Ti — 0.1 – 0.2 wt.%) grades, which provide weld metal with a different level of yield strength: 600, 800 and 1000 MPa, respectively. For the mechanized welding in CO_2 or Ar–CO_2 mixture a flux-cored wire PP-ANVP80 (C — 0.05; Cr — 13.0; Ni — 9.0; Mo — 2.0; Mn — 1.0; Si — 0.5; Ti — 0.1 wt.%) is recommended. For the submerged arc welding a new ceramic flux, solid wire EK-17VI (C — 0.03; Cr — 13.0; Ni — 9.0; Mo — 2.0; Mn — 1.0; Si — 0.5; Ti — 0.1 wt.%) and flux-cored wire PP-ANVP80 are recommended.

The above-mentioned welding consumables provide high welding-technological properties: stability of the arc process, self-removal of a slag crust, quality formation of the weld surface, absence of pores and slag inclusions in the deposited metal.

Figure 1. Microstructure of austenitic-martensitic weld metal (×320) (reduced by 2/3)

All these materials provide in welding of the high-strength steel, for example, 15Kh2N4MDA, the austenitic-martensitic weld metal of hardness at the level of *HV* 300 MPa. Mechanical properties of the weld are given in Table, and the typical microstructure is shown in Figure 1.

Steels and welds with a mentioned level of mechanical properties are rather sensitive to a delayed fracture and cold crack formation. One of the main factors, causing this, is hydrogen. Moreover, the higher level of the metal strength properties, the greater negative effect of hydrogen [5]. Therefore, when developing this group of welding consumables a special attention should be paid to minimizing the hydrogen concentration in the weld metal. The favourable combination of components included to the ceramic flux composition, electrode coatings and a core of the flux-cored wire, their optimum ratio in combination with a number of technological measures [6] could solve the mentioned problem positively. Thus, in DCRP welding the new consumables provide a low content of hydrogen in the weld metal, i.e. diffusion-mobile hydrogen, determined by a chromotographic method (GOST 23338–91) using OB2781 instrument, at the level of 1.3 – 2.0 cm³/100 g; residual hydrogen, determined by the fusion method in a gas-carrier jet, at the level of 0.3 – 1.0 cm³/100 g; total hydrogen, which is not more than 3.0 cm³/100 g. This hydrogen content does not cause the great effect on the resistance of the welded joint to the cold crack formation.

The resistance of welded joints, made by the suggested technologies, to crack formation, was

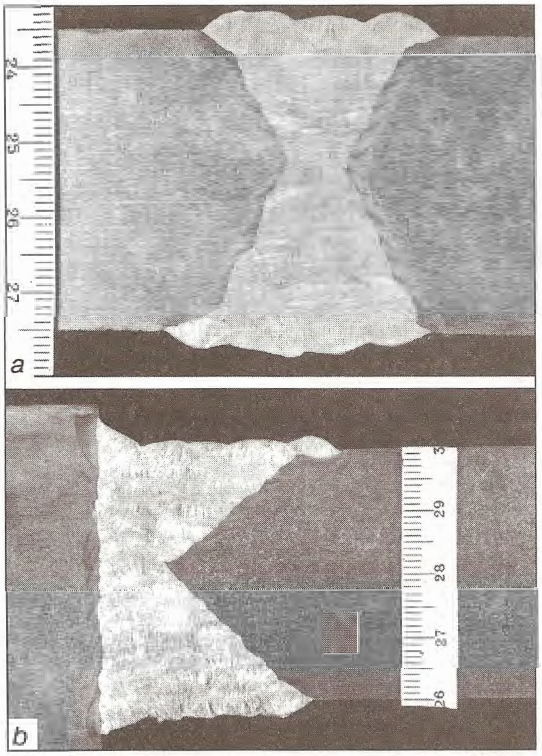

Figure 2. Macrosections of welded joints of rigid technological samples (*a* — TsNIITS, *b* — «round plug») made with electrodes ANVP-80

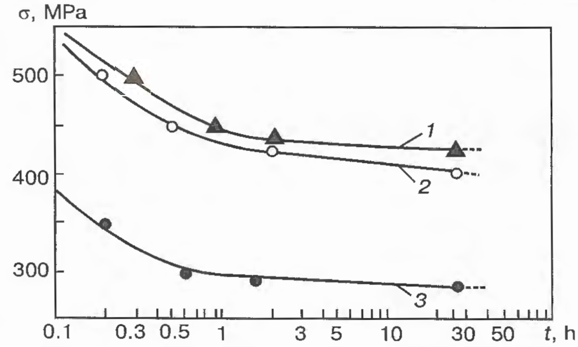

Figure 3. Resistance of 30Kh2N2M steel welded joints made without preheating and PWHT using electrodes to a delayed fracture: LO-1(*1*), ANVP-80 (*2*), UONI-13/45 (*3*)

assessed on 40 mm thick 15Kh2N4MDA steel using technological samples of «round plug» and Research Institute of Shipbuilding Technologies (TsNIITS) types [7, 8]. Welded joints of 30Kh2N2M (Cr-alloyed; Ni, Mo, Cu — up to 1.0 at C content of 0.15 – 0.40 wt.%) steel were tested on susceptibility to a delayed fracture [9].

The assessment showed that the test consumables can provide welded joints with a sufficient resistance to hot and cold crack formation and to a delayed fracture, close to the austenitic variant, during welding high-strength steels without preheating and PWHT. Figure 2 confirms this and shows a typical appearance of macrosections made from the above-mentioned technological samples, while Figure 3 presents the curves of a delayed fracture of the welded joints made with austenitic electrodes LO-1 (C — 0.1; Cr — 20.0; Ni — 9.0; Mn — 7.0; Ti — 0.7 wt.%), pearlitic electrodes UONI-13/45 (C — 0.1; Mn — 0.6; Si — 0.25; Fe — 0.05 wt.%) and austenitic-martensitic electrodes ANVP-80.

Weld metal made by the use of austenitic-martensitic materials is resistant to embrittlement at negative temperatures [10]. The cold resistance of this weld was evaluated by the determination of a critical temperature of brittleness from impact strength at negative temperature (T_{br}) and also from a relative fibrousness in fracture (T_{cr} at F = = 50 %).

It was established that T_{cr} = –70 °C, and T_{br} = = –(80 – 90) °C, i.e. the temperature of brittleness of the test metal is below the climatic temperature (–60 °C).

The fusion zone in the above-mentioned joints is not also sensitive to embrittlement. Here, the impact strength KCU^{+20} = 95 J/cm^2 and KCV^{-60} = = 45 J/cm^2. The absence of clearly expressed negative effect of the martensitic layer in the transition layer was due, in this case, to the formation of not a brittle acicular martensite, but a lath martensite [11] which is characterized by a sufficient ductility and does not deteriorate the welded joint serviceability.

The high-strength steel welded joints are often used in manufacture of structures operating in aggressive media, for example, in sea water, that is typical of joints of floating drilling rigs in particu-

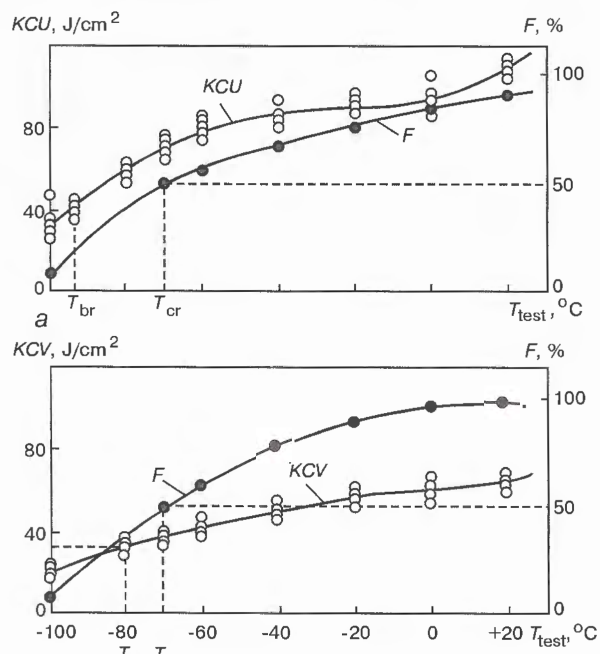

Figure 4. Relationship between the impact strength *KCU*, *KCV* and relative fibrousness *F* in the weld fracture and test temperature T_{test}: samples with a round (*a*) and sharp (*b*) notch

lar. The assessment of resistance to corrosion cracking in a synthetic sea water of 15Kh2N4MDA steel joints with an austenitic-martensitic weld showed that only a general corrosion without a fracture localizing is observed in the test joints, and the weld metal was not subjected to a corrosion cracking during testing for 100 h under the stress at the level of 80 % of its yield stress [12].

Sanitary-hygienic evaluation of the developed electrodes ANVP-60, ANVP-80 and ANVP-100 showed that the intensity of precipitation of hard constituent of the welding aerosol (HCWA) in welding with these electrodes is 1.5 times less than with austenitic electrodes EA-981/15 (C — 0.1; Cr — 16.0; Ni — 25.0; Mo — 6.0; Mn — 2.0; V — 1.0 wt.%) which are widely used for welding high-strength steels without preheating and PWHT. The specific precipitation of HCWA per 1 kg of electrodes of the developed series is 1.4 times lower than that of electrodes EA-981/15, and as to the content of most toxic components (manganese, chromium) in HCWA the comparing electrodes are at the same level.

It was established during the sanitary-hygienic evaluation of the developed flux-cored wire PP-ANVP80 that the intensity of precipitation of a hard constituent in CO_2 welding, the specific precipitation of HCWA per 1 kg of wire and the content of most toxic components (manganese, chromium) in HCWA do not exceed the corresponding characteristics of high-alloyed wires used in industry.

At present the above-described technologies and consumables are implemented in several branches of industry. Thus, the electrodes ANVP-80 are used successfully in restoration of bodies of adjustable valves and working surfaces of steam-water stop valves in power engineering, while the flux-cored wire PP-ANVP80 is used for welding and surfacing in restoration of automatic coupler equipment of freight cars.

The above-mentioned consumables are produced at the PWI. The technical documentation is available for their manufacture.

REFERENCES

1. Gotalsky, Yu.N., Snisar, V.V., Kuporev, A.L. *et al.* (1981) *Method of arc welding of hardenable steels.* USSR author's certificate **880671**, Int. Cl. B 23 K 28/00. Publ. 15.11.81.
2. Lipodaev, V.N., Gotalsky, Yu.N., Snisar, V.V. *et al.* (1991) *Welding electrode for welding without preheating and heat treatment of low- and medium-alloyed high-strength hardenable steels.* USSR author's certificate **1689007**, Int. Cl. B 23 K 35/365. Publ. 07.01.91.
3. Demchenko, E.L., Lyakhovaya, I.V., Snisar, V.V. *et al.* (1993) *Electrode for welding of high-strength steels.* USSR author's certificate **1785860**, Int. Cl. B 23 K 35/365. Publ. 07.01.93.
4. Gotalsky, Yu.N., Snisar, V.V., Demchenko, E.L. *et al.* (1990) Welding of high-strength steels with a yield strength of more than 800 MPa without preheating and heat treatment. *Avtomaticheskaya Svarka*, **10**, 38 – 40.
5. Kozlov, R.A. (1969) *Hydrogen in welding of hull steels.* Leningrad: Sudostroyeniye.
6. Demchenko, E.L., Snisar, V.V., Lipodaev, V.N. *et al.* (1991) Ways of reduction of hydrogen content in weld metal of 03Kh12N8M2GST steel in arc welding. *Avtomaticheskaya Svarka*, **10**, 23 – 27.
7. Makarov, E.L. (1981) *Cold cracks in welding of alloyed steels.* Moscow: Mashinostroyeniye.
8. Snisar, V.V., Demchenko, E.L. (1990) Prevention of cold cracks in 15Kh2N4MDA high-strength steel welded joints with austenitic-martensitic weld. *Avtomaticheskaya Svarka*, **2**, 24 – 27.
9. Snisar, V.V., Demchenko, E.L., Gaivoronsky, A.A. (1993) Effect of weld structure on properties of HAZ of welded joints of steel 30Kh2N2M. *Ibid.*, **9**, 43 – 45.
10. Snisar, V.V., Demchenko, E.L. (1988) Cold resistance of austenitic-martensitic weld in welded joint of steel 15Kh2N4MDA. *Ibid.*, **12**, 62 – 63.
11. Snisar, V.V., Novikova, D.P. (1984) Study of martensitic interlayer in fusion zone of high-strength steel of 15Kh2N4MDA type with austenitic-martensitic weld metal. *Ibid.*, **7**, 68 – 69.
12. Snisar, V.V., Yushkevich, Z.V., Demchenko, E.L. *et al.* (1984) Resistance to corrosion cracking of 15Kh2N4MDA high-strength steel welded joints with austenitic-martensitic weld. *Ibid.*, **10**, 69 – 71.

DESIGN OF AN INDUCTOR WITH A MAGNETIC CORE FOR HEATING FLAT SURFACES

A.S. PISMENNY[1], E.A. PANTELEJMONOV[1], A.S. PROKOFIEV[1] and Ch.V. PULKA[2]
[1]The E.O. Paton Electric Welding Institute, NASU, Kyiv, Ukraine
[2]I. Pulyuj Ternopol National Technical University, Ternopol, Ukraine

ABSTRACT

A procedure of design of a system of circular inductor with the magnetic core, namely a flat part (electric load), is described, based on application of the equivalent circuits and the results of calculation of the circuit electrical parameters. Calculation results and experimental data are given which demonstrate that the procedure is well-grounded and is sufficiently accurate for practical calculations.

Key words: *induction heating, welding, brazing, straightening of sheet structures, surfacing, inductors, equivalent circuits, electric parameters, calculations, examples, accuracy evaluation*

The inductors being discussed are single- or multi-turn flat water-cooled windings placed into the magnetic core slot, which are mounted in parallel to the item surface being heated (Figure 1). They are applied for heating the flat and end face surfaces of items prior to welding, brazing and heat-treatment (for instance, in flanged and tee joints, etc.). Application of such inductors is of interest in electrothermal straightening of sheet structures, whose design shape became distorted under the impact of residual stresses in welding.

Use of a magnetic core is known to increase the efficiency and power factor of any induction system. When inductors are used for heating the flat surfaces of items, the need to improve the above power characteristics is especially great, as in the case of application of an inductor without a magnetic core, the electromagnetic coupling of the inductor current with the eddy currents induced in the surface being heated, becomes very weak and is greatly inferior to that found in other types of induction systems, for instance, those consisting of an inductor which encloses the part being heated.

The designed induction system can be considered as a two-loop one, in which the primary loop is the inductor winding proper, while the secondary loop is the one equivalent to the eddy current field in the item being heated. This loop acts as the electric load for the inductor winding.

It is rational to perform the above induction system design by the method of equivalent circuits [1, 2]. The parameters of these circuits should be determined allowing for the structural features of the object under study.

For the two-loop system, the equivalent circuit [1, 2] shown in Figure 2, is valid where r_1 is the resistance of the inductor winding; r_2 is the resistance to passage of eddy currents in the item, while the reactive parameters of the equivalent circuit are given by the following equations:

$$\begin{aligned} X_{s1} &= 0.5\,(X_1 - X_2 + X_{k12}),\\ X_{s2} &= 0.5\,(X_2 - X_1 + X_{k12}),\\ X_{12} &= 0.5\,(X_1 + X_2 - X_{k12}), \end{aligned} \qquad (1)$$

where the design parameters of scattering (designated by s index) and of mutual inductance X_{12} depend on the ratio of the inherent reactances of the loops of inductor X_1, equivalent loop of currents in item X_2 and short-circuit resistance of these loops X_{k12}, determined allowing for the internal reactances of inductor x_{i1} and item x_{i2}. The following relationships $X_{s1} + X_{s2} = X_{k12}$; $X_{s1} + X_{12} = X_1$; $X_{s2} + X_{12} = X_2$ are valid, this meeting the necessary conditions of the equivalent circuit adequacy.

As can be seen from the structure of equations of system (1), X_{s1} parameter includes just x_{i1}, while X_{s2} includes only x_{i2}, whereas X_{12} does not include any internal reactances, as they are incorporated into the last equation of system (1) under different

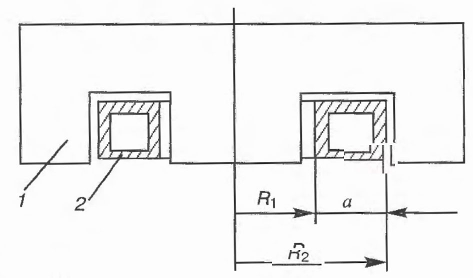

Figure 1. Schematic of an inductor with the magnetic core for heating flat surfaces of the items: *1* — magnetic core; *2* — turn (inductor winding)

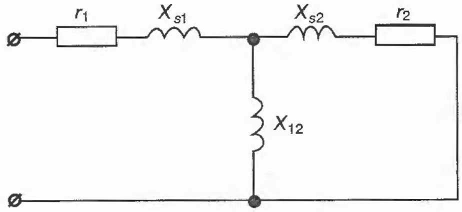

Figure 2. Equivalent circuit of two-loop induction systems

signs. This is in agreement with the physical concepts on the process of electromagnetic induction in two magnetically-coupled loops.

If the inductor winding has several turns, the resistances should be reduced to the same number of turns by calculation, using the method described in [1, 2]. In this case it is convenient to apply the method of reduction to one turn.

Based on the circuit given in Figure 2, for equivalent resistances of the system we can write [3]: $r = r_1 + r'_2$; $X = X_{s1} + X'_2$. Here r'_2 and X'_2 are secondary loop resistances reduced to inductor current

$$r'_2 = Cr_2, \tag{2}$$

$$X'_2 = C\left[X_{s2} + \frac{X_{s2}^2 + r_2^2}{X_{12}}\right], \tag{3}$$

while the coefficient of parameters reduction by current, is found from the following equation:

$$C = \frac{I_2^2}{I_1^2} = \left[\left(\frac{r_2}{X_{12}}\right)^2 + \left(1 + \frac{X_{s2}}{X_{12}}\right)^2\right]^{-1}. \tag{4}$$

The known methods of the electric circuit theory are used here to calculate from the equivalent circuit, the voltages, currents and powers in all the elements of the induction system.

The above procedure provides sufficiently accurate calculation results and has been tested many times when solving applied problems [1, 2]. The main issue here is the degree of substantiation in determination of r_1, r_2, X_1, X_2 and X_{12} parameters of the induction system. Let us consider this issue in greater detail.

Calculation of ohmic resistances. Inductor and load resistances can be found from the following equation:

$$r = \rho\,\frac{l_{av}}{\Delta\Pi}\,k_l a_R, \tag{5}$$

where ρ is the specific resistance measured on samples of inductor and load metal at constant current; $l_{av} = \pi d_{av}$ is the average length of current path; $\Delta = \sqrt{2\rho/\omega\mu}$ is the depth of current penetration into the inductor or load metal; $\omega = 2\pi f$ (f – frequency of inductor current); μ is the magnetic permeability of the inductor or load material; Π is the width of the zone of current flowing, for the inductor it is equal to inductor wire half-perimeter, for the load $\Pi_2 = a/k_R$ and $k_l = 1$ are assumed (k_R is the Rogovsky coefficient or similar values, allowing for the drop in resistance through current spreading in the load with the greater gap; which will be considered below); k_l is the coefficient of losses increase, as a result of non-uniform distribution of current density in the inductor winding [1]:

$$k_l = \left(\frac{(\alpha - 1)}{\ln\alpha}\right)^2 \frac{1}{\alpha}, \tag{6}$$

where $\alpha = R_2/R_1$ is the ratio of the outer and inner radius of the inductor turn.

Considering that the effects of losses increase because of non-uniform distribution of current density and losses decrease due to current flowing over onto the side surfaces of the inductor turn, are compensated to a certain degree, it can be assumed without impairing the accuracy of calculations, that the current in the inductor flows only on the turn surface that faces the item being heated, i.e. $\Pi = a$, $k_l = 1$. The known coefficient of current ousting in the turn, placed into the magnetic core slot, further contributes to the accuracy of such an assumption.

Equation (5) includes the Neumann coefficient a_R equal to a unity for nonmagnetic materials and determined for ferromagnetic materials from the following equation [4]:

$$a_R = \frac{4n}{3n + 1}\sqrt{1 + \sin\psi}, \tag{7}$$

where n is the power index of a parabola approximating the basic curve of steels magnetisation; ψ is the angle of hysteresis losses. The average value of this coefficient for structural steels is 1.4.

Complex impedances of the metal in case of current passage in the inductor winding and load, are calculated from the following equation:

$$Z_i = r + jx_i = (a_R + ja_X)\,\frac{\rho l_{av}}{\Delta\Pi}, \tag{8}$$

where $j = \sqrt{-1}$, while $a_X = \sqrt{1 - \sin\psi}$ is the Neumann coefficient for internal reactance x_i of ferromagnetic bodies [4], its average value for structural steels being $a_X \approx 0.85$. For non-magnetic materials it is equal to a unity.

Calculation of the inherent inductive reactance of the loops. These reactances are included into equations (1) and are determined only as inherent reactances, ignoring the influence of the other loop. In the theory of electrical generators, motors and transformers, the so defined reactances are called open-circuit resistances.

It is rational to assume the calculation model presented in Figure 3 for calculation of the inductive reactance of the loops in the presence of the magnetic core. The model assumes that practically all the current flows over the loop surface facing the load (which was substantiated above), and that the magnetic core can be replaced by a ferromagnetic half-space with magnetic permeability $\mu \to \infty$, as high-frequency magnetic cores are designed for operation at saturation levels significantly lower than the induction of the magnetic core material saturation. Therefore, calculation can be performed by the classical method of mirror reflections, which enables the inductive reactance of the loop with the magnetic core to be calculated as a double inductive reactance of the loop in a free space.

Inductive reactance at a high frequency can be found with not more than 10 % error, using the dual magnetic analog of the Holm equation for determination of contact resistance $X_x = \omega\lambda$ ($\lambda = \mu_0 2R_1$ is the permeance) [1]. Thus, for a loop with a magnetic core $X = 2X_x$.

Inductive reactance (allowing for the magnetic core) can be determined more precisely (with less than 3 % error) from the following equation [5]:

$$X = 0.81\omega\mu_0\pi R_1 k_i, \qquad (9)$$

where $k_i = 0.5(\alpha^2 - 1)/\ln\alpha$ for wide turns of the inductor winding allowing for the non-uniformity of current density distribution over their cross-section, or $k_i = (\alpha^2 + \alpha + 1)/3$ for thin turns and turns with a large radius of the inner hole. In the latter equation k_i coefficient tends to a unity at the ratio $R_2/R_1 = \alpha$ close to a unity.

With the increase of the gap between the inductor and the load, the radius of the equivalent turn of the load is reduced by a value determined with Rogovsky coefficient $R_{2\text{load}} = R_1/k_R$. When the inherent inductive reactance is calculated, this value is substituted into equation (9).

The reactance calculated from equation (9), is added to the internal reactance found from equation (8). This completes the calculation of the inherent inductive reactance of the inductor and load loops.

Note that for inductors with a wide turn, the inherent internal inductive reactance can be calculated from the following equation [1, 6]:

$$Z_i = r + jx_i = (a_R + ja_X)\frac{2\pi\rho}{\Delta\ln\alpha}. \qquad (10)$$

Short-circuit resistance of loops of inductor *1* and load *2* is calculated by the Kapp–Rogovsky formula for half of the air space between the thin windings located at the distance of $2g$ from each other (Figure 4) [1]:

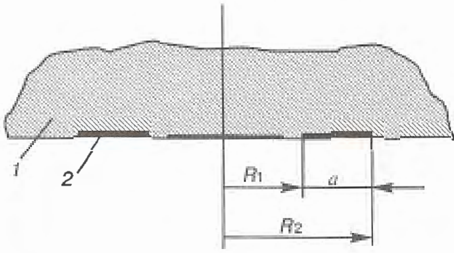

Figure 3. Design schematic for determination of the inherent reactance of flat closed electric loops in the presence of a magnetic core: *1* — magnetic mirror; *2* — inductor turn

$$X_{k12} = \omega\mu_0 \frac{l_{avg}}{a} k_R. \qquad (11)$$

The method of allowing for the load by its replacement by a mirror reflection of the inductor winding relative to the load surface, is frequently used in such calculations and does not introduce any significant error because of the non-ideal surface of the load as a magnetic mirror [1, 6]. In addition, such an approach allows taking into account the spreading of the current density in the load under the inductor turn, which is not always precisely known a priori.

Rogovsky coefficient $k_R = 1 - g/\pi a$ known from the theory of transformers, is determined for systems of rectilinear electric buses (windings) located between ideal magnetic cores. In this case, these are circular loops. On the other hand, it is desirable to apply the Rogovsky coefficient in calculations in view of the simplicity of its determination.

Earlier studies showed [6] that application of Rogovsky equation provides results with an acceptable engineering accuracy in calculation of the short-circuit resistance of circular loops provided $\beta > 4$ ($\beta = \pi R_1/2g$) at a given α. This condition is satisfied for a large number of induction systems of the type under consideration, as $R_1 > g$ is always selected to achieve an acceptable efficiency factor. Calculation error in this case is 4 – 8 %. At $\beta < 4$ Rogovsky coefficient has no physical meaning any more, as it becomes less than zero.

Under such conditions, short-circuit resistance should be calculated by equation (11), where $l_{av} = 2\pi R_{av} = 2\pi a/\ln\alpha$, while k_R coefficient is replaced by k_s coefficient equal to [6]

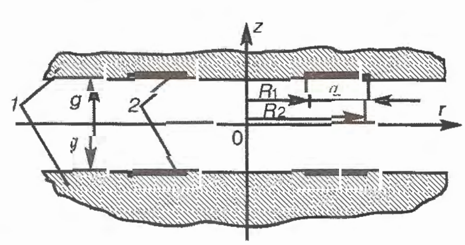

Figure 4. Calculation of the short-circuit resistance of cylindrical loops in the presence of magnetic cores: *1* — magnetic cores; *2* — inductor turns; *3* — air gap

$$k_s = 1 - 8(\pi^2 \ln\alpha)^{-1} \times \times \sum_{n=1,3,\dots}^{\infty} n^{-2}[K_0(n\beta\alpha)\, I_0(n\beta\alpha) + + K_0(n\beta)\, I_0(n\beta) - 2K_0(n\beta\alpha)\, I_0(n\beta)]. \quad (12)$$

It allows for the influence of the geometrical parameters of the studied system; $I_0(x)$ and $K_0(x)$ are zero order modified Bessel's functions of the first and second kind [7].

In terms of theory, it is interesting to determine the limit to which k_s tends, when the gap is increased to infinity, i.e. at $\beta \to 0$. Considering that $I_0(0) = 1$, $K_0(x \to 0) \approx -\ln(x)$ [8], substituting these expressions into equation (12), we will have

$$k_s = 1 - 8\pi^{-2} \sum_{n=1,3,\dots}^{\infty} n^{-2} = 0, \quad (13)$$

which corresponds to theoretical concepts of the nature of electromagnetic coupling of the electric loops, and is a test of the validity of the derived equations, as regards correspondence to their limit modes. The latter equation takes into account that [7]

$$\sum_{n=1,3,\dots}^{\infty} n^{-2} = \pi^2/8.$$

As $n = 1, 3, \dots$; $\beta = \pi R_1/2g$ and $\alpha = R_2/R_1$ is always greater than a unity, equation (12) can be simplified, using the known asymptotic expansions of the Bessel's functions [7], accurate to the second decimal digit with the Bessel's function argument greater than a unity, from which it follows that

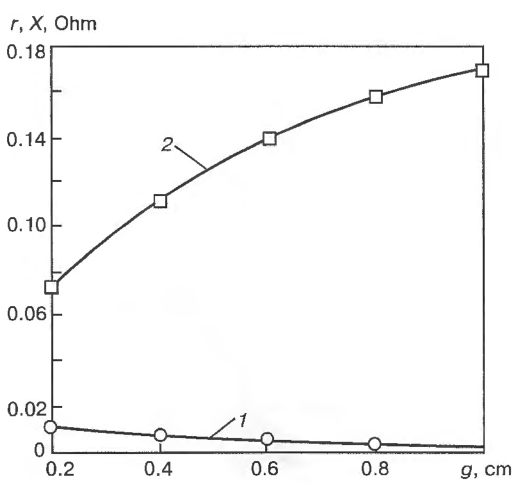

Figure 5. Dependence of electric parameters of the inductor on the gap between the inductor and load: *1* — ohmic resistance of the inductor; *2* — reactance of the inductor

$$K_0(cx)\, I_0(dx) = (2x)^{-1}(cd)^{1/2}\exp(-x(c-d)),$$

where x is the variable; c, d are the arbitrary parameters.

Taking into account the simplifications made, equation (12) can be written as

$$k_s = 1 - 4(\pi^2\beta \ln\alpha)^{-1} \sum_{n=1,3,\dots}^{\infty} n^{-3} \times \times [1 + \alpha^{-1} - 2\sqrt{\alpha^{-1}}\exp(-n\beta(\alpha - 1))]. \quad (14)$$

The sum of series $\sum_{n=1,3,\dots}^{\infty} n^{-3} = 7/(8\zeta(3)) \approx 1.052$, where $\zeta(p)$ is Riemann's function [7]. In view of that, equation (14) can be rewritten as

$$k_s = 1 - 4.208(\pi^2\beta \ln\alpha)^{-1}\, [(1 + \alpha^{-1}) - - 2\sqrt{\alpha^{-1}} \sum_{n=1,3,\dots}^{\infty} n^{-3} \exp(-n\beta(\alpha - 1))]. \quad (15)$$

It is obvious that the series in equation (15) diminishes very rapidly, and with the accuracy to the second decimal point, we can limit ourselves to calculation of just the first term of the series. Thus, we finally get

$$k_s = 1 - 4.208\, (\pi^2\beta \ln\alpha)^{-1}[(1 + \alpha^{-1}) - - 2\sqrt{\alpha^{-1}} \exp(-\beta(\alpha - 1))]. \quad (16)$$

Obviously, equation (16) is much more convenient for calculations, than equation (12).

In order to verify the proposed procedure of inductor design, we have performed calculations and measurement of the electrical parameters of the inductor–load system, in which an inductor with a ferrite magnetic core (see Figure 1) was used. The dimensions of the inductor turn $R_1 = 10$ mm, $R_2 = 18$ mm, $a = 8$ mm. The load was a steel plate, with its thickness ($d = 2$ mm) selected to be greater, than the depth of current penetration into the plate at the current density at which experiments were conducted (440 kHz). This allowed determination of the load parameters from the equations for the plane electromagnetic wave.

The equivalent ohmic resistance and reactance of the inductor–load system, was determined from the circuit shown in Figure 2, by the known equations of the theory of electric circuits. The results of calculation of the ohmic resistance and reactance of the inductor–load system, are given in Figure 5, and of the efficiency of power factor $\cos\varphi$ and co-

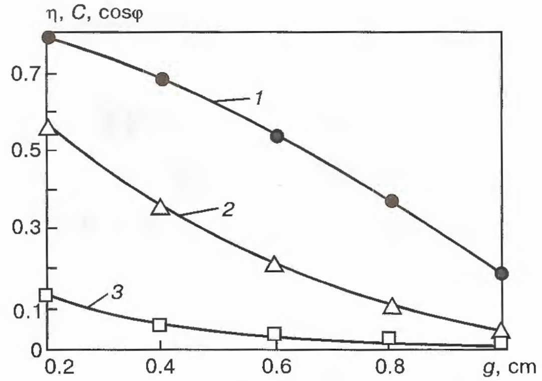

Figure 6. Dependence of the efficiency η (*1*), coefficient of parameter reduction *C* (*2*) and power factor cosφ (*3*) on the gap between the inductor and load

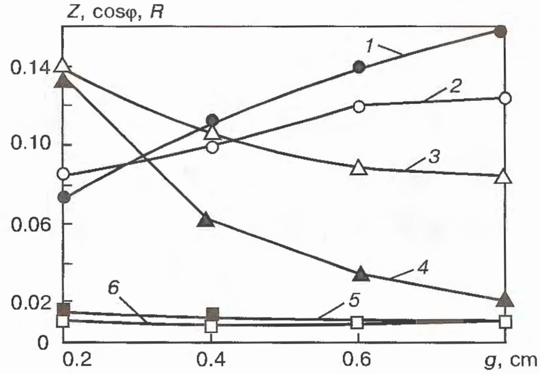

Figure 7. Results of comparison of the calculation and experimental data: *1* — *Z* (calc.), Ohm; *2* — *Z*, Ohm; *3* — cosφ; *4* — cosφ (calc.); *5* — *R* (calc.), Ohm; *6* — *R*, Ohm

efficient of parameters reduction *C* are shown in Figure 6, depending on the size of the air gap *g*. It is seen that a rational application for this inductor–load system would be with the air gaps less than 0.5 cm.

Figure 7 gives the calculated and measured values of the resistance and impedance, as well as the power factors of the studied inductor–load system.

Note that the coincidence of the calculated and measured resistances of the inductor–load system up to a gap of about 0.5 cm is satisfactory, and then the discrepancy of the results is increased. This is especially true for the power factor.

The performed analysis of this phenomenon showed that it is related to saturation of the inductor magnetic core with the increase of the air gap. This is due to the fact that in this case the magnetic coupling between the inductor winding and the field of current in the load deteriorates, magnetisation current rises, and the magnetic induction in the magnetic core also increases with lowering of the mutual inductive reactance X_{12} [2]. Calculation shows that in the case described in the paper, at the increase of the gap from 0.2 up to 0.8 cm, the magnetic induction in the magnetic core rises by 29 %, thus resulting in its saturation. This, in its turn, results in lowering of the inductor inherent reactance and further on, of the inductor–load reactance. In this case also, the degree of increase of the inductor–load system reactance becomes smaller as the air gap becomes larger, while the ohmic resistance of the system remains practically unchanged. This leads to a more slow decrease of the power factor with the gap increase, compared to the calculated value that can be traced directly by the equation $\cos\varphi = (1 + (X/R)^2)^{-1/2}$. With further increase of the gap, the reactance of the inductor–load system is transformed into the inherent reactance of the inductor with a magnetic core, with an appropriate mode of its saturation, the power factor being equal to cosφ of the inductor at no load.

As was noted above, however, these modes of inductor–load system operation are beyond the recommended modes, in terms of reaching the admissible efficiency of the item and magnetic core heating. Therefore, ignoring the saturation is reasonable for practical calculations and provides a simplified procedure of valid engineering calculations with an accuracy sufficient for practical purposes.

REFERENCES

1. Lebedev, V.K., Pismenny, A.S., Yavorsky, Yu.D. (1976) Design of an inductor for high-frequency welding. *Avtomaticheskaya Svarka*, **3**, 29 – 34.
2. Pismenny, A.S. (1994) Equivalent diagrams and procedures of calculation of the induction welding and electrothermal devices. *Ibid.*, **4**, 1 – 4.
3. Slukhotsky, A.E., Ryskin, S.E. (1974) *Inductors for induction heating*. Leningrad: Energia.
4. Pismenny, A.S. (1988) Calculation of a two-dimensional electromagnetic field at an excitation field sinusoidal in space. *Tekhn. Elektrodinamika*, **4**, 25 – 30.
5. Pismenny, A.S. (1997) Electromagnetic field and inherent resistances of inductors for heating flat surfaces of items. *Avtomaticheskaya Svarka*, **11**, 28 – 31.
6. Pismenny, A.S. (1979) Calculation of the inherent reactance of the pole winding. *Tekhn. Electrodinamika*, **2**, 4 – 8.
7. Dwait, G.B. (1973) *Tables of integrals and other mathematical equations*. Moscow: Nauka.
8. (1979) *Reference book on special functions with equations, graphs and a table*. Ed. by M. Abramovits and I. Stigan. Moscow: Nauka.

EFFECT OF METHOD OF WEAR-RESISTANT SURFACING ON THE DISTRIBUTION OF A STRENGTHENING PHASE IN DEPOSITED METAL

V.A. BAGROV and **V.N. KALIANOV**
Ukrainian Engineering-Pedagogical Academy, Kharkov, Ukraine

ABSTRACT

Peculiarities of effect of the method of surfacing on distribution of a strengthening phase in height of the deposited metal depending on endogeneous or exogeneous nature of its formation are considered. It was established experimentally that the application of surfacing with a dead filler «levels» the distribution of strengthening phases and stabilizes the characteristics of wear resistance and microhardness of the deposited metal.

Key words: *surfacing, flux-cored wire, endo- and exogeneous carbides, wear resistance*

The increase in service life of machines and mechanisms is one of the most important links of a general problem of improving the quality of products. The wear of materials depends on many quite different technological situations and service conditions. According to data of [1, 2] the following types of wear are most often observed: corrosion, selective, abrasive, etc.

At present the surfacing materials and technologies of their deposition on the components operating under different conditions of wear have been developed [3]. When surfacing materials are improved a special attention is paid to the materials science developments of wear-resistant sparsely-alloyed alloys [4]. Service characteristics of the deposited metal designed for operation under different conditions of wear are determined, first of all, by the system of alloying, different phase composition and structure. Here, the deposited metal has a heterogeneous structure consisting of a tough matrix (bainite, austenite, etc.) and hard crystals of a strengthening phase (TiC, $(FeMo)_3C$, $(FeCr)_{23}C_6$, etc., which are introduced for increasing the level of wear resistance and hardness. The increase in wear resistance is of a special interest in use of sparsely-alloyed alloys with a structure of a metastable austenite of C–Cr–Mn–Ti system on iron base in which carbon is bound into carbides Ti–C and Cr–C. Titanium is a main carbide-forming element in these alloys. Titanium carbides have a higher hardness than carbides Cr_7C_3, VC, Mo_2C, $(FeCr)_{23}C_6$ that influences the wear resistance [2, 5].

Table 1. Properties of deposited metal

No. of alloy	*Content of carbide phase, vol.%*	*Heat of carbide formation, J*	*HRC hardness*	*Coefficient of relative wear resistance,* ε
1	12.25	42666.75	51 – 52	~ 3.50
2	12.76	44443.00	49 – 52	~ 3.40
3	11.30	39358.00	49 – 52	~ 3.50
4	2.58	8986.00	48 – 52	~ 1.59
5	3.31	11529.00	48 – 50	~ 1.80
6	5.30	18460.00	49 – 52	~ 2.35
7	3.26	Not determ.	47 – 49	~ 1.60
8	4.08	Same	48 – 50	~ 2.00
9	2.32	»	46 – 48	~ 1.40
10	3.04	»	46 – 49	~ 1.60

Note. Reference of relative wear resistance is alloy with $Ni_{eq} = 4 - 8$; $Cr_{eq} = 8 - 10$

Table 2. Chemical composition of deposited alloys

No. of alloy	*Methods of surfacing and use of strengthening phase*	*Mass share of elements, %*				
		C	*Cr*	*Mn*	*Ti*	*Si*
1	Under agglomerated flux	2.8	4.80	9.70	5.00	1.4
2	Ti + C	2.6	4.80	9.00	5.60	1.3
3		2.3	4.80	9.80	5.20	1.4
4	Flux-cored wire with a dead filler Ti + C	0.5	3.36	5.86	1.69	1.8
5		0.7	4.36	7.60	2.19	1.7
6		1.2	4.72	8.22	2.38	1.8
7	The same	0.7	3.60	6.10	2.00	1.4
8	TiC	0.9	3.00	7.40	2.20	1.7
9	Flux-cored wire	0.5	3.20	5.90	1.40	1.3
10	TiC	0.7	3.10	6.10	1.30	1.5

Note. Surfacing conditions are as follows: $I = 310 - 330$ A; $U_a = 34 - 36$ V; $v_s = 23.7$ m/h; electrode stickout $l = 45$ mm.

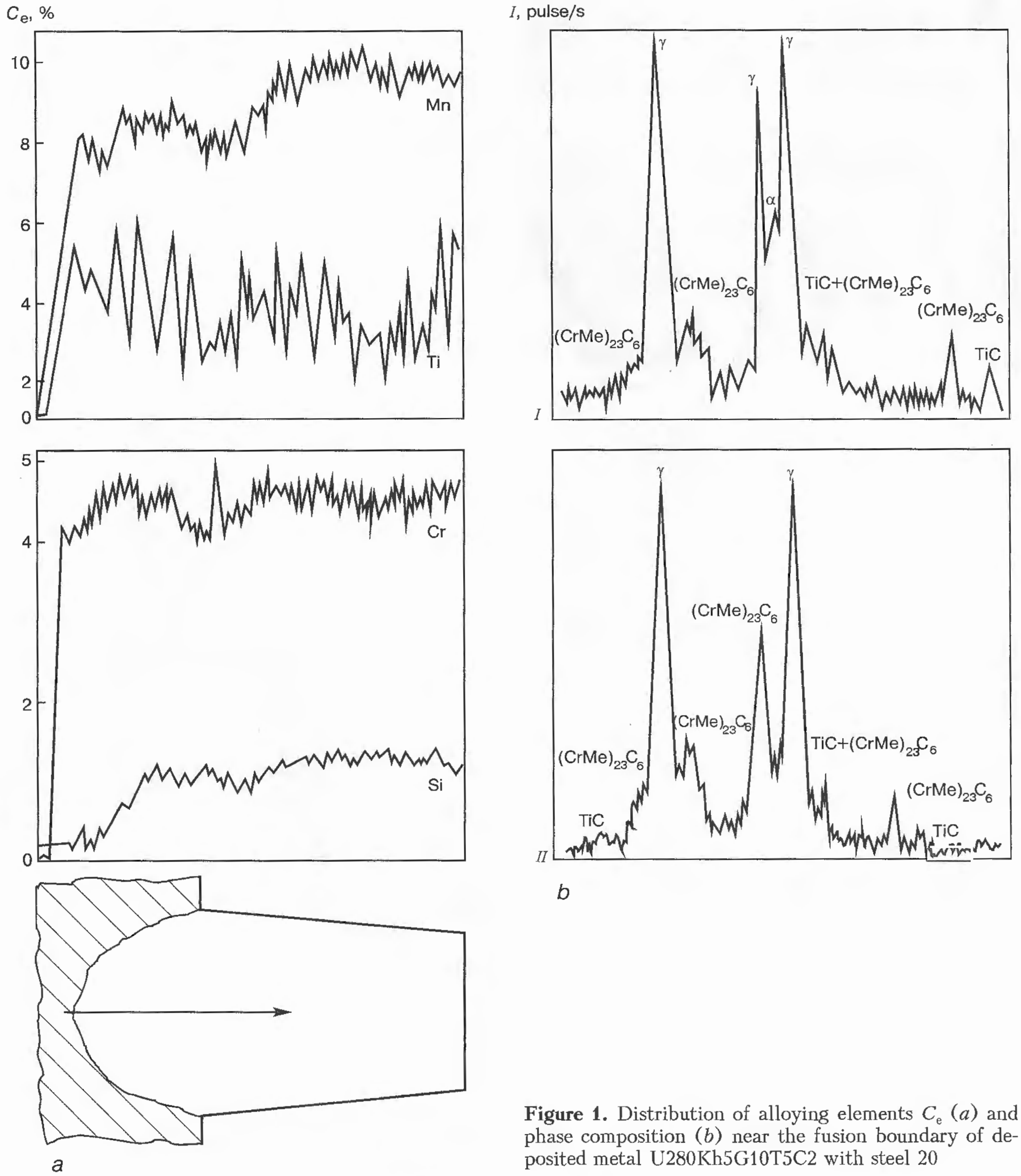

Figure 1. Distribution of alloying elements C_e (*a*) and phase composition (*b*) near the fusion boundary of deposited metal U280Kh5G10T5C2 with steel 20

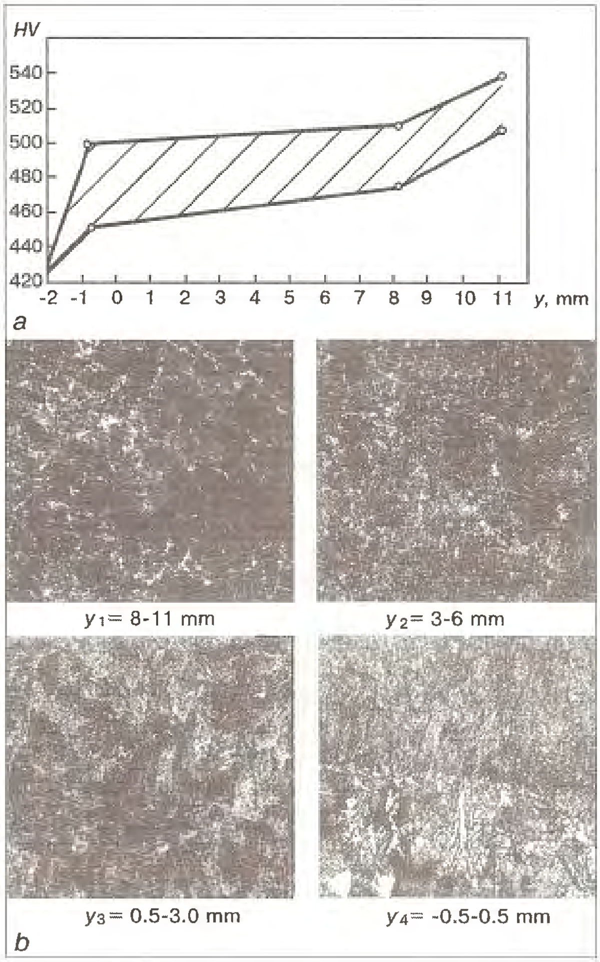

Figure 2. Change in *HV* hardness (*a*) and microstructure (*b*) in height y of deposited metal U280Kh5G10T5S2

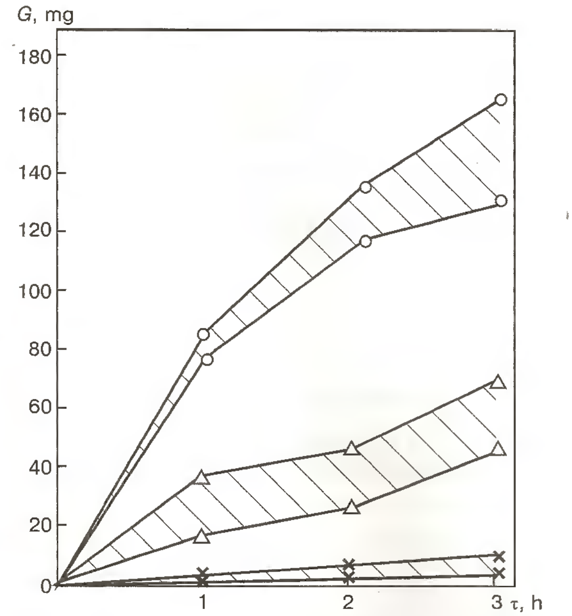

Figure 3. Wear G of steel and deposited metal: O — 50KhV2F; Δ — 60Kh5M1FT; × — 120Kh4T3GS

Analysis of parameters that influence the dissolution of alloying elements in iron-carbon melts shows that the rates of dissolution are decreased in the Ti–Si–Cr–Mo system. In addition, the decrease in carbon content in the melt leads to the increase in rate of dissolution of chromium. However, for the titanium carbides the rate of dissolution is constant and does not depend on the concentration of carbon in the liquid metal [6].

The structure formation during solidification of Fe-based alloys with a concentration of 0.5 – 2.0 % C and 0.5 – 2.0 % Ti was examined in [7]. First, the titanium carbide is formed, the liquid around it is depleted with carbon and titanium. When concentrations of carbon or titanium are changed the hypereutectic, hypoeutectic and eutectic alloys, containing titanium carbides, can be formed. The carbide phase in the deposited layer can be produced by two methods, such as endogeneous (MeC) and exogeneous (Me + C).

The use of the exogeneous method promotes the increase in an internal heat both of the weld pool and the metal during solidification (Table 1). The depletion of solidifying melt with carbon due to carbide formation changes the temperatures of a martensitic transformation and, probably, the susceptibility of the deposited metal to the formation of crystalline cracks. The distribution of a carbide phase in the deposited metal influences greatly the wear resistance.

The effect of method of using a strengthening phase on its distribution in electric arc surfacing with coated electrodes was investigated [8].

The distribution of carbides in the deposited metal was investigated for different types of a mechanized surfacing (Table 2). The surfacing was performed on 25 mm thick plates of steels 20 and 45 by a tractor TS-17 and a head A-1416 using experimental flux-cored wires, suspended devices for feeding dead flux-cored wire to a head part of the weld pool and flux AN-22 and also using 2 mm diameter wire of Sv-08A grade and an agglomerated flux on CaF_2 + (Na_2O–K_2O) base of the similar system of alloying. Hardness was measured by TK-2 meter (in scale C) and by Vickers in TP unit. Determination of hardness and examination of structure in height of the deposited metal were performed in the following ranges: upper bead — y_1 = = 8 – 11 mm (n = 12, x = 520, s^* = 2.57); near the upper bead — y_2 = 3 – 6 mm (n = 11, x = 502, s^* = 2.84); middle of lower bead — y_3 = 0.5 – 3.0 mm (n = 7, x = 501, s^* = 3.64); in fusion line — y_4 = –0.5 – 0.5 mm (n = 8, x = 495, s = 1.936), where n is the number of measurements, x is the mean arithmetic value of hardness, s^* is the root mean square deviation. Quantitative carbide analysis was made by a spot method of A.A. Glagolev [9]. Microhardness was measured in PMT-3 unit at 1 and 2 N loading on «finger-type» samples of

10 mm diameter with an oblique cutting of the working part (10 – 15°). X-ray phase analysis of samples was performed in DRON-3 unit at K_{α}-Co radiation (monochromatic) using Bregg-Brentano scheme.

The effect of number of titanium carbides after wear on microhardness scattering in height of samples made from 60Kh5M1FT (C — 0.6; Cr — 5.0; Mo — 1.0; V — 1.0; Ti — 0.5 wt.%), 120Kh4T3GS (C — 1.2; Cr — 4.0; Ti — 3.0; Mn — 1.0; Si — 1.0 wt.%) alloys and steel 50KhV2F (C — 0.5; Cr — 1.0; W — 2.0; V — 1.0 wt.% after oil quenching at 1153 K, air tempering at 733 K) was examined. Test conditions for wear were as follows: test duration $\tau = 3$ h, temperature of friction rod $T = 1023$ K, pressure $P = 1.5$ MPa, rate of displacement of samples $v = 16.66$ cm/s, material of friction rod — steel R18.

Samples for microanalyzing were subjected to a combined etching (base metal was etched in 4 % alcohol solution of the nitric acid, and deposited metal — in electrolyte, mass share, %: 17 — chomium anhydride; 230 — orthophosphoric acid; 100 — sulphuric acid; 17 — water). Before measurements of microhardness and X-ray analysis the surface cold-worked layer was etched in 50 % HCl solution or concentrated perchloric acid with an addition of a hydrogen peroxide. Mixture of nitric and perchloric acids was also used (1:3). The properties of the deposited metal were estimated from wear resistance [5, 10], hardness and microhardness.

The distribution of alloying elements and phase composition of the deposited metal is given in Figure 1, where each peak has its phase. During phase composition analysis TiC, $(CrMe)_{23}C_6$, γ-Fe, α-Fe were revealed. In all deposits the metal hardness was equal to *HRC* 48 – 52 (Table 1).

At three-layer surfacing using an agglomerated flux the microstructure of the bead at the upper edge was as follows: ledeburite (austenite 60 – 70 %) and inclusions of thread-like carbides.

In flux-cored wire surfacing with a feeding of a dead filler (Table 2) the more uniform distribution of carbides as compared with surfacing using an agglomerated flux is observed. The flux-cored wire surfacing with a titanium carbide in the charge of a dead filler provides also a uniform distribution of carbides in the weld section. However, 3 – 4 layer surfacing is required to produce a preset chemical composition of the deposited metal.

Distribution of hardness and change of structure in the height of the deposited metal is shown in Figure 2.

The noticeable improvement of wear resistance and stability of the wear were attained when a large amount of titanium carbides are present (Figure 3). In alloys with a large amount of titanium carbides after wear tests the scattering of microhardness was by 20 – 25 % less in height of the samples ($z = 0 - 900$ μm) as compared with alloys 60Kh5M1FT ($\Delta H\mu = 2000$ MPa in the deposited metal 120Kh4T3GS against $\Delta H\mu = 3700$ MPa in alloy 60Kh5M1FT).

CONCLUSIONS

1. The distribution of a strengthening phase in the deposited metal depends greatly not only on the endogeneous or exogeneous method of introducing carbides, but also on the technology of surfacing.

2. Stable characteristics on wear resistance and microhardness of the deposited metal make it possible to use surfacing with a dead filler and large amount of titanium carbides.

REFERENCES

1. Garkunov, D.N. (1985) *Tribotechnique*. Moscow: Mashinostroyeniye.
2. Eyre, T.S. (1979) Wear resistance of metals. *Treatise on Materials Science and Technology*, **13**, 363 – 442.
3. Livshits, L.S. (1991) Surfacing materials and technology of surfacing for increase in wear resistance and restoration of machine parts. *Svarochnoye Proizvodstvo*, **1**, 15 – 17.
4. Paton, B.E. (1998) Problems of welding at the threshold of centuries. In: *Proc. of Int. Conf. on Welding and Related Technologies to the XXI Century*. Kyiv: PWI.
5. Kalianov, V.N. (1997) Structure and characteristics of wear-resistant sparsely-alloyed deposited metal. *Svarochnoye Proizvodstvo*, **4**, 13 – 17.
6. Lepinskikh, B.M., Vostryakov, A.A. (1978) *Dissolution of solid phases on metallurgical melts*. Moscow: Nauka.
7. Snagovsky, L.M., Snagovsky, V.M., Taran, Yu.N. *et al.* (1976) Crystallization of eutectics on phase of niobium and titanium carbides in iron alloys. In: *Carbides and alloys on their base*. Kyiv: Naukova Dumka.
8. Kakovkin, O.S., Darakhvelidze, Yu.D., Starchenko, G.G. (1989) Peculiarities of alloying of deposited metal with titanium carbide in arc wear-resistant surfacing. *Svarochnoye Proizvodstvo*, **5**, 41 – 42.
9. Pilyushenko, V.L., Vinokur, B.B., Kondratyuk, S.E. *et al.* (1984) *Handbook on practical metals science*. Kyiv: Tekhnika.
10. Danilchenko, B.V. (1992) Selection of wear-resistant deposited metal for operation in the conditions of abrasive wear. *Svarochnoye Proizvodstvo*, **5**, 31 – 32.

UPDATING OF WELDING RECTIFIER VDU-504

S.V. PUSTOVOIT
The E.O. Paton Electric Welding Institute, NASU, Kyiv, Ukraine

ABSTRACT

The updated power source VDU-504 which can provide current pulses of 0.1 – 4.0 s duration periods is described. The schematic diagram of the source, calculation of its elements, table of conditions and an oscillogram of the output voltage are given.

Key words: *arc welding, electromagnetic control, power source, electromagnetic forces*

Over the recent years the great attention is paid to the effect of welding current pulses on the pool, processes of its solidification and service characteristics of the weld metal [1 – 4]. The effect of a pulsed condition on the weld quality was proved experimentally.

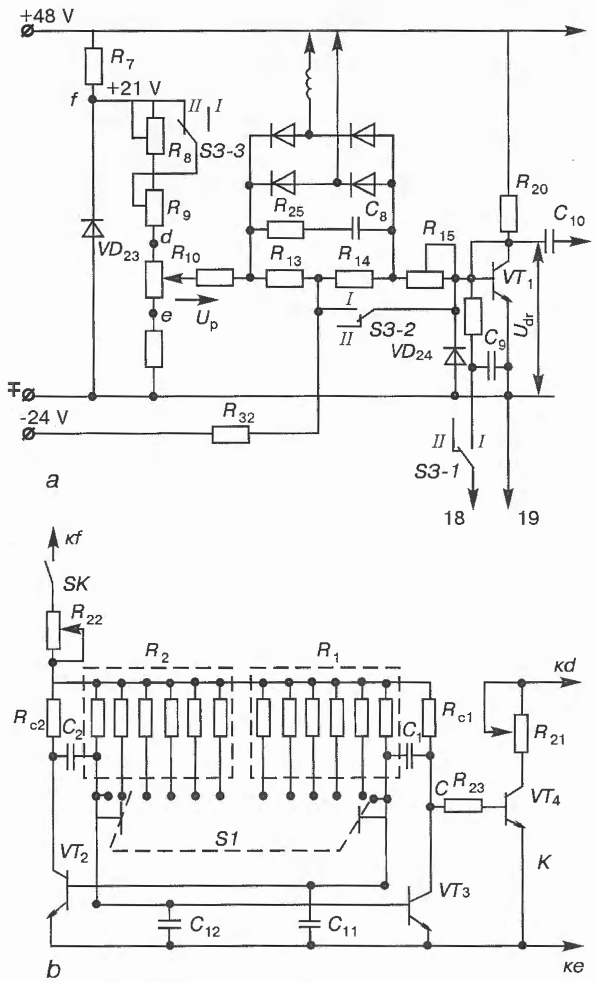

Figure 1. Schematic electrical diagram of system for the rectifier phase control: *a* — VDU-504; *b* — developed system

In addition, when the periodicity of pulses with free oscillations of the pool are matched the penetration depth is increased [2], all other conditions being equal, the welding efficiency is increased and the electric energy is saved essentially. To attain this matching it is necessary to investigate additionally the movement of pools of different sizes and compositions, because of a lack of information on this phenomenon.

Unfortunately, the pulsed-current sources, used in the experiments, are not described sufficiently (there is only advertising information about a unit of a synergetic control of the process of a pulsed-arc welding [5], used in a set with a rectifier VDU-1201 and a welding tractor ADF-1201).

In the present article a pulsed-current source developed on the basis of the welding rectifier VDU-504 is described. The high duration of the current pulses made it possible to use a phase method of their amplitude control. The simplified schematic diagram of control of thyristors of the rectifier VDU-504, used as a technical base, is given in Figure 1, *a* [6]. Its welding current determines the preset voltage U_p acting in the circuit of the thyristor VT_1 base.

A special device has been created which controls the value of this voltage, shape and current of welding. It consists of a key K, an adjustable resistor R_{21}, connected to a resistor R_{10} and supplied by a stabilized voltage of 21 V (Figure 2).

At an open key K the arc current dependence on a preset voltage has a form

$$I_a = kU_{p\,\max}\,(l_p/l), \tag{1}$$

where l_p/l is the ratio between the length of a wire potentiometer R_{10}, from which U_p is taken, and entire its length l; k is the coefficient of proportionality between the preset voltage and value of welding current (at a linear relation between U_p and I_a).

For the above-mentioned rectifier $U_{p\,max} = 2.8$ V, $l_p = l$ and maximum value of current is equal to 500 A. Therefore, $k = 178$ A/V. When the key is closed, the value $U_{p\,max}$ is changed and arc current will be determined not only by ratio l_p/l. At series-parallel connection of R_8, R_{10}, R_{21}

$$U_{p\,max} = R_{eq} \frac{U_s}{R_8 + R_{eq}},$$

where $R_{eq} = \dfrac{R_{10} R_{21}}{R_{10} + R_{21}}$.

At preset values U_s, R_8, R_{10} we shall obtain

$$U_{p\,max} \cong \frac{3R_{21}}{200 + R_{21}}. \tag{1}$$

Therefore, the relation between I_a and U_p has a form

$$I_a \cong 178 \frac{3R_{21}}{200 + R_{21}} \cdot \frac{l_p}{l}. \tag{2}$$

Table gives data of welding current I_a at open and closed key K, $l_p/l = 0.25$; 0.50; 0.75; 1.00 and $R_{21} = 30$; 60; 90; 120; 150 Ohm.

At a periodic closing of key K the pulsed current passes the rectifier output. Its maximum value will be determined by the condition (1) and the minimum value — by the expression (2).

Key K is assembled on transistor KT315E. It is controlled by the voltage pulses supplied to its base. As the most widely used shape of the arc pulsed current is rectangular [7], so a generator of pulses of the same shape is used for the key control. Such their shape can be obtained by using multivibrators [8]. The schematic diagram of the multivibrator (Figure 1, *b*) consists of crossing collector-base links of transistors VT_2 and VT_3, realized via capacitors C_1 and C_2.

The pulse duration in transistor VT_3 (point C) is determined by the time of its staying in a closed state

$$t_{pulse} = 0.7 R_2 C_1. \tag{3}$$

The duration of period is equal to $T = t_{pulse} + t_p$, where T_p is the pause duration, determined by a duration of the capacitor discharge.

In a symmetric multivibrator $t_{pulse} = t_p$, as $R_1 = R_2$ and $C_1 = C_2$. Consequently,

$$T = 1.4\, R_2 C_1.$$

Transistors in the multivibrator circuit should operate in the saturation condition determined mainly by the value of the base current I_b. Collector current $I_c \approx \beta I_b$, therefore, the use of transistors with a high coefficient of amplification β makes it

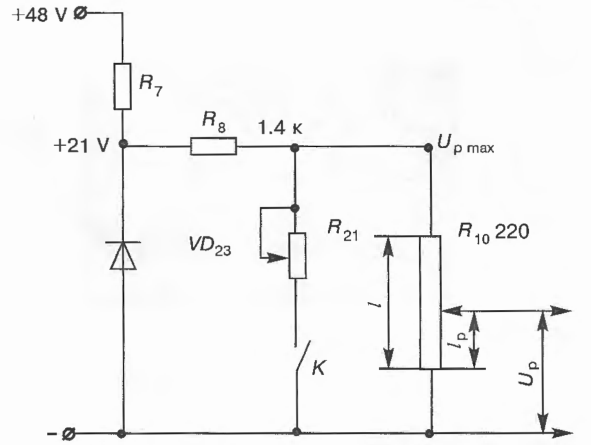

Figure 2. Simplified electrical diagram of control unit for derivation of relation between I_a and U_p

possible to obtain the saturation condition at low values of I_b. As I_b is equal to the ratio of voltage of the circuit supply to the resistance in the base circuit, then, in accordance with equation (3), the use of such transistors can control the change in pulse duration not only at the expense of the capacitance of the capacitor, but also (to a larger degree) by the resistance in the circuit of bases of the transistors. Therefore, to produce pulses of different duration at a fixed value of capacitances of the capacitors for a step adjustment of the duration a system of resistors R_1 and R_2 was used. Switching is made by a packet switch S_1.

The application of transistors with a high coefficient of amplification β can also increase the ratio between $R_1(R_2)$ and $R_{c1}(R_{c2})$ by more than 5 – 10 times (that is necessary for a stable operation of the multivibrator) [8]. This gave an opportunity to keep the steepness of the leading edge of a pulse constant in changing the pulse duration within the wide ranges. This steepness is determined by values $R_{c1}(R_{c2})$ and C (constant time of charging capacitors $Q_{ch} = R_c C$). The highest value β is typical of

Values of pulsed current I_a

l_p/l	*Resistance of shunt R_{21}*				
	30	*60*	*90*	*120*	*150*
0.25	125/17.5	125/30	125/41	125/50	125/57
0.50	250/35.0	250/61	250/82	250/100	250/114
0.75	375/52.0	375/92	375/123	375/150	375/171
1.00	500/70.0	500/123	500/165	500/200	500/229

Note: Numerator gives maximum values (open key) and denominator — minimum values (clossed key) of current.

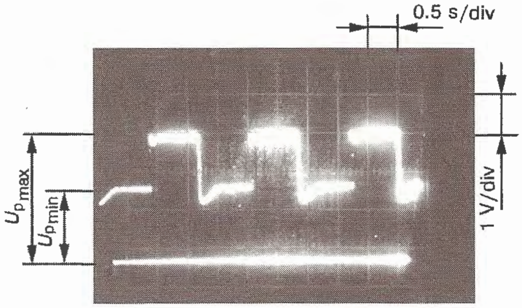

Figure 3. Oscillogram of a preset voltage

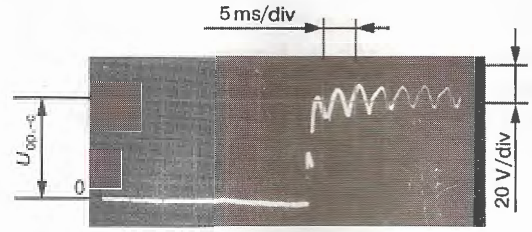

Figure 4. Oscillogram of a pulsed voltage at VDU-504 output

transistor KT315E, whose other parameters (voltage of collector-emmiter $U_{c.\text{-}e\ max}$ = 35 V, constant current of collector $I_{c\ max}$ = 100 mA) could supply multivibrator with voltage +21 V from the circuit of a phase shifting device (stabilitron VD_{23} point *f*).

The developed device was made on a separate board and connected to the circuit of VDU-504 in points *d* and *e* (Figure 1, *a*). The pulsed condition of operation of the rectifier is switched on by a switch *SK* (Figure 1, *b*). The preset voltage U_p has successive rectangular pulses with values $U_{p\ max}$ and $U_{p\ min}$ (Figure 3). At open *SK* the rectifier is operated as a direct current power source.

The smooth setting of the pulse duration inside the step is performed by an adjustable resistor R_{22} = 2.2 kOhm (Figure 1, *b*). At $R_{22} > 0$ the current of a capacitor charging is decreased, thus leading to the increase in duration of a charge and pulse.

It was established during study of a force action of the arc on the molten metal of the weld pool that the steepness of a leading edge of a pulse of the loading current is important [1]. Figure 4 shows an oscillogram of the transition process in the circuit illustrating the steepness of the leading edge.

To prevent the effect of the electromagnetic interferences on high-sensitivity circuits of bases of transistors the capacitors C_{11} and C_{12} of 0.1 μF, connected between the base and emmiter (VT_2 and VT_3, respectively) are introduced to the circuit of the multivibrator.

CONCLUSIONS

1. It was established that the updated rectifier VDU-504 makes it possible to obtain pulses of welding current with a wide range of changing the pulse amplitude and duration (from 0.1 to 4.0 s).

2. A feasibility of use of the pulsed power source in equipment with a sinergetic control of the welding condition parameters and for study of dynamic processes in the pool is demonstrated.

REFERENCES

1. Calon, K., Varga, T. (1990) On pulsed submerged arc (SA) welding. In: *Doc. Ann. Ass. of IIW Comm. IX*, Montreal, July 2 – 12, 1990. Montreal.
2. Pokhodnya, I.K., Golovko, V.V., Sheiko, P.P. (1996) Effect of conditions of submerged pulsed-arc welding on penetration depth of parent metal. *Avtomaticheskaya Svarka*, **5**, 3 – 7.
3. Pokhodnya, I.K., Golovko, V.V., Grabin, V.F. *et al.* (1997) Peculiarities of thermal cycle of submerged pulsed-arc welding. *Ibid.*, **9**, 3 – 8.
4. Grabin, V.F., Golovko, V.V., Novikova, D.P. (1995) Peculiarities of structure of weld metal in submerged pulsed-arc welding. *Ibid.*, **8**, 3 – 11.
5. Sheiko, P.P., Shevchuk, S.A., Zhernosekov, A.M. (2000) Unit of synergetic control of submerged pulsed-arc welding process. *Svarshchik*, **1**, 1 – 4.
6. Zaks, M.I., Ryvkin, A.L. (1979) Updating of welding rectifier. *Electrotech. Industry, Ser. Electric Welding*, Issue 2(53).
7. Zaruba, I.I., Lebedev, V.K., Sheiko, P.P. *et al.* (1968) Welding with a modulated current. *Avtomaticheskaya Svarka*, **11**, 35 – 40.
8. Blanter, S.G. (1967) *Industrial electronics*. Moscow: Nedra.

IN-CHAMBER LEAK DETECTION

K.S. AKOPYANTS
The E.O. Paton Electric Welding Institute, NASU, Kyiv, Ukraine

ABSTRACT

The device described is intended for detection of leaks on the side of vacuum, i.e. from the inside of a work chamber. The device comprises a funnel with a pressure gauge tube installed at its neck. The funnel is moved over the surface being examined. The leak is detected by deterioration of vacuum in the funnel registered by a vacuum gauge.

Key words: *leak detection, vacuum chamber, electron beam welding*

Manufacture of vacuum chambers for electron beam welding units involves their testing to vacuum tightness and leak detection. For this it is necessary to fix a place where air leaks from the outside into the vacuum volume, localize this place and stop the leak. The leaks are most often found in welds and seals of vacuum chambers formed during their manufacture.

Special leak detectors, e.g. of the halogen or mass-spectrometric type [1, 2], are used in vacuum facilities to detect leaks. The leak detector is connected to a chamber to be tested and the chamber is evacuated to achieve a maximum possible vacuum in it. The chamber is blown from the outside with a halogen-containing gas (in the case of using the halogen type of the leak detector) or helium (in the case of using the mass-spectrometric type of the leak detector). The gas flows into the chamber through a leak. This is registered by the leak detector, which thus determines the leak location.

However, this method is suitable only for a case where, when you blow the chamber with a gas from the outside, you know for sure whereto this gas goes. If the place in the chamber you test has some externally mounted elements (mechanisms, extra structures, coverings, etc.), blowing with gas from the outside does not allow location of the leak to be fixed.

For this case it is advisable to do leak detection from the inside of the chamber, i.e. on the side of vacuum. The E.O. Paton Electric Welding Institute made a simple device for the in-chamber detection of leaks. Schematic of the device is shown in the Figure. The device comprises funnel *1* with a pressure gauge tube *2* installed at its neck. The device is mounted on a mechanism which provides its longitudinal movement over the surface being examined (the movement mechanism is not shown in the Figure). The device and the movement mechanism are placed over the surface to be examined at a minimum gap S along the entire length of their movement. For detection of leaks at a medium vacuum in the chamber equal to $1\cdot10^{-3} - 1\cdot10^{-5}$ mm Hg, we used the PMI-2 tube (ionization pressure gauge) and the VIT-3 ionization-thermocouple vacuum gauge. For detection of leaks at low vacuum (below $1\cdot10^{-3}$ mm Hg) it is possible to use the PMT-2 tube (thermocouple pressure gauge) and the same VIT-3 vacuum gauge.

Detection of a leak is done as follows. The chamber is evacuated to achieve the maximum possible vacuum. The tube is switched on and readings of the corresponding vacuum gauge are registered. They should coincide with readings of the other vacuum gauge which measures general vacuum in the chamber. The device is moved over the surface examined. If during its movement the vacuum gauge fixes deterioration of vacuum in the funnel, this indicates that the funnel is just over the place in which the leak is located.

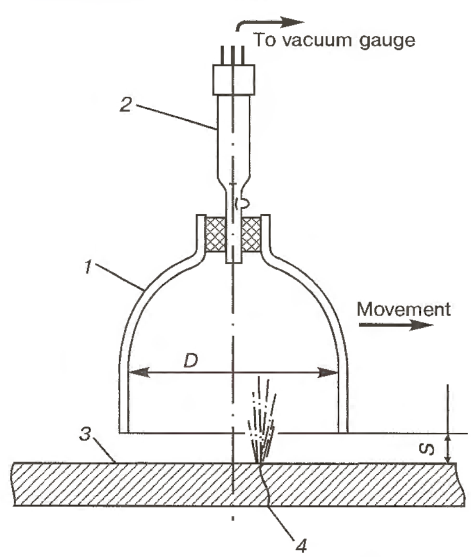

Schematic of the device for detection of leaks from the inside of a vacuum chamber: *1* — funnel; *2* — tube (pressure gauge); *3* — surface of the vacuum chamber being examined; *4* — leak

During detection of the leak the gap S between the funnel and the surface examined was set at about 10 mm (or less). The speed of movement of the device over the surface was 10 mm/s. Diameter D of the funnel was 90 mm. The presence of the leak was fixed by a change of ΔN (division) in readings of the ionization part of the vacuum gauge, as compared with a current value of N, which is calculated using the following relationship:

$$k\Delta N = \frac{D}{S},$$

where k is the dimensionless coefficient equal to 0.1 (the vacuum gauge scale has 100 divisions).

During detection of leaks the device demonstrated a high sensitivity: at a gap of $S \approx 10$ mm movement of the funnel to the place of location of a leak leads to an increase of an order of magnitude in readings of the vacuum gauge.

This device was employed for detection of leaks in manufacture and field testing of large (12 – 25 m^3) vacuum chambers of the electron beam welding units. It helped detect and then stop a number of leaks. The resulting vacuum in the chambers was at a level of $(2-3)\cdot10^{-5}$ mm Hg.

Characteristic feature of this leak detection device is that detection of a leak does not depend upon its size (in l/mm Hg/s). The leak size and the evacuation efficiency determine the maximum achievable vacuum in the chamber. The device registers a relative (in divisions of the scale) deterioration of vacuum in the funnel when it is located over the place of the leak. This relative deterioration does not depend upon the specific value of vacuum in the chamber, but is determined only by the geometry of the device (gap S and funnel diameter D).

Therefore, the use of the device proved its efficiency in detection of leaks from the inside of an evacuated volume. The device is characterized by a high sensitivity (at a level of the vacuum gauge readings).

REFERENCES

1. Lanis, V.A., Levina, L.E. (1963) *Vacuum test procedure*. Moscow: Gosenergoizdat.
2. Chvertko, A.I., Nazarenko, O.K., Nekrasov, A.I. *et al.* (1973) *Equipment for electron beam welding*. Kyiv: Naukova Dumka.

COMPUTER ATLAS OF THE DIAGRAMS OF AUSTENITE DECOMPOSITION AND MECHANICAL PROPERTIES OF THE HAZ METAL OF WELDED JOINTS ON STRUCTURAL STEELS

A.F. MUZHICHENKO
The E.O. Paton Electric Welding Institute, NASU, Kyiv, Ukraine

ABSTRACT

The paper describes a program package which includes spline-approximated plots of austenite decomposition diagrams for various steel grades. The bank provides information storage and updating. The computer atlas is stored in a form convenient for computerized forecasting of the HAZ metal mechanical properties.

Key words: *computer atlas, program package, mechanical properties, spline-approximation*

Important characteristics of a steel weldability are the nature of phase transformations, change of the structure and mechanical properties of the metal of the HAZ as a reaction to the thermal cycle of welding. For various steel grades these data were generalised in the form of atlases [1 – 4]. The phase composition and mechanical properties of the metal in the HAZ can be determined from these atlases and calculation of the steel cooling time in the temperature range of 800 to 500 °C ($t_{8/5}$). However, the information presentation in the form of hard copies (books) as graphs and tables makes it more difficult to enter the data for calculations into the modern computer systems.

The tasks of entering the textual and tabulated information can be accomplished using such well-known programs as FineReader, CuneiForm, etc. However, the software market does not offer any programs which would allow entering the graphs of the diagrams of anisothermal decomposition of austenite (ADA) and mechanical properties in a form convenient for further use and computation in personal computers.

This created the need for development of specialised software for digitising and entering graphic information from atlases of ADA diagrams into the computer and presentation of this information in a vector form convenient for further computations. A scanner and mouse were selected, as well as subsequent displaying of the image (or its part) in the display, which allows using the feedback between the scanned image and the introduced spline-approximation.

Digitising of plots was performed using spline-approximation constructed by reference points chosen by the operator visually during processing of the scanned image on the display.

Construction of the cubic spline of $y = f(x)$ curve is described in [5]. With this method the spline-function $y = f(x)$ can be constructed only for single-valued functions, i.e. a monotonically rising sequence of x_i is required in $x0 < x_1 < \dots$ $\dots x_{N-1} < x_N$ grid, one x value cannot correspond to several values of y. Some curves of phase transformations do not meet this requirements.

A non-single-valued, also a closed curve (periodical spline) can be plotted, using parametric assignment of the function. For this purpose an independent variable t is chosen and $x(t)$ and $y(t)$ spline-approximations are calculated, which is followed by plotting a curve passing through points x_i, y_i, corresponding to the selected t_i [6].

Two methods of assigning t parameter are proposed in [7]. According to the first method t is assigned as a sequence of integer numbers $t_i = i$. With the second method, t_i corresponds to the total length of the chords which is an approximation of the length of the arc between the first and i-th points. In this case at $t_1 = 1$, $t_2 = 2$.

$$t_i = t_{i-1} + \sqrt{\frac{(x_i - x_{i-1})^2 + (y_i - y_{i-1})^2}{(x_2 - x_1)^2 + (y_2 - y_1)^2}}.$$

The spline is constructed allowing for the position of all n points, therefore, n equations should be solved. In [6] it was demonstrated that the influence of the boundary conditions on the next points quickly attenuates and is only manifest in the intervals, closest to the ends, i.e. just the position of three to five adjacent points closest to this

No.	Action
1	Image scanning
2	Saving the images in one of the graphic formats (PCX TIF or BMP)
3	Creation of a list of files of the scanned images
4	Selection of the next image from the list and its representation in the display
5	Entering the ranges of the graph co-ordinates
6	Recording the origin of the system of co-ordinates of the graph and the final points of the coordinate axes
7	Calculation of the angle of inclination of the axes of the system of co-ordinates relative to the horizontal and vertical and to each other (this operation is due to the inevitable error in the graph positioning in the scanner, as well as in preparation of the art work)
8	Selection of the colour for the curve which is to be digitised
9	Marking the system of reference points on the curve
10	Recording the co-ordinates of the reference points in accordance with the angle of deviation of the system of co-ordinates
11	Plotting the curve spline-approximation by the co-ordinates of the basic points
12	The graphs of spline-approximation are superposed onto the earlier scanned image of the graphs in the display; in case of unsatisfactory accuracy, the system of reference points can be edited

section, is taken into account. Such an approach to construction of splines in [6], was called local splines. When the scanned image is represented in the display in the mode of 800×600 points, the thickness of the graph lines is 2 to 3 pixels, using the mouse the reference point can be positioned with an accuracy of up to 1 pixel, i.e. the error does not exceed $0.5 - 1.0$ %.

The algorithm of the software operation is presented in the Table.

The time for scanning and digitising one of the diagrams from the atlas [1] is about 10 min. This software was used to create the «Electronic atlas of diagrams of austenite decomposition, change of phase composition and mechanical properties of the HAZ in steel welding» data base, which includes more than 200 steels from the atlases [1, 2] and is used for calculation of the mechanical properties allowing for $t_{8/5}$ [7].

This software can be used also for digitising the graphs from reference books; plotting the graphs when entering the tabulated information; automated entering into the computer of the shapes of various flat parts.

The electronic atlas can be used independently or with other software and can be continuously complemented by new steel grades.

REFERENCES

1. Seyffarth, P. (1982) *Großer Atlas Schweiß-ZTU-Schaubilder*. Dusseldorf: DVS-Verlag.
2. Shorshorov, M.Kh., Belov, V.V. (1977) *Phase transformations and changes of the steel properties in welding*. Atlas. Moscow: Nauka.
3. (1995) *An atlas of continuous cooling transformation (CCT) diagrams applicable to low-carbon low-alloy weld metals*. Ed. by Zhuyao Zhang, R.A. Farrar. Ashgate.
4. (1991) *Atlas of time-temperature diagrams for irons and steels (Materials data series)*. Ed. by G.F. Vander Voort. ASM Int.
5. Marchuk, G.I. (1977) *Methods of computational mathematics*. Moscow: Nauka.
6. Bayakovsky, Yu.M., Galaktionov, V.A., Mikhailova, T.N. (1985) *GRAFOR. Graphic extension of FORTRAN*. Moscow: Nauka.
7. Muzhichenko, A.F. (1996) Program of forecasting the microstructure and mechanical properties of the HAZ in welding the structural steels. *Avtomaticheskaya Svarka*, **6**, 40 – 43.

ON THE FEATURES OF FLUX MELTING IN ELECTRIC ARC WELDING

V.G. KUZMENKO
The E.O. Paton Electric Welding Institute, NASU, Kyiv, Ukraine

ABSTRACT

Features of flux melting in the zone in front of the arc are discussed, in particular the probability of formation of a discontinuity of the slag skin in this section in SAW. It is shown that in the actual welding processes no slag film forms in front of the moving arc due to the high heat-insulating properties of the fluxes.

Key words: *electric arc welding, fluxes, slag skin*

The author would like to once more discuss the features of flux melting and the associated issue of the continuity of the slag skin in electric arc welding [1, 2].

In [2] B.N. Badianov focused his principal criticism on the assumption made by the author of [1] of the weld pool front edge being incompletely covered by the slag skin, because of limited transfer of the arc heat through it to the flux. The other remarks are of a methodological nature and do not influence the conclusions of [1].

In order to study the nature of flux melting in front of the arc, B.N. Badianov in [2] used N.N. Rykalin's equation of a limit quasi-stationary state for a mobile point source [3]

$$T = \frac{q_m}{2\pi\lambda R} \exp\left(-\frac{VR}{2a} - \frac{VX}{2a}\right). \quad (1)$$

In the calculations it was presented as

$$X = -\frac{2a}{V} \ln \frac{2\pi\lambda T}{q_m} - \frac{2a}{V} \ln R - R. \quad (2)$$

Application of these equations for calculation of heat transfer from the arc to the flux through the slag skin already is rather abstract, as the assumptions used by N.N. Rykalin in studying the features of the metal heated by the arc (point source, uniform medium, absence of transformations), do not imply formation of liquid metal, including the slag skin.

Nonetheless, by substituting the appropriate parameters of the welding process and using for the flux the value of thermal diffusivity $a = \lambda/c\gamma = 0.06$ cm^2/s for SiO_2, B.N. Badianov determened the distance between 3000 and 1300 °C isotherms that, in his opinion, corresponds to the thickness of the slag skin in front of the arc. It is equal to 24 mm for welding speed v_w = 0.01 cm/s (0.36 m/h), and to 0.55 mm for 0.60 cm/s (21.00 m/h), respectively.

As regards the value of the flux thermal diffusivity a proper, assumed in the above calculations, first of all selection of an abstract SiO_2 as the flux analog is puzzling. SiO_2 can be present both in the form of a monolithic (quartz), and granular (sand) material, while having different ratios of the crystalline and vitreous phase. The differences in the thermophysical properties will also be significant in each case, accordingly. If selection of SiO_2 is to be accepted after all, dry sand will probably be the most suitable for the case under consideration. According to the reference book on thermophysical properties of inorganic materials [4], thermal diffusivity of quartz sand is $(0.044 - 0.058) \cdot 10^{-2}$ cm^2/s. If this value of thermal diffusivity is to be used in equation (2), the distance between 3000 and 1300 °C isotherms in the flux bulk in front of the arc will be 0.20 mm for v_w = 0.36 m/h, and at v_w = 21.00 m/h it will take a really negligible value of 0.005 mm. This practically completely eliminates the probability of slag skin formation in front of the arc in the actual welding processes.

In order to understand the reason for the excess values of thickness of the slag skin in front of the arc, derived by B.N. Badianov in his calculations, let us compare the values of the coefficient of thermal diffusivity of the flux of 0.06 cm^2/s selected in [2], and used by N.N. Rykalin [3] in calculation of steels heating by an electric arc. So, in the latter study they are equal to 0.08 cm^2/s for low-carbon steel and 0.053 cm^2/s for chromium-nickel austenitic steel, respectively. This means that B.N. Badianov, using in [2] the value of the flux thermal diffusivity coefficient equal to 0.06 cm^2/s, actually performed calculations for heat propagation in steel.

Thus, the calculations performed by B.N. Badianov, did not deny, but rather confirmed the fact of the absence of a slag skin in front of the moving arc in submerged-arc welding.

REFERENCES

1. Kuzmenko, B.G. (1999) Features of melting and solidification of flux in welding. *Svarochnoye Proizvodstvo*, **10**, 13 – 22.
2. Badianov, B.N. (1999) On a new procedure of submerged-arc welding. *Ibid.*, **11**, 8 – 11.
3. Rykalin, N.N. (1951) *Calculation of the thermal processes in welding*. Moscow: Mashgiz.
4. Krzhizhanovsky, R.E., Shtern, Z.Yu. (1973) *Thermophysical properties of non-metallic materials*. Leningrad: Energia.